Universidade do Minho
Escola de Ciências

Maria Carolina Morais Amorim

Investigating bolaamphiphilic bis-dehydropeptide hydrogels as drug delivery systems

February 2021

Maria Carolina Morais Amorim **Investigating bolaamphiphilic bis-dehydropeptide hydrogels as drug delivery systems**

UMinho | 2021

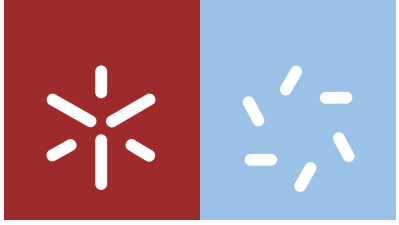

Universidade do Minho
Escola de Ciências

Maria Carolina Morais Amorim

Investigating bolaamphiphilic bis-dehydropeptide hydrogels as drug delivery systems

Master's Dissertation
Master in Medicinal Chemistry

Performed under supervision of
Professor Doctor Peter John Jervis
and
Professor Doctor Paula Margarida Ferreira

February 2021

DIREITOS DE AUTOR E CONDIÇÕES DE UTILIZAÇÃO DO TRABALHO POR TERCEIROS

Acknowledgement

This work was only possible with the contribution and guidance of many people. I am grateful to all whom in one way or another contributed to this work.

First, I would like to thank my supervisors, Dr. Peter Jervis and Dra. Paula Margarida Ferreira, and to Dr. José Alberto Martins for all their support during the development of this work and for the opportunity of working in a new field. Their confidence, encouragement, energy and guidance helped me to overcome difficulties during this time.

I would like to express my gratitude to Dr. Loic Hillou from the Instituto de Polímeros e Compósitos (IPC) for all the help and for making available the equipment where the rheology assays were carried out. I also thank Dr. David Pereira from Faculdade de Farmácia of Universidade do Porto for conducting the cytotoxicity tests.

I thank to the Centro de Química and the Departamento de Química of the Universidade do Minho for offering the necessary resources for the development of this project. A special thanks to Elisa Pinto and Vânia Azevedo for the NMR spectra. I also thank the NMR Portuguese network (PTNMR (Portuguese NMR network) PINFRA/22161/2016 financed by FCT and Portugal 2020).

I would like to thank to Fundação para a Ciência e a Tecnologia for funding through project PTDC/QUI-QOR/29015/2017.

Thank you to my lab colleagues for the good lab environment and the help provided.

To my friends who have helped me in all situations, academic or otherwise, for making difficult times easier.

Finally, I would like to thank my family, especially my parents and my sister for their support, encouragement, understanding, patience and strength I needed to continue following my dreams.

FCT Fundação para a Ciência e a Tecnologia

REPÚBLICA PORTUGUESA

STATEMENT OF INTEGRITY

I hereby declare having conducted this academic work with integrity. I confirm that I have not used plagiarism or any form of undue use of information or falsification of results along the process leading to its elaboration. I further declare that I have fully acknowledged the Code of Ethical Conduct of the University of Minho.

Investigating bolaamphiphilic bis-dehydropeptide hydrogels as drug release systems

Abstract

Self-assembly is a phenomenon which is ubiquitous in nature with examples ranging from the complementarity of DNA base pairs to the folding of proteins. Self-assembled peptides has emerged as a novel class of biomaterials with diverse therapeutic applications. In this work four symmetrical bolaamphiphiles based on dehydrodipeptides (phenylalanyldehydrophenylalanine and tyrosyldehydrophenylalanine) linked through phenyl or naphthyl linkers (terephthalic acid and 2,6-naphthalenedicarboxylic acid) were prepared and their self-assembly properties studied. The results showed that all compounds with the exception of the bolaamphiphile of tyrosyldehydrophenylalanine and 2,6-naphthalene dicarboxylic acid gave self-standing hydrogels with critical gelation concentrations of 0.3 and 0.4 wt% using a pH trigger.

Scanning transmission electron microscopy images showed a network of entangled fibres for all three hydrogelators and vesicular structures for the bolaamphiphile that failed to give hydrogels in the conditions tested. Circular dichroism spectroscopy was performed to evaluate the aggregation of peptides into characteristic secondary structures. The results point to β-sheet or random coil. According to rheology the dehydrodipeptide bolaamphiphile hydrogelators are viscoelastic materials with an elastic modulus G' that falls in the range of native tissue (0.37 kPa brain – 4.5 kPa cartilage). The cytotoxicity of the new compounds was tested using human keratinocytes (HaCaT cell line). The molecules under study have no identifiable impact in cell proliferation, despite having a small impact in cell viability although none of the molecules elicited loss of membrane integrity in the concentrations tested.

In sustained release assays, the effect of the charge present on model compounds on the rate of cargo release from the hydrogel networks was evaluated. The hydrogels provide a sustained release of the methyl orange (anionic) and of ciprofloxacin (neutral), while the methylene blue (cationic) is retained by the hydrogels network.

The bolaamphiphiles prepared constitute promising materials to be used as drug delivery platforms.

Keywords: bolaamphiphiles, dehydrodipeptide, drug delivery, self-assembly, supramolecular hydrogelators.

Investigando hidrogéis de bis-desidropéptidos bola-anfifílicos como sistemas de libertação de drogas

Resumo

A auto-associação é um fenómeno onipresente na natureza, com exemplos que vão desde a complementaridade dos pares de bases do DNA até ao enrolamento de cadeias proteicas. A auto-associação de péptidos deu origem a uma nova classe de biomateriais com diversas aplicações terapêuticas. Neste trabalho foram preparados quatro compostos bola-anfifílicos baseados em desidrodipéptidos (fenilalanildesidrofenilalanina e a tirosildesidrofenilalanina) ligados por grupos fenilo ou naftilo (ácido tereftálico e o ácido 2,6-naftalenodicarboxílico) e estudadas suas propriedades de auto-associação. A formação de hidrogéis a partir dos compostos preparados foi avaliada tendo-se verificado que todos os compostos, com exceção do bola-anfífilo de tirosildesidrofenilalanina e ácido 2,6-naftaleno dicarboxílico, deram hidrogéis com concentrações críticas de gelificação de 0,3 e 0,4 wt%.

As imagens de microscopia eletrónica de transmissão de varrimento mostraram uma rede de fibras entrelaçadas para os três compostos que deram origem a hidrogéis e estruturas vesiculares para o bola-anfífilo que não formou hidrogéis nas condições estudadas neste trabalho. Ensaios de espectroscopia de dicroísmo circular foram efetuados para avaliar as estruturas secundárias resultantes da agregação dos péptidos. Os resultados evidenciaram estruturas em folha β e *random coil*. Estudos de reologia mostraram que que os hidrogéis são materiais viscoelásticos com valores para o módulo de elasticidade G' situados entre os encontrados para os vários tecidos biológicos (0,37 kPa cérebro - 4,5 kPa cartilagem). A citotoxicidade dos novos bola-anfifílos foi testada em queratinócitos humanos, (HaCaT). Os resultados obtidos mostram que as moléculas em estudo não têm impacto identificável na proliferação celular, apesar de terem um pequeno impacto na viabilidade celular. No entanto, nenhuma das moléculas provocou perda de integridade de membrana nas concentrações testadas.

Nos ensaios de liberação controlada, foi estudado o efeito da carga dos compostos modelo na sua taxa de libertação a partir dos hidrogéis. Os resultados mostraram a libertação do alaranjado de metilo (aniónico) e da ciprofloxacina (neutra). O azul de metileno (catiónico) permaneceu retido nos hidrogéis.

Os novos compostos preparados poderão no futuro vir a ser utilizados como plataformas para a entrega de fármacos.

Palavras-chave: auto-associação, bola-anfífílos, desidrodipéptidos, hidrogeladores supramoleculares, libertação de fármacos.

Índice

Index of figures

Index of tables

Index of schemes

Abbreviations and Acronyms

3D	Three-dimensional
BAs	Bolamphiphiles
Boc	*Tert*-Butyloxycarbonyl
Boc_2O	*tert*-Butyl dicarbonate
CD	Circular dichorism
$CDCl_3$-d_1	Deuterated chloroform
cgc	Critical gelation concentration
COX-1	Cyclooxygenase-1
COX-2	Cyclooxygenase-2
DMAP	4-dimethylaminopyridine
DMSO-d_6	Deuterated dimethylsulfoxide
DNA	Deoxyribonucleic acid
ESI	Electrospray Ionization
Et_3N	Triethylamine
FF	Phenylalanylphenylalanine
FGI	Functional Group Interconversion
Fmoc	Fluorenylmethoxycarbonyl
G*	Complex modulus
G'	Elastic modulus
G''	Viscosity modulus
GdL	D-glucono-δ-lactone
HBTU	*N,N,N',N'*-Tetramethyl-*O*-(1*H*-benzotriazol-1-yl)uronium hexafluorophosphate
HRMS	High Resolution Mass Spectrometry
J	NMR coupling constant in Hz
LDH	Lactate dehydrogenase
LMWHs	Low molecular weight hydrogelators
MB	Methylene blue
MeCN	Acetonitrile
MO	Methyl orange
Naph	Naphthalene

NMR	Nuclear magnetic resonance
Npx	Naproxen
Cbz	Benzyloxycarbonyl / carboxybenzyl
NSAID	Nonsteroidal anti-inflammatory drug
PAG	Photoacid generators
ppm	Parts per million
rt	Room temperature
STEM	Scanning transmission electron microscopy
SEM	Scanning electron microscopy
TFA	Trifluoroacetic acid
THF	Tetrahydrofuran
TLC	Thin layer chromatography
TMG	*N*,*N*,*N*',*N*-tetramethylguanidine

Chapter 1

Introduction

1 Introduction

1.1 Hydrogels

Over the last few decades, hydrogels have attracted considerable attention as promising biomaterials for various biotechnological and biomedical applications such as drug delivery, regenerative medicine, tissue engineering, diagnosis and cell culture. [1-5]

Hydrogels are solid-like materials made of a three-dimensional (3D) network of self-assembled building blocks that capture large numbers of water molecules. [1-7]

Hydrogels according to the macromolecular architecture of the 3D network can be either chemical or physical gels. Chemical hydrogels or covalent hydrogels comprise molecular scaffold chains covalently linked to each other. These hydrogels are strong and irreversible. Physical hydrogels rely on self-assembly, a phenomenon ubiquitous in nature that is involved in many of the most fundamental biological processes. Self-assembly is the spontaneous association of individual molecules into unique supramolecular well-ordered structures held together by non-covalent interactions such as hydrogen bonding or π-π stacking interactions, hydrophobic interactions, electrostatic interactions. [1, 8-10] Physical hydrogels are reversible and usually weaker than chemical hydrogels. Moreover, the transition from a solution form into a gel state (sol-to-gel) is usually more rapid in physical gels than the cross-linking that leads to the formation of chemical hydrogels (Figure 1).

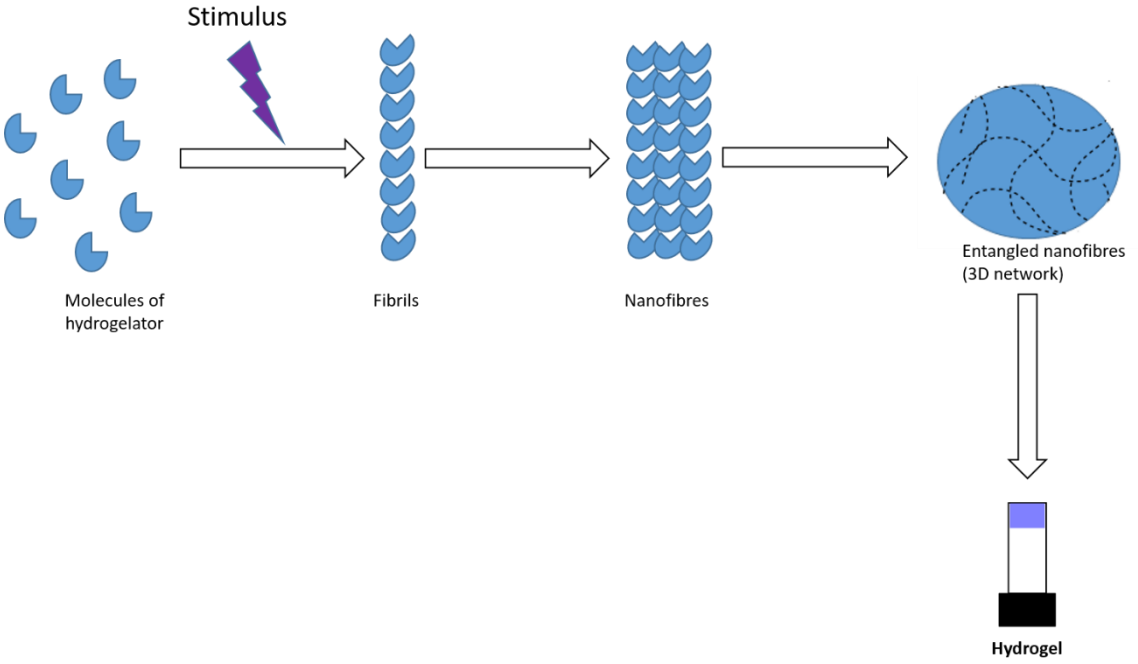

Figure 1: Hierarchical process that leads to physical hydrogels. (adapted from ref. 11) [11]

1.2 Self-assembled Low Molecular Weight Peptide hydrogels

Low molecular weight hydrogelators (LMWHs) are small molecules that self-assemble into gel-phase materials. Among LMWHs amino acid derivatives and small peptides have attracted a substantial research interest due to their modular and tunable functionality, ease of synthesis and scalability, ability to associate spontaneously and biocompatibility. In general, these hydrogelators are constructed by conjugating an amino acid or small peptide with aromatic systems such as fluorenylmethoxycarbonyl (Fmoc), naphthaloyl or carboxybenzyl, to promote self-assembly. The shorter the peptide sequence the lower will be the cost of production and the ease of its scale-up. Thus, amino acids derivatives have been studied as potential hydrogelators and although, 20 natural amino acids are known only a few have elicited hydrogels easily and with low minimum gelation concentration when functionalized with aromatic moieties. These include phenylalanine (Phe, F), tyrosine (Tyr, Y) or tryptophan (Trp, W) (Figure 2). [1, 12-14]

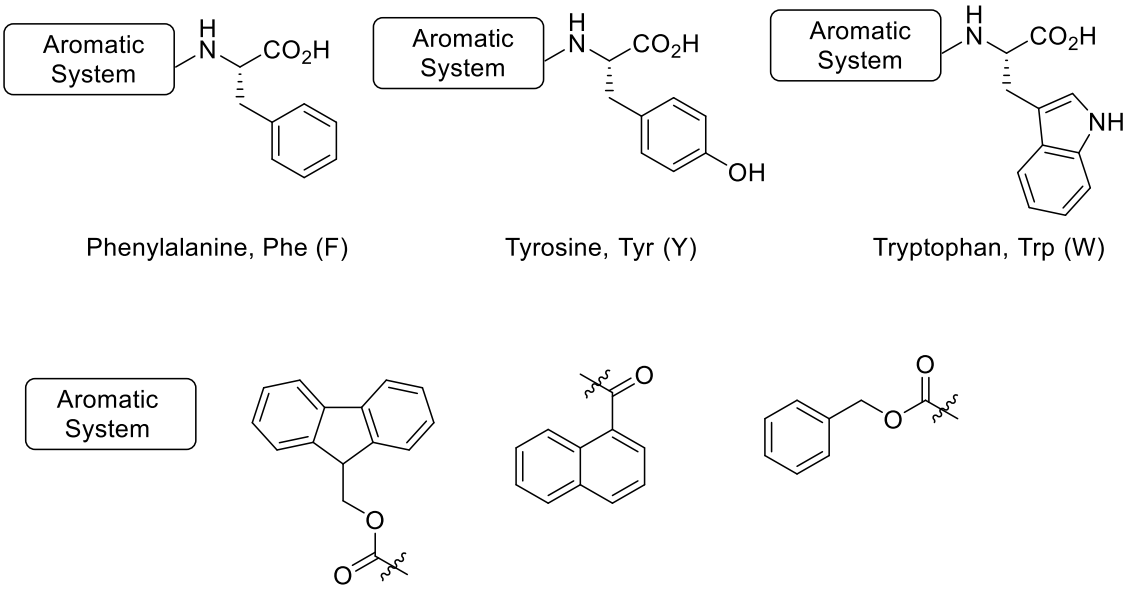

Figure 2: Structures of supramolecular hydrogelators based on amino acid derivatives.

Most of the peptide LMWHs contain one or more aromatic amino acid residues especially phenylalanine. One of the aggregation sequences of the amyloid protein, the dipeptide phenylalanylphenylalanine (FF) has been extensively studied. This sequence alone does not give hydrogels but rather forms crystalline nanotubes. However, the dipeptide Fmoc-FF gives a self-supporting hydrogel. (Figure 3) The ease of synthesis is one of the reasons that explain the popularity of this *N*-protected dipeptide as a hydrogelator for a variety of applications. [15-17]

The Fmoc group is susceptible to cleavage at pH values above 10 which can be problematic since this type of gelators are usually dissolved in basic aqueous solutions prior to gelation. Also, the cleavage product of Fmoc, the dibenzofulvalene show some cytotoxicity. Thus, in order to overcome this drawback a wide range of *N*-capping groups have been used to prepare small peptide hydrogelators (naphthalene or carboxybenzyl based groups). [18]

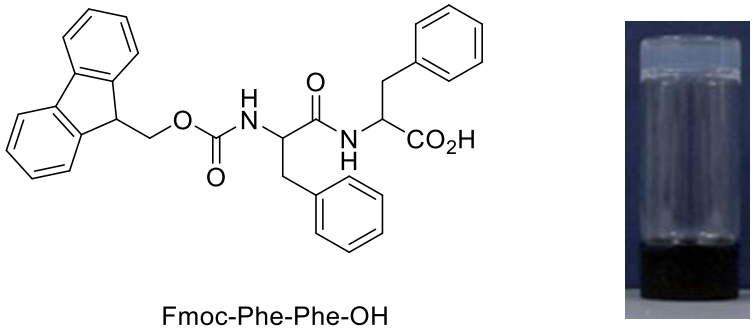

Figure 3: Structure and optical image of Fmoc-Phe-Phe-OH hydrogel. (adapted from ref 17) [17]

The FF dipeptide *N*-protected with the 2-naphthyloxyacetyl group gives different types of networks using several triggers (Figure 4). [14, 19]

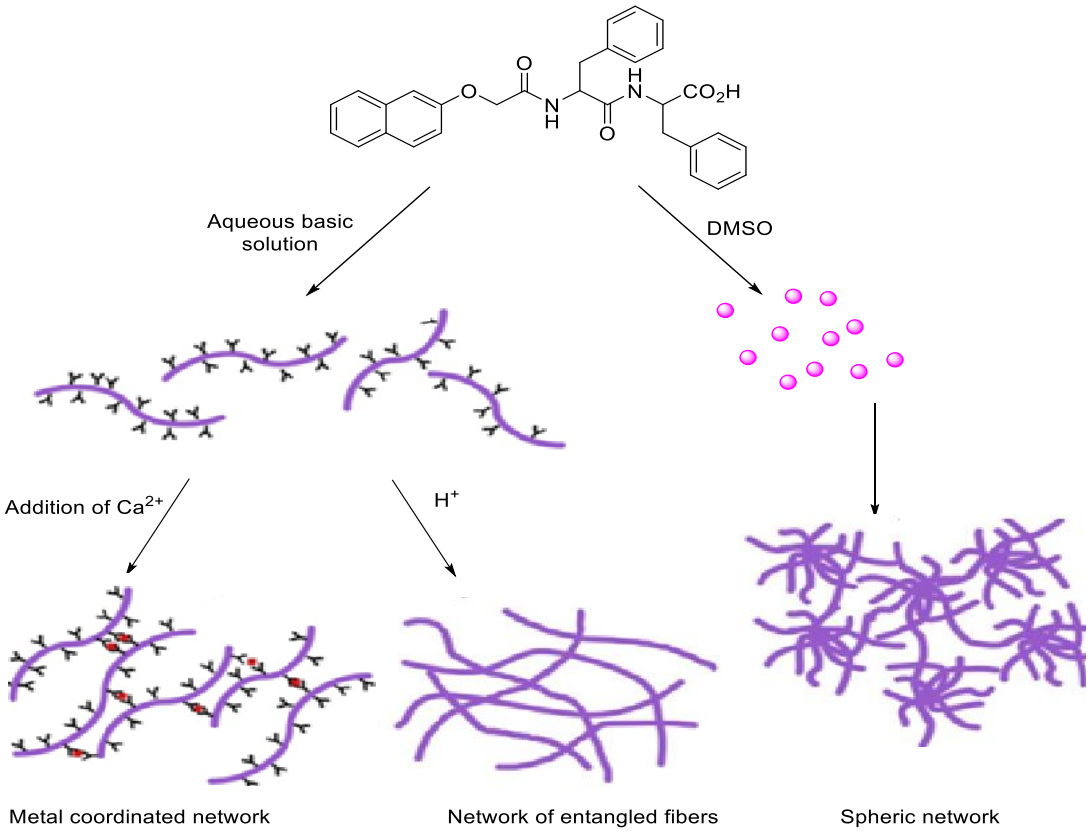

Figure 4: Self-assembly of FF dipeptide *N*-capped with 2-naphthyoxyacetyl. (adapted from ref. 14) [14]

The tuning of small peptides self-assembly and hydrogelation can be accomplished not only by alteration of the *N*-capping group but also by a careful selection of the amino acid sequence and by the choice of the gelation method.

There are many reports in the literature emphasizing the importance of the Phe residue in the development of small peptide supramolecular hydrogelators. [18] However, the importance of aromatic amino acids in the design and development of this type of hydrogelators is not yet clearly understood. Bowerman *et al.* [20] studied the hydrogelation of an octapeptide with Phe by replacing it with a cyclohexylalanine residue. The results showed that given the complexity of the self-assembly process the precise contribution of aromaticity was quite difficult to detect. Thus, in order to simplify the system, Shaummugam *et al.* [21] compare a phenylalanine residue *N*-capped with Fmoc with a cyclohexylalanine with the same *N*-protecting group. Both compounds gave hydrogels, which suggests that the hydrophobicity of the phenyl ring contributes to the formation of the hydrogel rather than its aromaticity. The results also point that the aromaticity of the phenyl ring of phenylalanine imparted thermal stability to the hydrogel through additional π-π interactions.

Gelation is initially evidenced by inverting the vial and observing a lack of flow under the force of gravity. The majority of supramolecular hydrogels are formed as apparently homogeneous materials in vials by treatment of a gelator solution with a stimulus such as heat, pH, light, ultrasound, enzymes or metal ions. [12] These triggers produce a disturbance on the gelation system that induces the transition between the solution and the gel phase. [22] When peptide molecules start to assemble from a super-saturated solution, three situations are possible (Figure 5):

1. Crystallization, in response to highly ordered packing;
2. A random aggregation resulting in a precipitate;
3. Aggregation process giving a gel (intermediate between 1 and 2). [23]

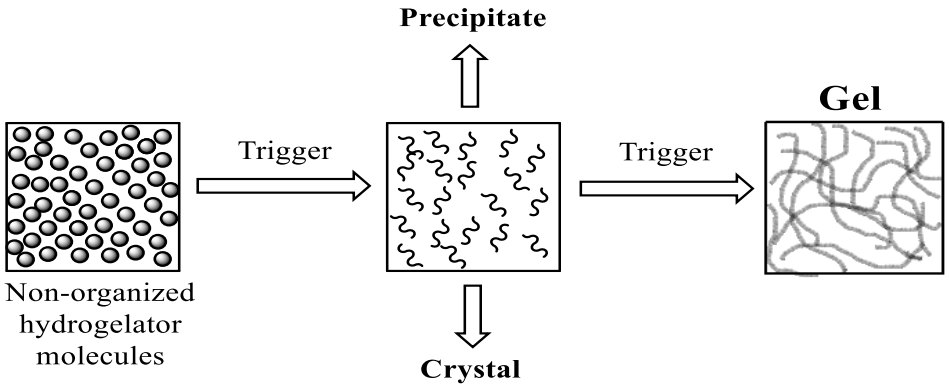

Figure 5: Self-assemble of molecules from a saturated solution. [23]

The most frequently used trigger of gelation is acidification of a basic solution of hydrogelator. [1] The pH drop can be accomplished by the addition of a solution of HCl or of glucono-δ-lactone (GdL). The addition of HCl induce a decrease in pH that is faster than the mixing of the acid leading to heterogeneous hydrogels. [24] This inconvenient can be circumvent by using the slow hydrolysis in water of glucono-δ-lactone to gluconic acid (Scheme 1, Figure 6). As the rate of dissolution of GdL is higher than the rate of hydrolysis, the result is a uniform decrease in pH across the entire sample. This methodology also allows targeting a specific final pH. [25-29]

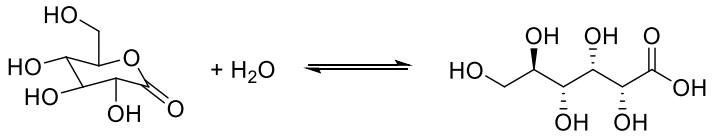

Scheme 1: The hydrolysis of GdL to gluconic acid in water. [24]

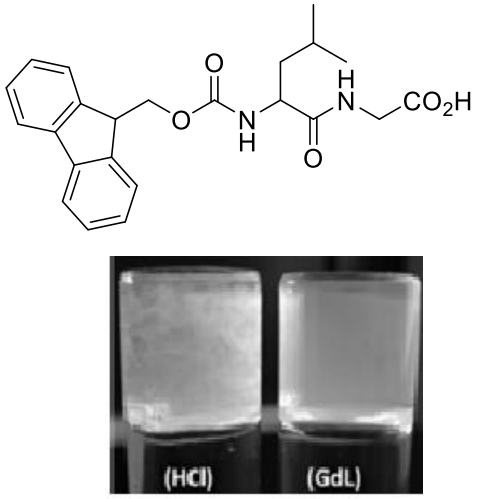

Figure 6: Photographs of hydrogels prepared from Fmoc-L-Leu-Gly-OH. On the left, the pH was changed with HCl, turbid inhomogeneities can be seen in this hydrogel. On the right, the pH was changed using GdL. Here, a transparent, uniform gel is formed. In both cases the final pH is 3.9 (adapted from ref. 26). [26]

The simplest method to obtain supramolecular hydrogels is the use of a change in temperature. Several LMWHs are soluble in water at low concentration at high temperature. This approach consists in heating the solution/suspension of the hydrogelator and, upon cooling, a hydrogel is formed. As the temperature decreases, so does the solubility and, because of the presence of one-dimensional non-covalent forces, fibrous structures are formed, resulting in a hydrogel. [14, 24, 30, 31]

Xu *et al.* [32] and Ulijn *et al.* [33] described another method for hydrogel formation, where dipeptide or tripeptide conjugate hydrogelators are formed *in situ* from soluble precursors, via a reaction catalysed by enzymes. Enzymes can either make or break a bond and convert a precursor into

a hydrogelator which can self-assemble to form a hydrogel. The kinetics of gel formation can be controlled by adjusting the concentration of enzyme. When high concentrations of enzyme are used, gels with higher elastic moduli are formed. At low enzyme concentration, the fibres formed are thinner and more uniform, resulting in a hydrogel with weaker mechanical properties. [24, 34] One example of this methodology is the cleavage of the phosphate group from a peptide with an *O*-phospho-tyrosine residue with a phosphatase. This reduces the water solubility of the compound leading to self-assembly (Scheme 2). [34, 35]

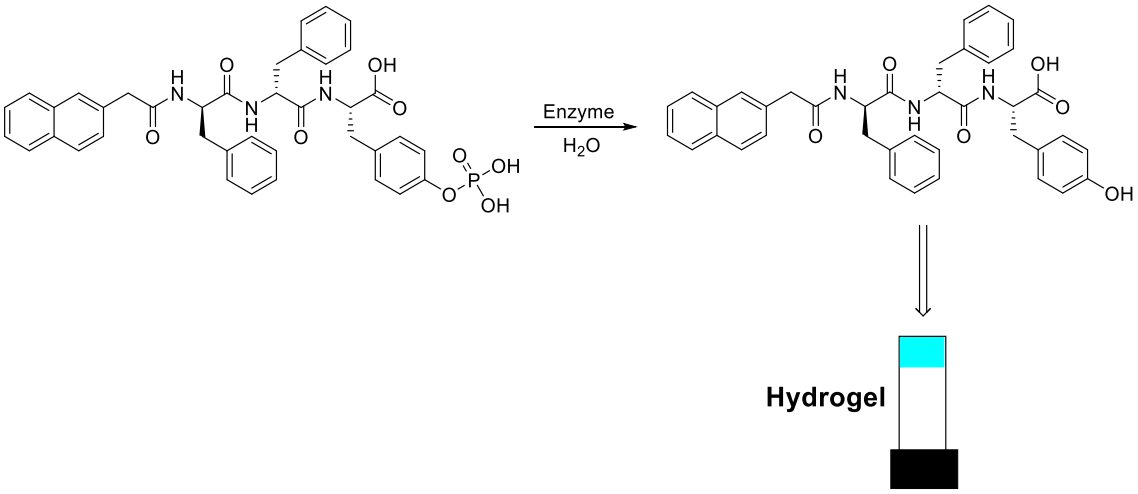

Scheme 2: Enzymatic *in situ* generation of a hydrogelator by dephosphorylation of a tyrosine phosphate. [35]

Gelation can also be achieved by the addition of ions to the hydrogelator solution. Shi *et al.* reported the use of calcium ions (Ca^{2+}) to cross-link the nanofibers of self-assembled small peptides namely 2-Naph-L-Phe-L-Gly-L-Leu-L-Asp-L-Asp-OH, 2-Naph-L-Phe-L-Phe-L-Cys-L-Gly-L-Leu-L-Asp-OH and 2-Naph-L-Phe-L-Phe-L-Cys-L-Gly-L-Leu-L-Asp-L-Asp-OH, allowing the formation of self-healing hydrogels (Figure 7). The properties of the hydrogels can be controlled in terms of their function by the amount of calcium ions added, which regulates the density of crosslinks. [36]

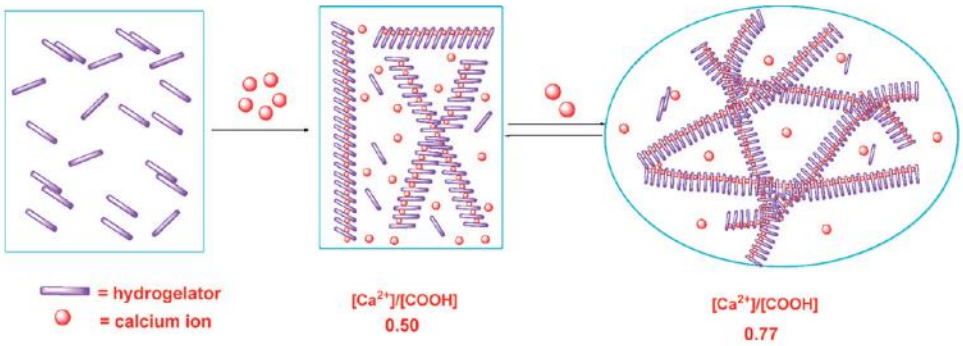

Figure 7: Illustration of the hydrogelation process induced by calcium ions suggested by Shi *et al.* (adapted from ref 36). [36]

Chen *et al.* [37] also described the hydrogelation of a series of dipeptide derivatives by the addition of cations. When solutions containing long and worm-like micelles were treated with cations crosslinks between the micelles were created, leading to hydrogelation (Figure 8).

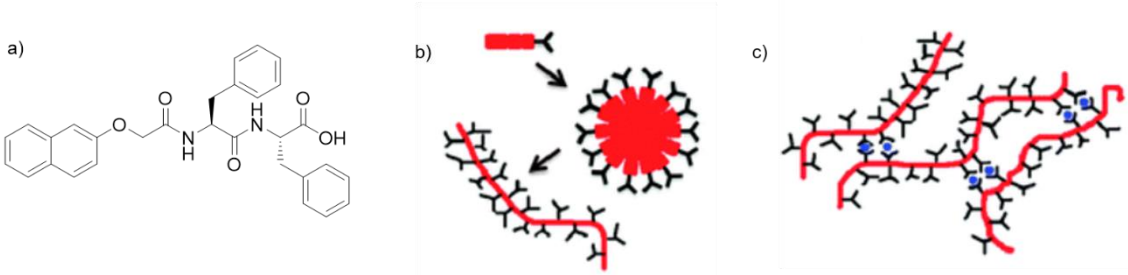

Figure 8: a) Structure of 2-Naph-L-Phe-L-Phe-OH; b) Schematic assembly of this dipeptide into worm-like micelles above the critical micelle concentrations; c) Schematic illustration of worm-like micelles crosslink on addition of a divalent ion (blue) (Adapted from ref. 37). [37]

The characterization of peptide hydrogels relies on several techniques such as spectroscopy, electronic microscopy or rheology. Given the complex nature of supramolecular hydrogels, complementary techniques are usually combined to fully characterize their properties.

The macroscopic properties of hydrogels can be determined by rheology. Rheology is the study of the deformation and flow of matter under the influence of an applied stress. When a stress is continuously applied to a material, two extreme behaviours are possible:

- The material deforms slightly, but eventually resists to further stress and is considered a solid;
- The material flows continuously and is a liquid.

However, there are some materials that cannot be considered neither a solid nor a liquid and behave as a solid or as a liquid depending on the time scale of the deformation process. For this reason, it is easier to classify materials in terms of their rheological behaviour as elastic or viscous. If the amount of deformation of the material is proportional to the applied force or stress, the material is

elastic. However, if it is the deformation rate that is proportional to the force or stress the material is considered viscous. [38, 39] Supramolecular hydrogels are viscoelastic materials that exhibit both elastic and viscous characteristics. Oscillatory rheology can give information about the nature of the network of a hydrogel namely type, number and strength of the crosslinks. [38] In this technique the sample is placed between two plates (or cylinders) and an oscillatory strain (or stress) is applied to one of the plates. The induced movement of the other plate is decomposed into an in- and out-of-phase component. Several properties can be determined using this methodology: complex modulus, G*; elastic or storage modulus, G' and loss or viscous modulus, G''. [10, 39] A material is considered a viscoelastic gel, when G' is independent of the frequency until a particular yield point and G' exceeds G'' by at least one order of magnitude. [39, 40, 41].

The supramolecular structure of low molecular weight peptide hydrogels can be determined using spectroscopy techniques. Among these, circular dichroism (CD) is a valuable tool for the elucidation of intra- and intermolecular interactions of chiral structures. Thus, is particular useful to determine the secondary structures of peptides and proteins. [10, 39-42] The amide bond chromophore has two absorption bands corresponding to the n-π* and π-π* transitions, at 230-210 nm and 200-180 nm, respectively. [43] The CD spectra of the major secondary structural motifs of peptides and proteins are shown in Figure 9 and are: α-helix, β-sheet and random coil. [44] α-Helical peptides have negative bands at 222 nm and 208 nm and a positive band at 193 nm, peptides with antiparallel β-sheets have negative bands at 218 nm and positive bands at 195 nm, while a random coil peptide show low ellipticity above 210 nm and negative bands near 195 nm (Figure 9). [45]

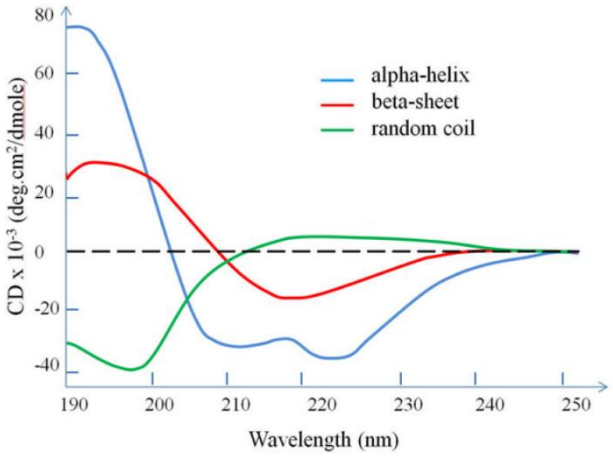

Figure 9: CD spectra of the secondary structures of peptides. [46]

Another technique used to characterize hydrogels is scanning transmission electron microscopy

(STEM). It is a powerful imaging technique, suitable for the characterization of the micro- and nano-structure of the hydrogel network. Images are formed by electrons passing through a sufficiently thin sample. [47]

1.3 Supramolecular hydrogels with non-proteinogenic amino acids

Biomaterials based on α-peptides are known to be unstable towards proteolytic enzymes. [48] This is the main reason why their long-term application *in vivo* is not possible. In order to circumvent this limitation several strategies have been envisage. The most frequently used is the introduction of non-natural amino acids into the peptide chain. These synthetic peptides can incorporate among others *D*-amino acids, β- or γ-amino acids, dehydroamino acids or α,α -disubstituted amino acids. Peptides with non-protein amino acids are endowed with higher proteolytic stability when compared with their natural amino acid peptide counterparts. [49]

Xu *et al.*, described new hydrogelators based on dipeptides containing *D*-amino acids and *N*-capped with the non-steroidal anti-inflammatory drug (NSAID) naproxen. [50] The presence of *D*-amino acids in the hydrogelators not only increased the proteolytic stability but also enhanced their selectivity for inhibiting cyclooxygenase-2 (COX-2) over cyclooxygenase-1 (COX-1). The COX-1 has mainly a physiological role in kidneys and the stomach, and is responsible for maintaining homeostasis, whereas COX-2 induces the inflammatory response, producing the formation of prostaglandins, prostacyclin and thromboxane. Inhibition of COX-1 is responsible for the adverse gastrointestinal and renal effects of NSAIDs while the inhibitions of COX-2 accounts the therapeutic effects of NSAIDs. Selective COX-2 inhibition was also observed with peptides *N*-conjugated to other NSAID drugs, such as: ibuprofen and flurbiprofen. [25]

Yang *et al.* developed a hydrogel made of a small peptide with β-amino acids which displayed a 3D-fibrillar morphology and proteolytic stability to be applied in drug delivery. [51]

The self-assembly of a conformationally restricted dipeptide, H-Leu-ΔPhe-OH, containing an α,β-dehydrophenylalanine residue into a highly stable and mechanically strong hydrogel was described by Thota and co-workers [52]. The gel was able to entrap hydrophobic and hydrophilic drugs and released them in a controlled manner being an attractive candidate for the development of a drug delivery platform (Figure 10).

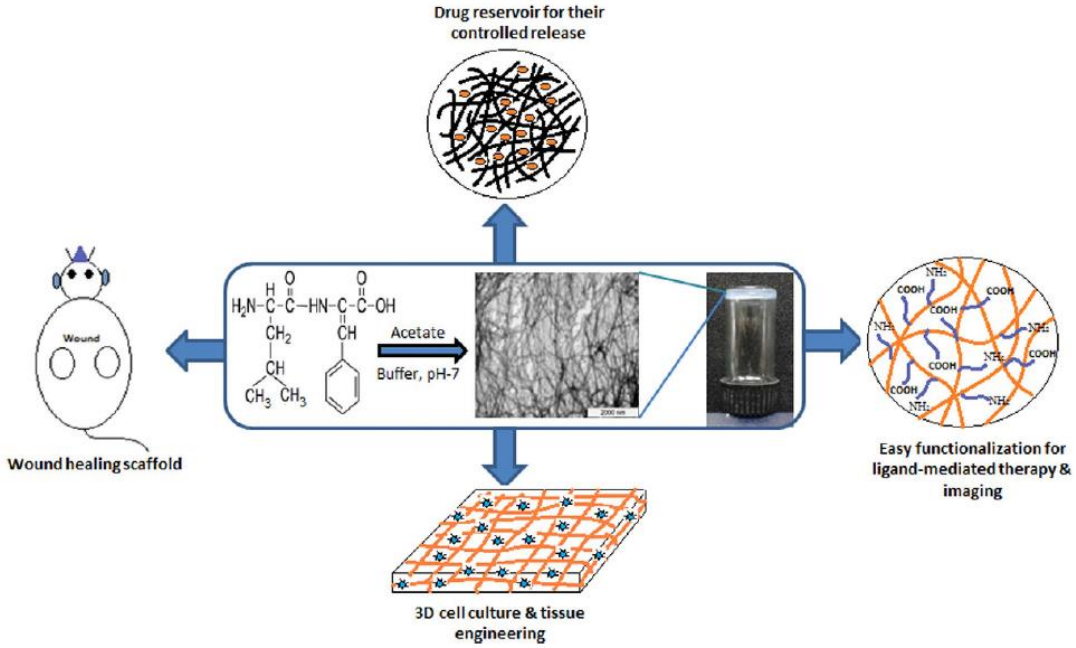

Figure 10: Instant self-assembly of Leu-ΔPhe into a highly stable hydrogel at room temperature and its possible applications in biomedical field. [52]

In our research group, new dehydropeptides capable of forming hydrogels are being developed (Figure 11). [25, 53-55] The presence of the dehydroamino acid residue impart increased proteolytic resistance to the hydrogels and impose conformational constraints in the peptide backbone.

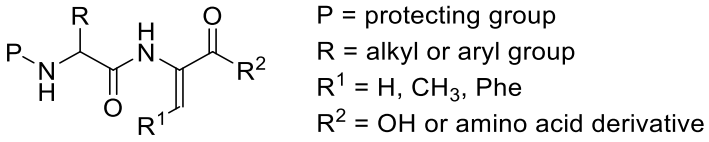

Figure 11: Structure of dehydropeptide hydrogelators developed in our research group.

Several dehydrodipeptides *N*-capped with the naproxen (Npx) were prepared and tested as hydrogelators (Figure 12). Some of these compounds gave hydrogels with critical gelation concentrations (cgc) between 0.4 and 0.6 wt% and a gelation pH of 5 and 8. The use of these materials as controlled drug delivery systems was also tested using model molecules such as curcumin. [22, 25]

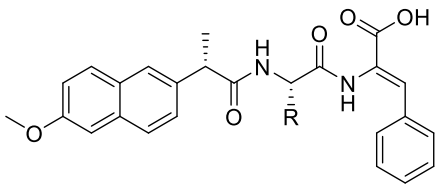

R = Amino side-chain.

Figure 12: Structure of the dehydrodipeptides *N*-protected with naproxen.

The hydrogels based on the dehydrodipeptides tyrosyldehydrophenylalanine and aspartyldehydrophenylalanine *N*-capped with naproxen (Npx-L-Tyr-*Z*ΔPhe-OH and Npx-L-Asp-*Z*ΔPhe-OH) were endowed with magnetic properties by incorporating of superparamagnetic iron oxide nanoparticles (SPION) (Figure 13). The resulting magnetic hydrogels displayed concentration-dependent T2-MRI contrast enhancement and upon magnetic excitation (alternating magnetic field –AMF–) the SPION were able to generate a significant amount of heat. These composites have potential to be used as new theranostic platforms. [55]

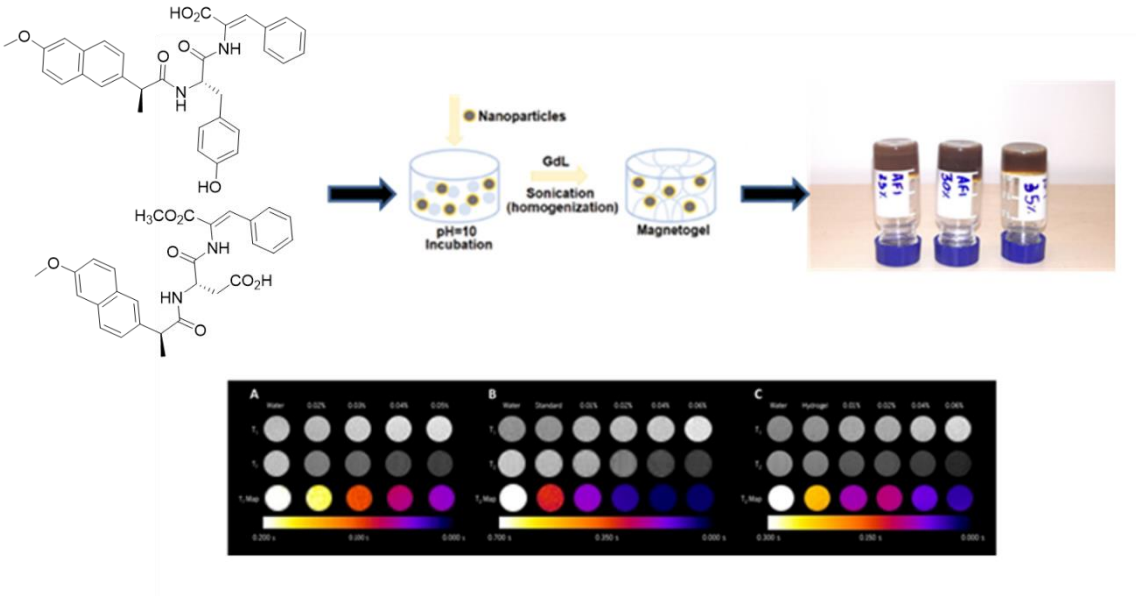

Figure 13: Naproxen-Tyr-ΔPhe-OH and Naproxen-Asp-ΔPhe-OH (0.8 wt%) with 25%, 30% and 35% of SPIONs and T1w- and T2w -MRI phantom images and T2 relaxation maps (25 °C, 3 T): A) SPION in water B) SPION incorporated into Tyr hydrogel (0.8 wt %); C) SPION incorporate into Asp hydrogel (0.8 wt%). The T2-MRI relaxation map was acquired using the MEMS (multi-echo-multi-spin) sequence.

More recently, *N*-protected dehydrodipeptides with carboxybenzyl (Cbz) group were developed and the physico-chemical properties of the resulting hydrogels were investigated. The hydrogels were also tested with promising results as nanocarriers for the natural compound curcumin and the antitumor drug doxorubicin. [56]

1.4 Hydrogels based on peptide bolaamphiphiles

Bolaamphiphiles (BAs) comprise two functional hydrophilic head groups connect by a hydrophobic core (Figure 14).

Figure 14: Scheme of a bolaamphiphile molecule.

BAs can be divided in two main categories: symmetric with the same polar head groups at both ends and asymmetric having different polar head groups at both ends. This type of molecules is capable of self-assembling to give several types of nanostructures. [57] A large variety of BAs with diverse structures based on lipids, peptides and carbohydrates has been reported in literature. [58-61] BAs are attractive building blocks to give hydrogels as their amphiphilicity promotes intermolecular interactions (hydrogen bonding, π-π interactions, aromatic interactions, and hydrophobic effects). Figure 15 show the structure of peptide bolaamphiphiles used as hydrogelators. [62]

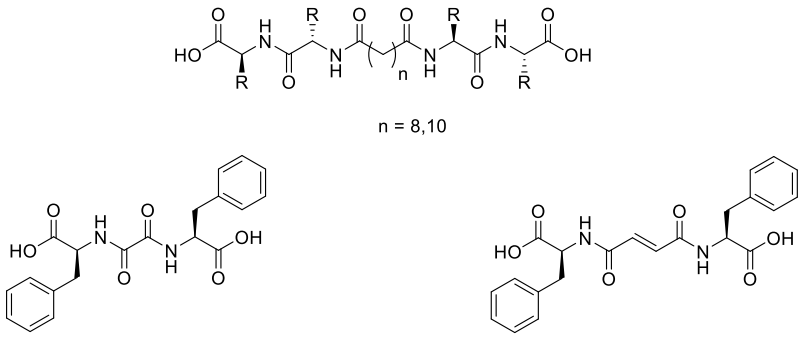

Figure 15: Structures of bolaamphiphiles used as hydrogelators. (adapted from ref. 62). [62]

Feng *et al.* [63] developed two new bolaamphiphiles based on phenylalanine and terephthalic acid (Figure 16a and 16b). These compounds originate hydrogels with a cgc of 0.25 wt% and were capable of controllable adsorption of 97–99% of certain organic dyes (methylene blue and methyl violet 2B) within two minutes.

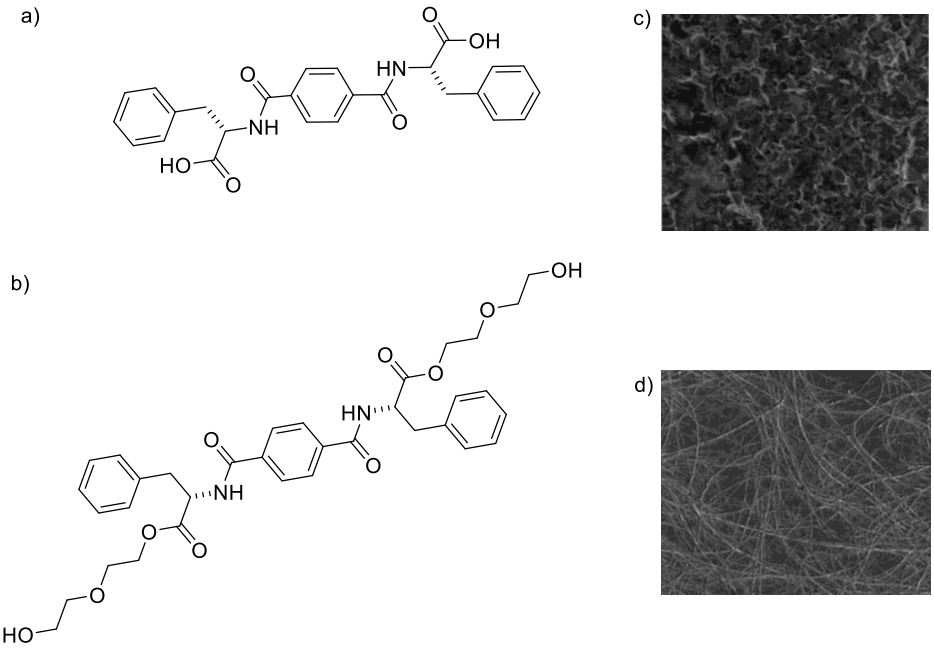

Figure 16: a) and b) Structures of the bolaamphiphiles based on phenylalanine and terephthalic acid. c) and d) SEM image of the hydrogels of a) and b). (adapted from ref. 63) [63]

Das and co-workers developed peptide symmetrical bolaamphiphiles based on dipeptides and succinic acid. These compounds were activated to self-assemble by reaction with 4-hydroxy benzylalchool catalysed by lipase (Figure 17). [64]

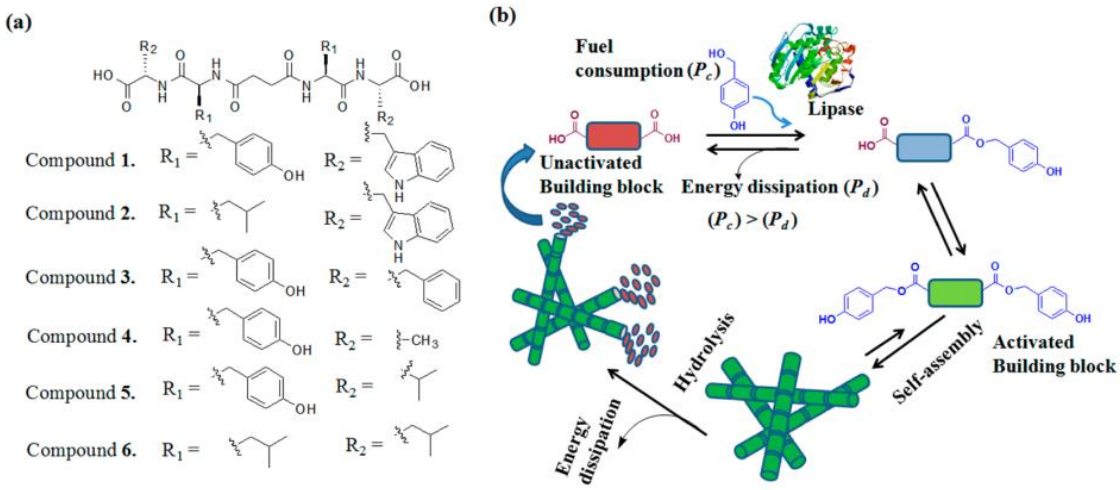

Figure 17: (a) Structures of peptide bolaamphiphiles (1–6). (b) Dissipative reaction cycle of the system. (from reference [64])

Unactivated peptide bolaamphiphile 1 (Figure 17) incorporates energy in the form of *p*-hydroxy benzylalcohol to give the monoester and then diester. The diester self-assembles into nanofibers and forms hydrogel. The subsequent hydrolysis leads to dissipate the energy of the diester which results in the collapse of the hydrogel. The rate of enzymatic energy dissipation (Pd) (ester hydrolysis) is lower than the consumption of the energy (Pc) to allow the formation of self-assembled architecture. [64]

Recently, Yan and co-workers described a symmetric BA based on a phenylalanylphenylalanine and *bis*(10-carboxydecyle)disulphide as an efficient hydrogelator. The resulting injectable hydrogel was studied as a drug-carrier with the prodrug 5-aminolevulinic acid hydrochloride that, upon release from the hydrogel, biosynthetically initiate the production of an active photodynamic therapeutic agent (Figure 18). [65]

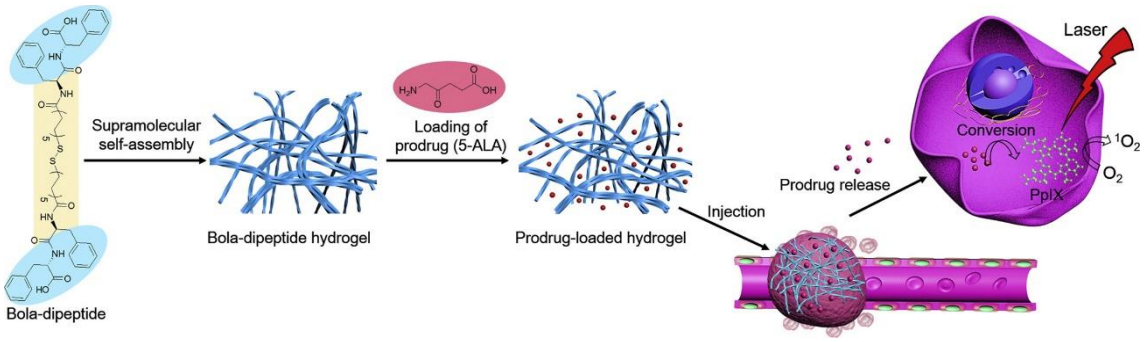

Figure 18: Schematic illustration of bola-dipeptide-based injectable hydrogels for localized and sustained prodrug (5-aminolevulinic acid hydrochloride, 5-ALA) delivery and in situ prodrug-to-drug (protoporphyrin IX, PpIX) conversion toward enhanced photodynamic a antitumor therapy. (from reference [65])

1.5 LMW peptide hydrogels as drug delivery systems

One of the advantages of using self-assembled peptides as therapeutic materials include the possibility to generate modular platforms toward patient- or disease-specific therapies. Another benefit of these materials is their ability to rapidly respond to stimuli through dynamic and reversible changes in their properties. Moreover, the building blocks are ease to prepare and in most cases are low cost compounds. Accordingly, small peptides that self-assemble afford a variety of useful properties for the design of drug delivery systems. [66-69]

Conventional drug delivery strategies can be restricted by rapid metabolism, the need for repeated dosing, undesirable drug absorption and easy degradation under physiological conditions. The hydrogel network formed by amphiphilic peptides is an obvious choice for use as a delivery vehicle for drugs, due to their biocompatibility, bioavailability, non-cytotoxic nature and responsiveness to enzymatic, hydrolytic or environmental stimuli. Both hydrophilic and hydrophobic drugs can be encapsulated into polymer nanostructures depending on their characteristics and can be released in a controlled way at the targeted sites. Peptide-based hydrogels as drug nanocarriers can improve the pharmacokinetic parameters of drugs *in vivo*; increase the drug curative effects; reduce the drug toxicity and thus decrease the side effects through drug encapsulation and targeted delivery. [66, 70, 71]

Xu *et al.* showed the controlled release of a pamidronate using a hydrogel formed from a mixture of two Fmoc-based amino acid derivatives (Fmoc-L-Leu-OH and Fmoc-L-Lys-OH). This system has also proven to be effective in the recovery of uranium-infected skin. [72]

Chauhan *et al.* reported the entrapment and controlled release of a number of drugs, both hydrophilic and hydrophobic, from two dipeptides hydrogels (H-L-Phe-*Z*-ΔPhe-OH and H-L-Leu-*Z*-ΔPhe-OH), which have been shown to be pH sensitive. One example is the anticancer drug, mitoxantrone, entrapped with H-L-Leu-*Z*-ΔPhe, which resulted in significant regression of tumours, when injected into tumour-bearing mice. [52]

Dipeptides conjugated to several non-steroidal anti-inflammatory drugs (NSAID), such as naproxen, flurbiprofen, ibuprofen and aspirin (Figure 19) self-assemble to give multifunctional hydrogels. [73]

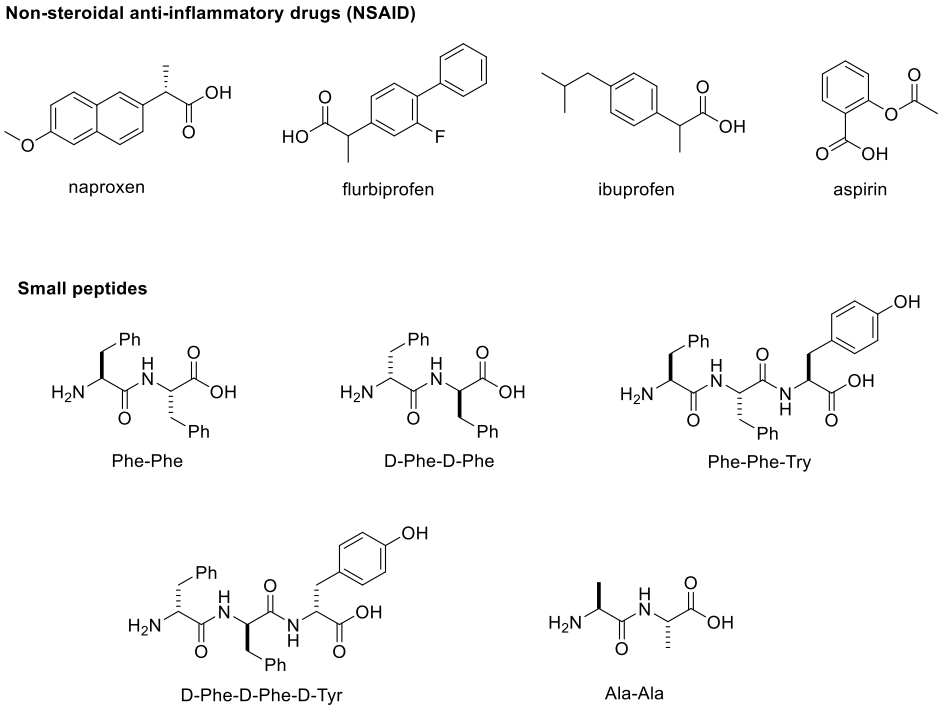

Figure 19: The structures of the NSAIDs and peptides explored as the building blocks of hydrogelators in the work of Xu and co-workers. [73]

The latter approach contributes to the development of bioactive molecules that have dual or multiple roles, in this case combining hydrogelation properties with therapeutic activity. [74]

Chapter 2

Results and discussion

2 Results and discussion

Dehydroamino acids are known to impart proteolytic resistance to peptides and also to impose conformational constraints. In our research group we developed an easy and efficient method for the synthesis of these compounds. The dehydroamino acid derivatives were then used to prepare a library of non-proteinogenic amino acids using several types of reactions including Michael additions, substitution reactions, cyclizations and palladium catalysed cross-couplings. [75] Furthermore, it was found that small peptides with dehydroamino acid residues and *N*-capped with aromatic groups were able to self-assemble to give hydrogels. [22, 25, 53-56, 75] Thus, recently the research efforts have been focussed on the design, synthesis and characterization of new self-assembly dehydroamino acid derivatives for biomedical applications. The work described in this thesis is part of the research carried out in this area by our group.

Taking into consideration all the work already done in the area of dehydroamino acid derivatives self-assembly, it was decided to conjugate dehydroamino acids with aromatic systems to obtain new symmetrical bolaamphiphiles (BAs) and study their properties as building blocks for supramolecular hydrogels. Hence two dipeptides with a dehydrophenylalanine residue were coupled with two aromatic moieties namely terephthalic acid and 2,6-naphthalene dicarboxylic acid (Figure 20). The two carboxylic acid functions constitute the hydrophilic heads of the BAs linked by a hydrophobic system made of an aromatic moiety together with the dipeptide chain. The symmetry and low molecular weight of the new BAs are important synthetic features, simplifying procedures by reducing the number of synthetic steps and therefore allowing faster, greener and more atom efficient preparations. [18]

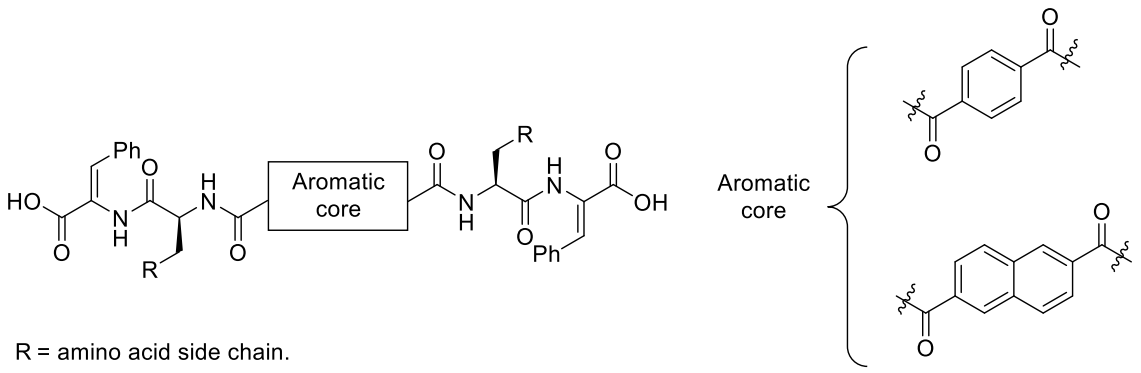

Symmetric dehydrodipeptide bolaamphiphiles

Figure 20: Structure of bolaamphiphiles prepared in this work.

The structures of the BAs **1-4** developed in this work are shown in Figure 21.

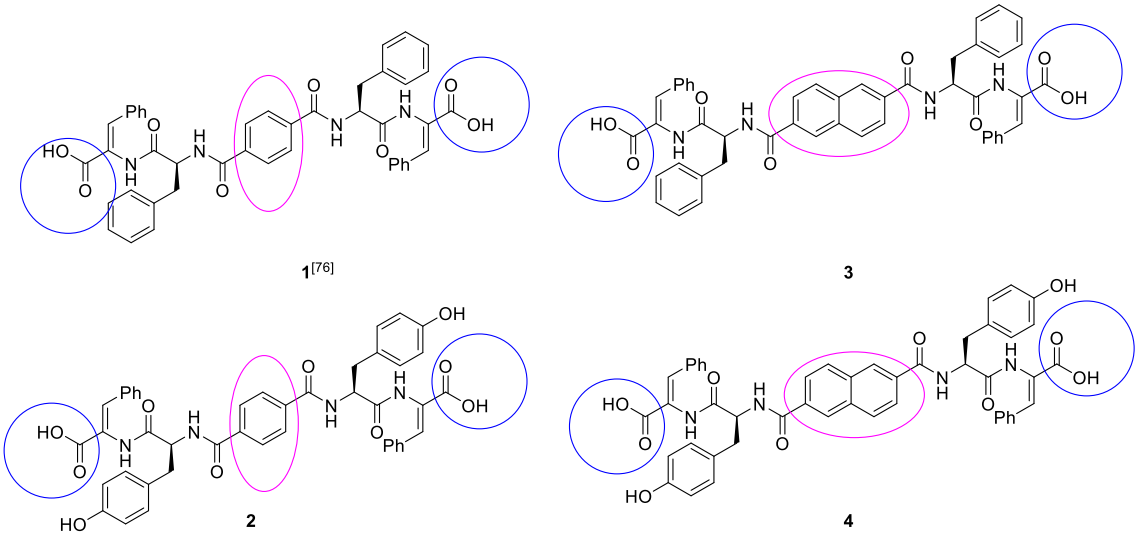

Figure 21: Chemical structures of the symmetrical BAs based on dehydrodipeptides and aromatic systems prepared.

The first step in the retrosynthetic analysis of the target molecules **1-4** (Scheme 3) is a functional group interconversion (FGI) of carboxylic acids to esters to give the methyl esters **5-8**. Two disconnections of the aromatic core gave the two dehydrodipeptides **11a** and **11b**. At this stage, two possible synthons for the carbonyl component were considered: the acid chloride, **9** and the carboxylic acid, **10**. The *N*-deprotected dehydrodipeptides can undergo a FGI to give the corresponding dehydrodipeptides protected at the *N*-terminus with a *tert*-butoxycarbonyl (Boc) group (**12a, 12b**). Another FGI converts a dehydroamino acid residue into a β-hydroxyamino acid residue, providing dipeptides **13a** and **13b**. Finally, there is a disconnection of the peptide bond to obtain the methyl ester of D,L-β-hydroxyphenylalanine, **14** and the *N*-Boc amino acid (**15a** and **15b**).

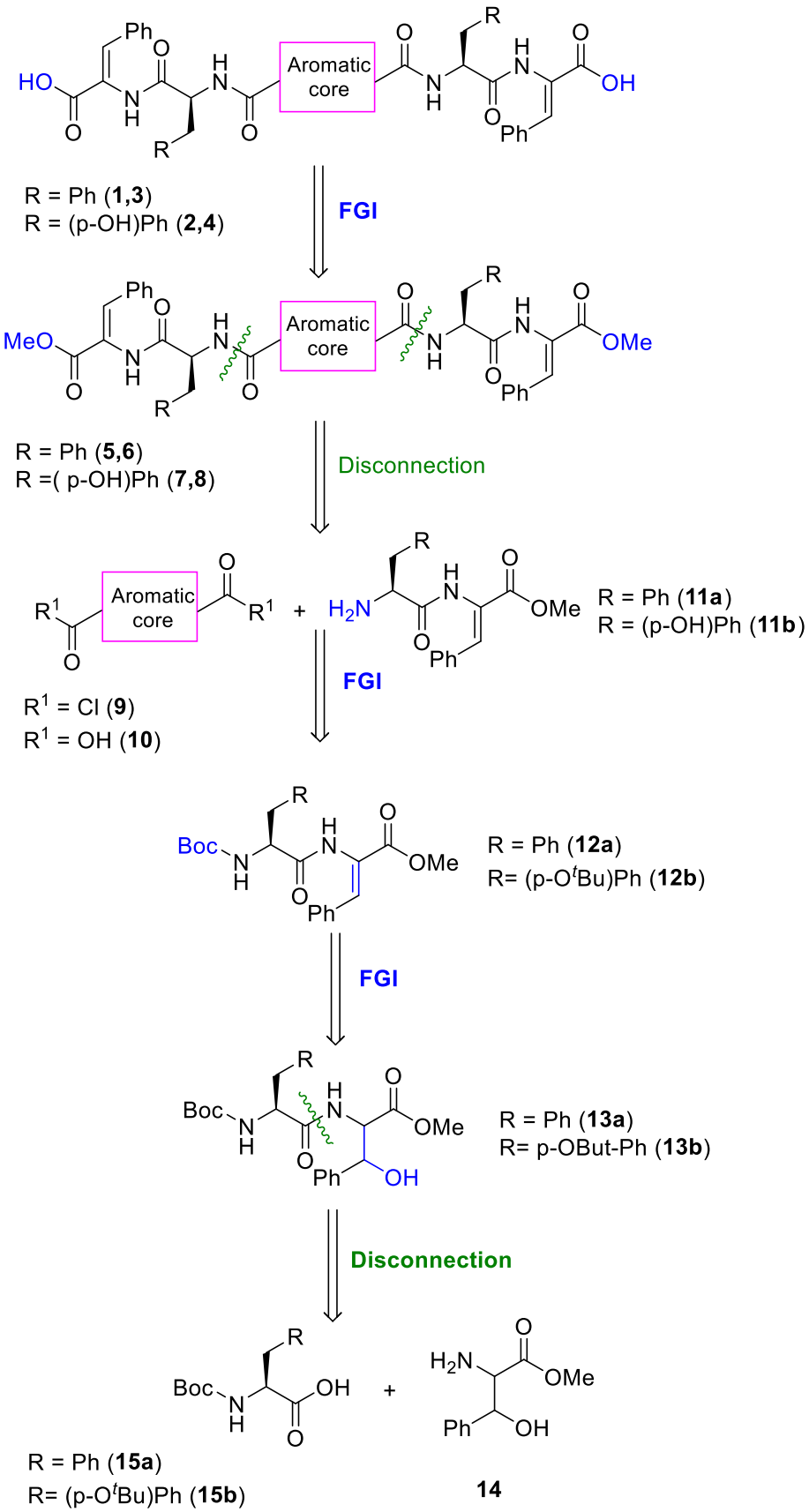

Scheme 3: Retrosynthetic analysis of BAs (**1**-**4**).

The key step in the synthetic route involves the coupling reaction between the dehydrodipeptides and the central aromatic moiety, followed by an ester hydrolysis to give the final bola-dehydrodipeptides derivatives.

2.1 Synthesis of *N*-deprotected dehydrodipeptides

N-deprotected dehydrodipeptides **11a** and **11b** were prepared using a conventional stepwise solution protocol developed within our research group (Scheme 4). [77]

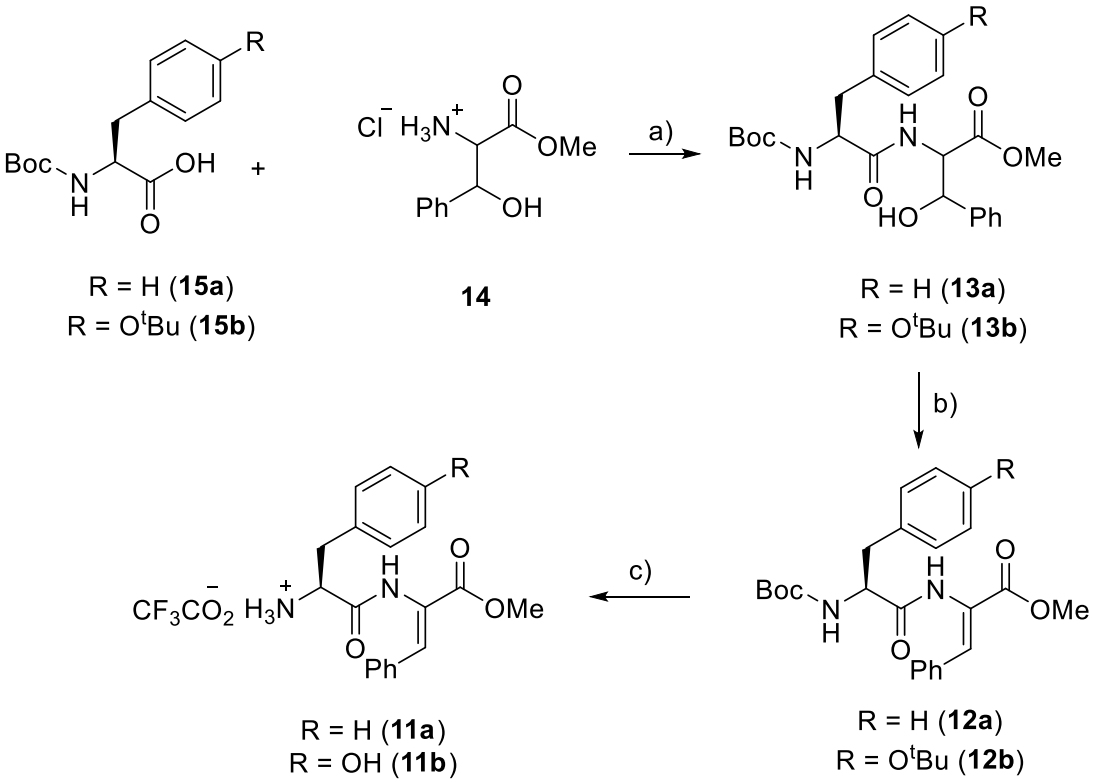

Scheme 4: Synthesis of the *N*-deprotected dehydrodipeptides **11a** and **11b**. **a)** MeCN, Et_3N, HBTU; **b)** 1. Boc_2O, DMAP, dry MeCN, 2. TMG; **c)** TFA, rt

The coupling of *N*-*tert*-butoxycarbonyphenylalanine (Boc-L-Phe-OH, **15a**) with the methyl ester of D,L-β-hydroxyphenylalanine (HCl.H-D,L-Phe(β-OH)-OMe, **14**) afforded dipeptide **13a** as a diastereomeric mixture, in excellent yield, using a standard 2-(1*H*-benzotriazole-1-yl)-1,1,3,3-tetramethylaminium hexafluorophosphate (HBTU) procedure. The mechanism of the coupling reaction with HBTU involves the deprotonation of the amino acid carboxylic acid, followed by attack on the imine carbon atom of HBTU, producing an *O*-acyl urea derivative and the anion of 1-hydroxybenzotriazole. The latter reacts with the *O*-acyl urea to give the tetramethylurea and the activated ester. Finally, reaction of the activate ester with the amine gives the amide and 1-hydroxybenzotriazole (Scheme 5). [78]

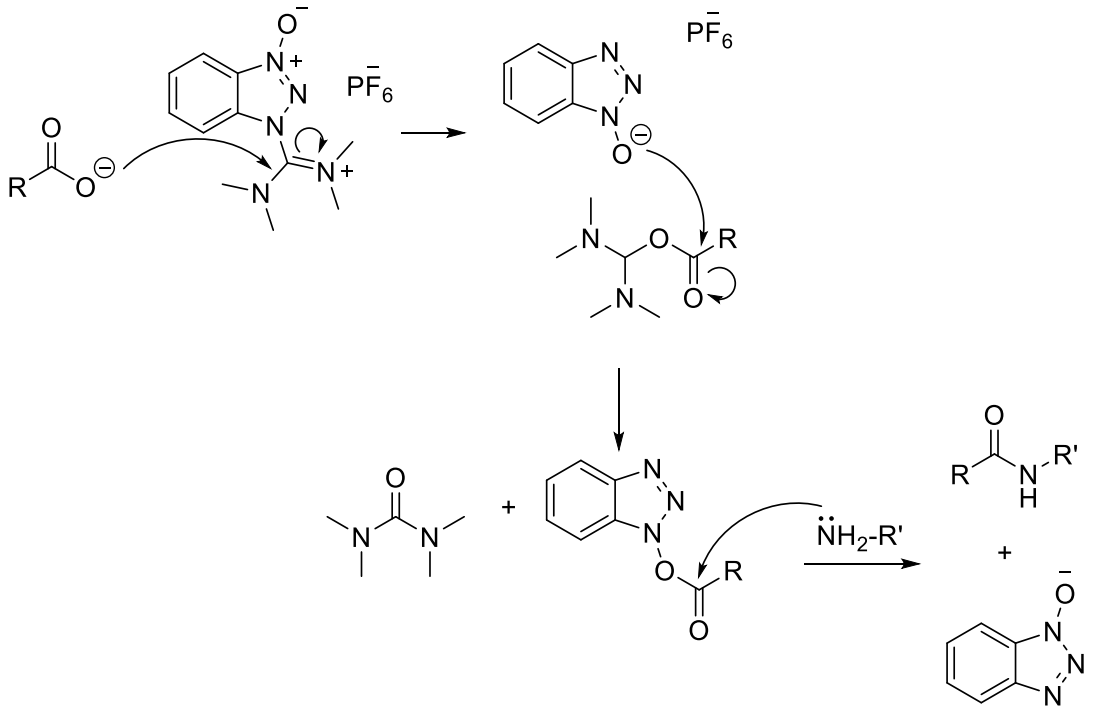

Scheme 5: Coupling mechanism using HBTU. [78]

The β-hydroxydipeptide **13a** was dehydrated by treatment with di-*tert*-butyl dicarbonate (Boc_2O) in the presence of 4-dimethylaminopyridine (DMAP), followed by *N,N,N′,N′*-tetramethylguanidine (TMG), to afford compound **12a** with 69% yield. This reaction involves the formation of a carbonate intermediate which is eliminated by treatment with base (TMG). The reaction is stereospecific towards the more thermodynamically stable *Z*-isomer (Scheme 6). [77]

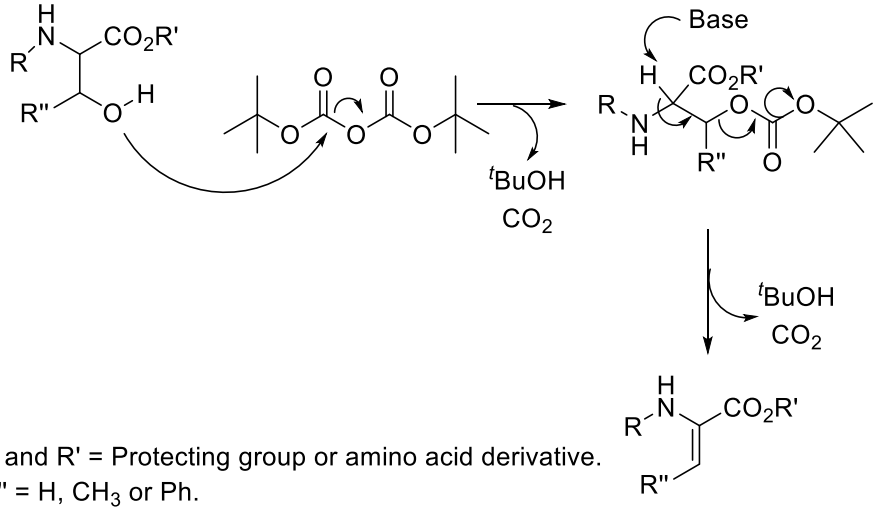

Scheme 6: Mechanism of dehydration of β-hydroxyamino acid derivatives with Boc_2O/DMAP and TMG. [77]

The stereochemistry of the dehydrodipeptides prepared in these work was confirmed by NOE difference experiments by irradiating the α-NH proton and observing an NOE effect on the β-phenyl protons of the dehydropheylalanine residue.

The *N,C*-protected dehydrodipeptide, **12a** was treated with trifluoroacetic acid (TFA) to remove the *tert*-butoxycarbonyl group affording compound **11a** as a trifluoroacetate salt in quantitative yield.

The proton ^{1}H NMR spectrum of compound **11a** in DMSO-d_6 (Figure 22) shows a three-proton singlet at 8.25 ppm which corresponds to the NH_3^+, along with the absence of a nine-proton singlet at 1.41 ppm assigned to the *tert*-butyl group.

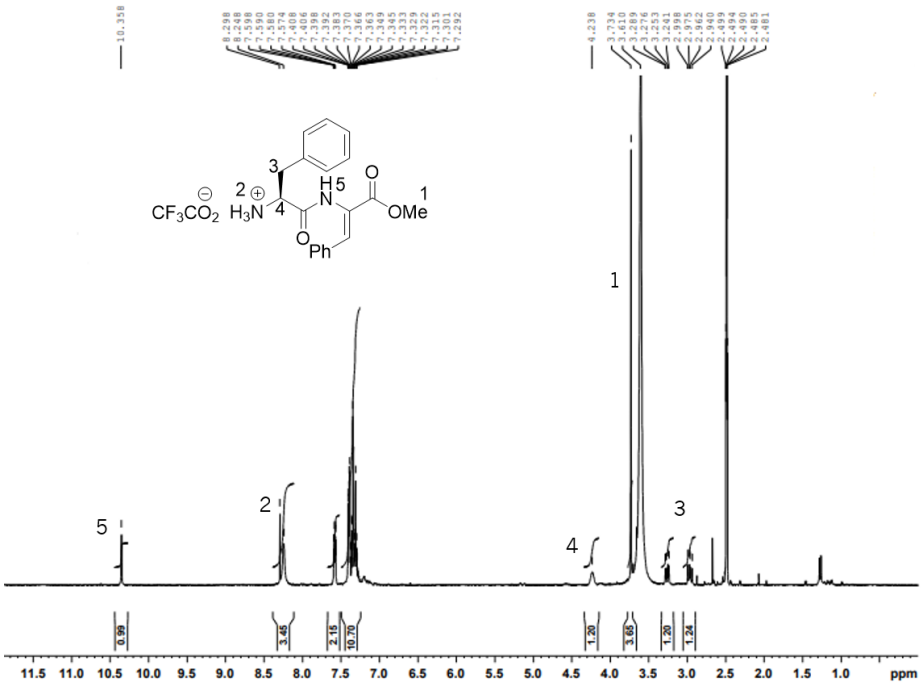

Figure 22: ^{1}H NMR spectrum of compound **11a** in DMSO-d_6.

The compound **11b** was prepared using a strategy similar to that described for compound **11a** (Scheme 4). In this case, TFA was used to remove two protecting groups simultaneously, the Boc group from the *N*-terminus and the side chain *tert*-butyl protecting group of the tyrosine residue. The proton ^{1}H NMR spectrum of compound **11b** in DMSO-d_6 (Figure 23) reveals a singlet at 8.17 ppm which corresponds to the NH_3^+, along with the absence of two singlets at 1.26 ppm and 1.31 ppm which were assigned to the *tert*-butyl groups of Boc and *tert*-butyl ether, respectively.

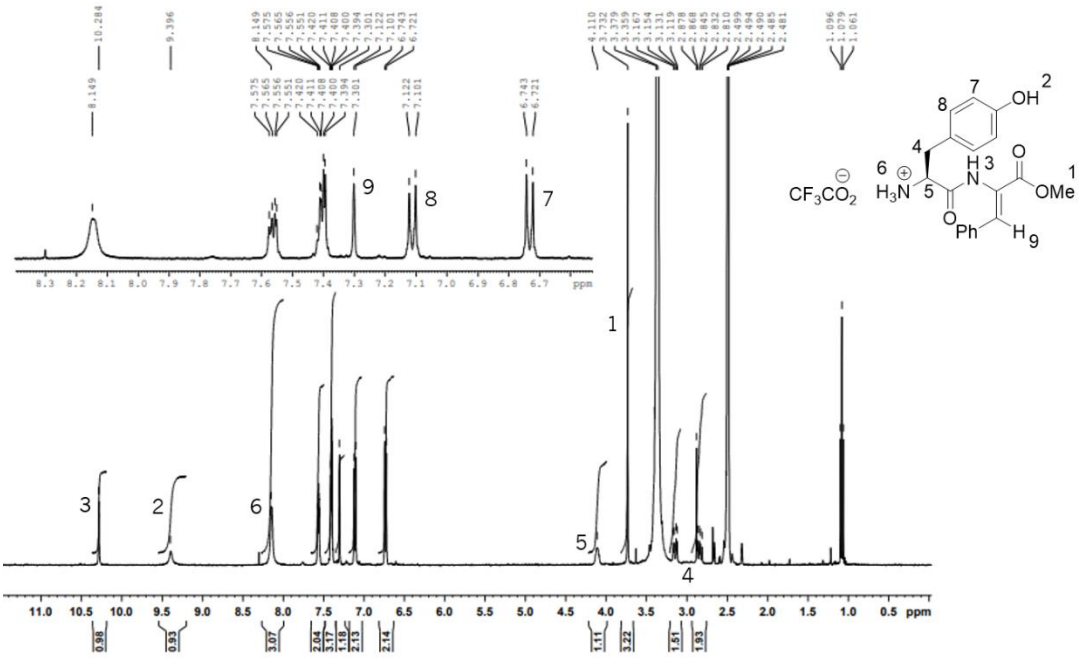

Figure 23: ^{1}H NMR spectrum of compound **11b** in DMSO-d_6.

2.2 Synthesis of symmetric bolaamphiphilic bis-dehydrodipeptides

Bolaamphiphiles **1-4** were prepared from terephthaloyl chloride (**16**) and naphthalene-2,6-dicarboxylic acid (**19**) and *N*-deprotected dehydrodipeptides **11a** and **11b**.

Compounds **1** and **2** were obtained by a double addition-elimination reaction using the terephthaloyl chloride followed by a standard methyl ester basic hydrolysis (Scheme 7). Terephthaloyl chloride, **16** was reacted with dehydrodipeptides **11a** or **11b** in the presence of triethylamine to give compounds **17** and **18** in 44% and 73% yield, respectively. These compounds were then treated with a solution of NaOH (1M) in dioxane to afford compounds **1** and **2**.

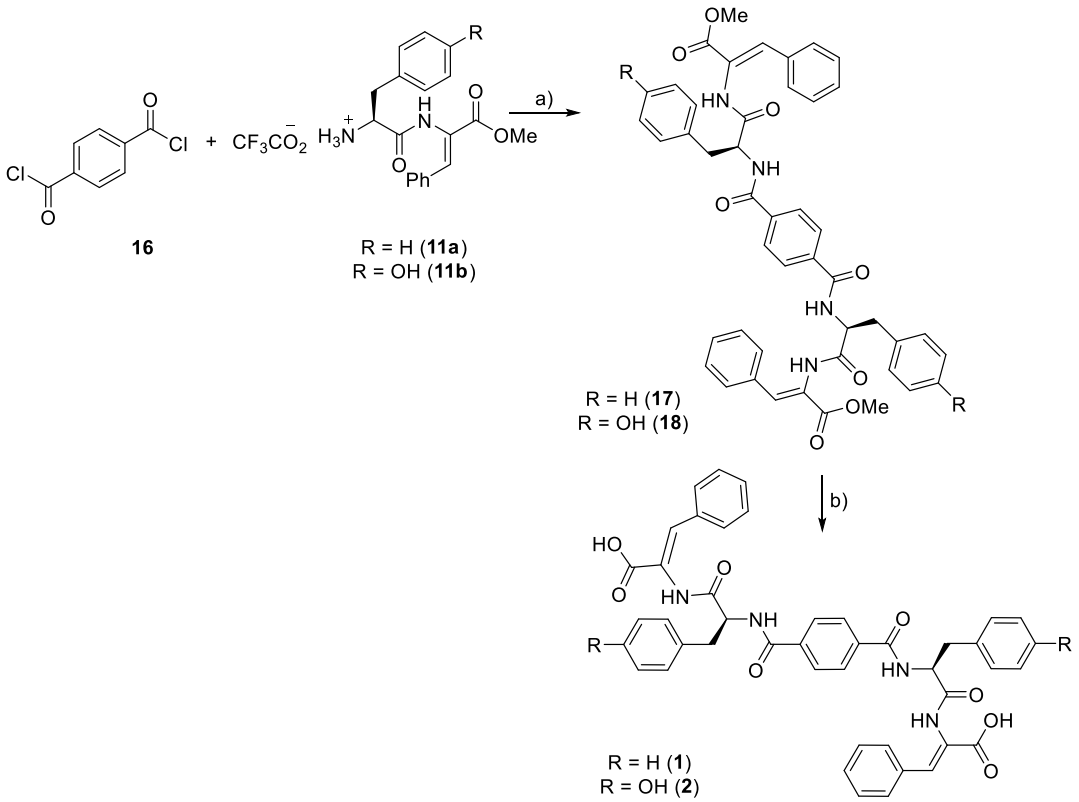

Scheme 7: Synthesis of the compound **1** and **2**. a) Et_3N, dry THF, N_2 atm, reflux, 80 °C; b) 1. NaOH, 1,4-dioxane, 2. $KHSO_4$.

Figures 24 and 25 show the proton ^1H NMR spectra of compounds **17** and **18** in DMSO-d_6. The spectrum of compound **17** (Figure 24) shows two doublets of doublets at 3.06 and 3.22 ppm, which correspond to the β-CH_2 of the phenylalanine residue, one multiplet at 4.83-4.89 ppm assigned to the α-CH of phenylalanine residue and two singlets at 3.70 ppm and 7.88 ppm that correspond to the methyl ester and to the aromatic protons of the terephthaloyl moiety, respectively. In the spectrum of compound **18** (Figure 25) it is possible to observe two singlets at 3.70 ppm and 7.90 ppm that correspond to the methyl ester and to the aromatic protons of the terephthaloyl moiety and two doublets at 6.65 ppm and 7.19 ppm, assigned to the aromatic protons of tyrosine.

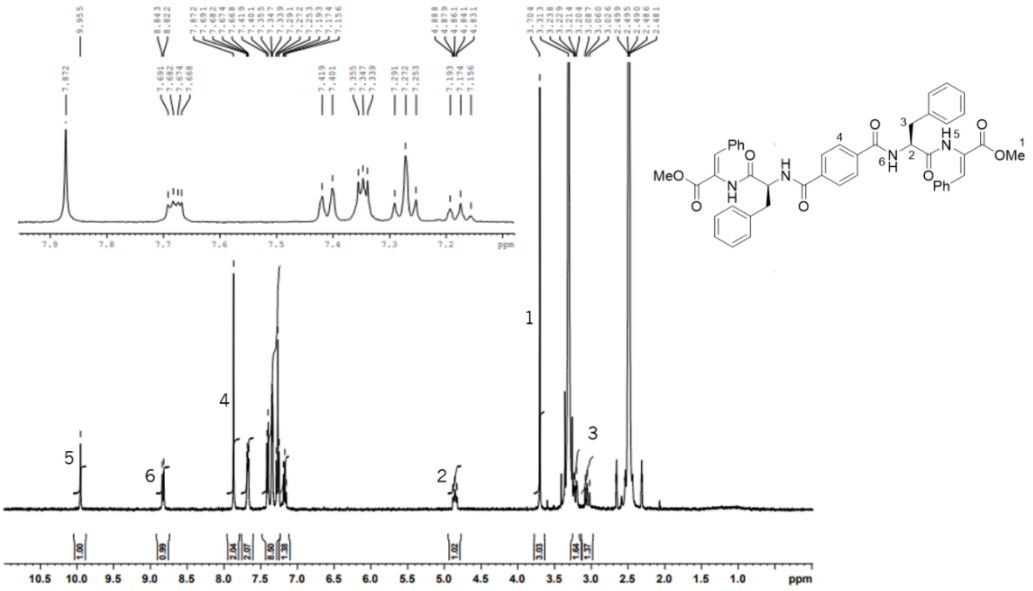

Figure 24: ^{1}H NMR spectrum of compound **17** in DMSO-d_6.

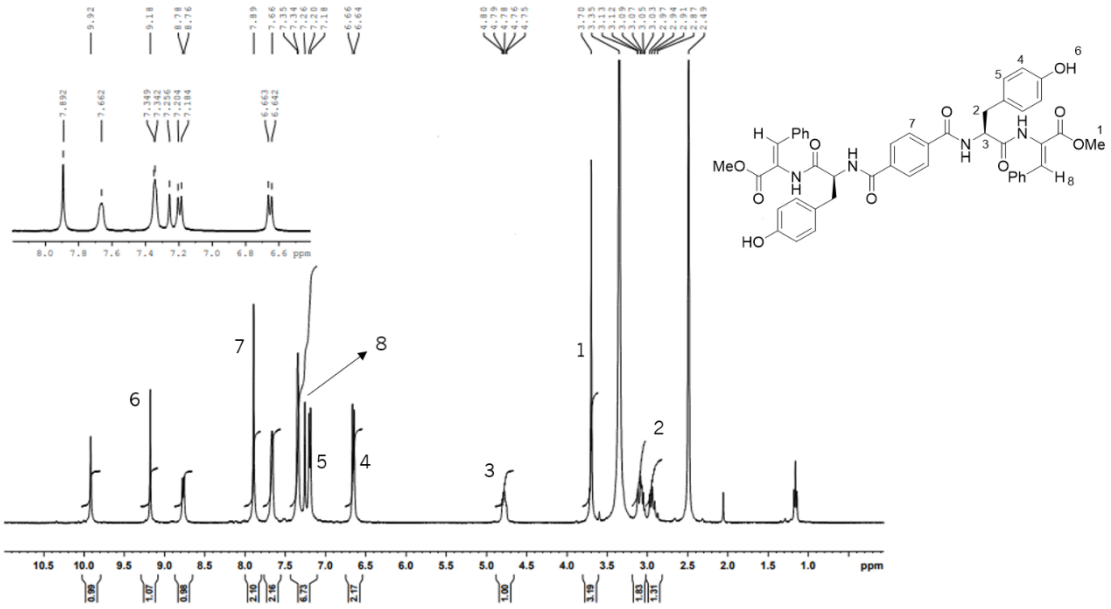

Figure 25: ^{1}H NMR spectrum of compound **18** in DMSO-d_6.

The basic hydrolysis of the methyl ester of compounds **17** and **18** gave hydrogelators **1** and **2** in 82% and 81% yield, respectively. The ^{1}H NMR spectra of compounds **1** and **2** in DMSO-d_6 (Figures 26 and 27) show broad singlets at 12.7 ppm and 12.5 ppm due to the carboxylic acid protons (COO*H*), along with the absence of the singlet at 3.70 ppm assigned to the CH_3 of the methyl esters.

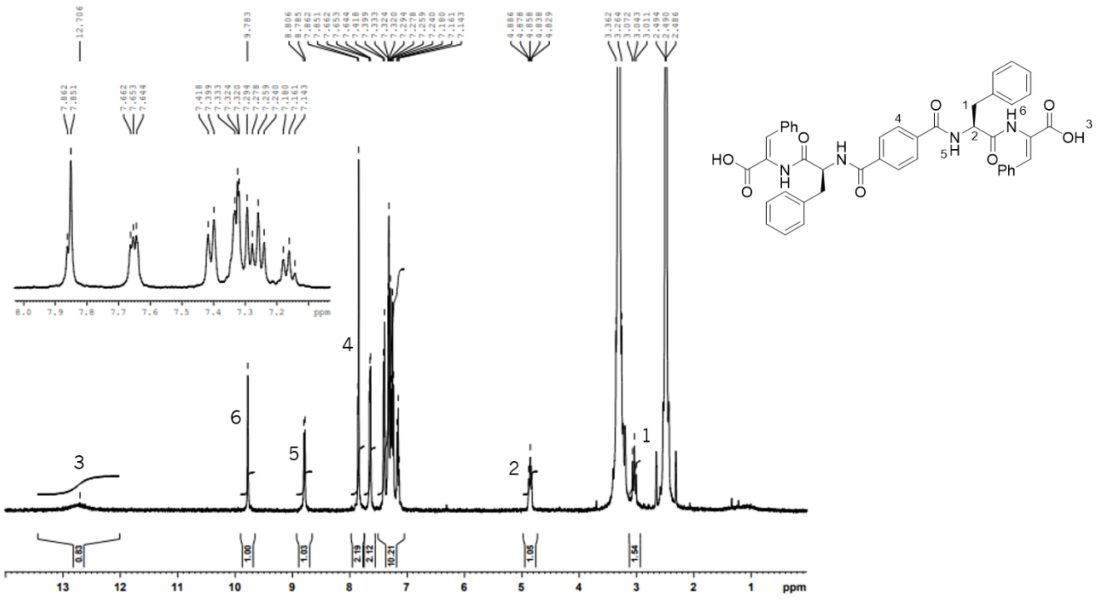

Figure 26: ^{1}H NMR spectrum of compound **1** in DMSO-d_6.

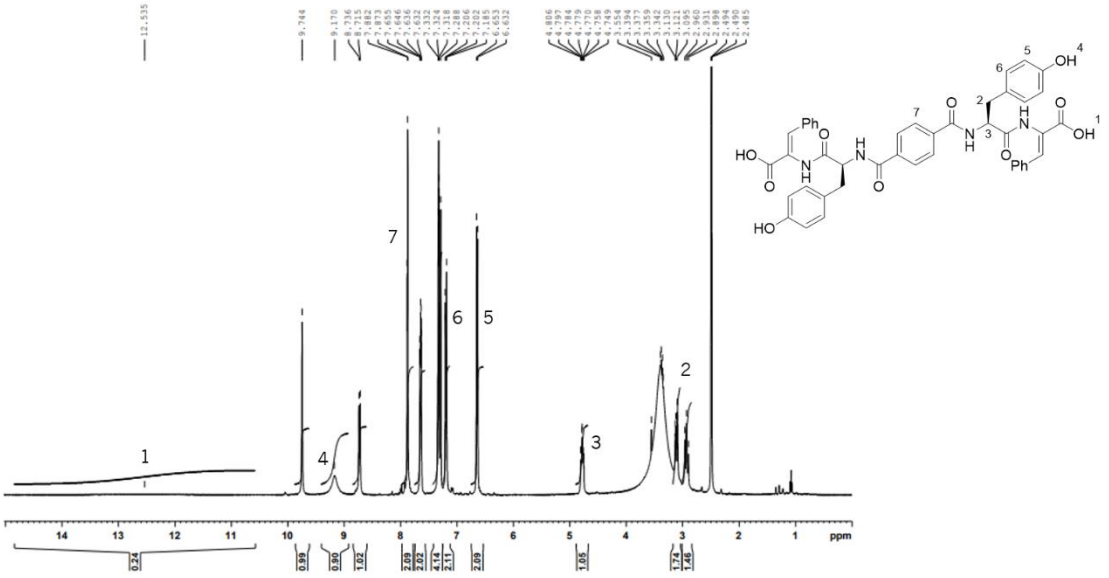

Figure 27: ^{1}H NMR spectrum of compound **2** in DMSO-d_6.

Bolaamphiphiles **3** and **4** were prepared from dehydrodipeptides **11a** and **11b** and naphthalene 2,6-dicarboxylic acid, **19** using an amide coupling protocol with HBTU, similar to that used for the synthesis of dipeptides **13a** and **13b** (Scheme 8).

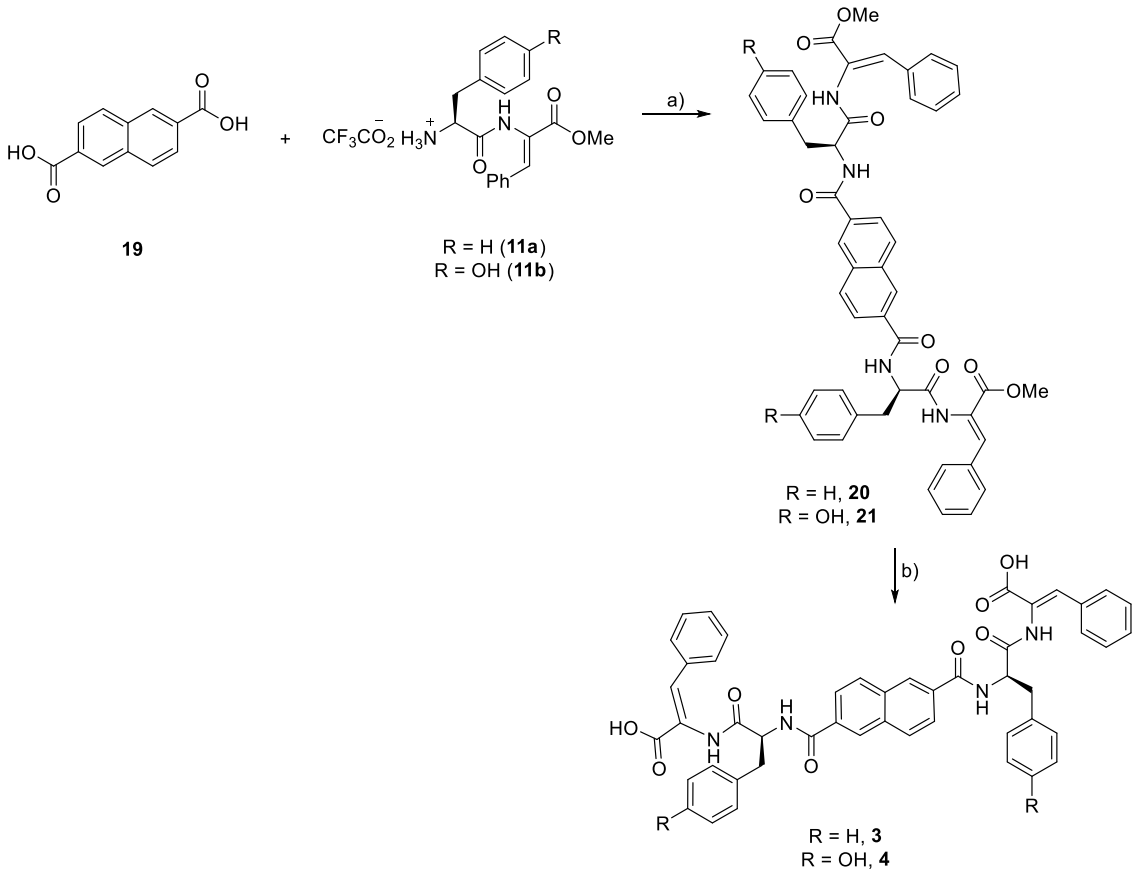

Scheme 8: Synthesis of the compound **3** and **4**. a) MeCN or DMF, Et_3N, HBTU; b) 1. NaOH, 1,4-dioxane, 2. $KHSO_4$.

The coupling of the naphthalene-2,6-dicarboxylic acid with the *N*-deprotected dehydrodipeptides **11a** and **11b** afforded compound **20** and **21** in 96% and 98% yield, respectively. The proton ^{1}H NMR spectrum of compound **20** in DMSO-d_6 (Figure 28) shows one apparent triplet and one doublet at 3.05 ppm and 3.14 ppm that correspond to the β-CH_2 of phenylalanine. The multiplet at 4.90-4.96 ppm corresponds to the α-CH of the phenylalanine residue and the two doublets and singlet observed at 7.97 ppm, 8.10 ppm and 8.50 ppm are assigned to the naphthalene protons.

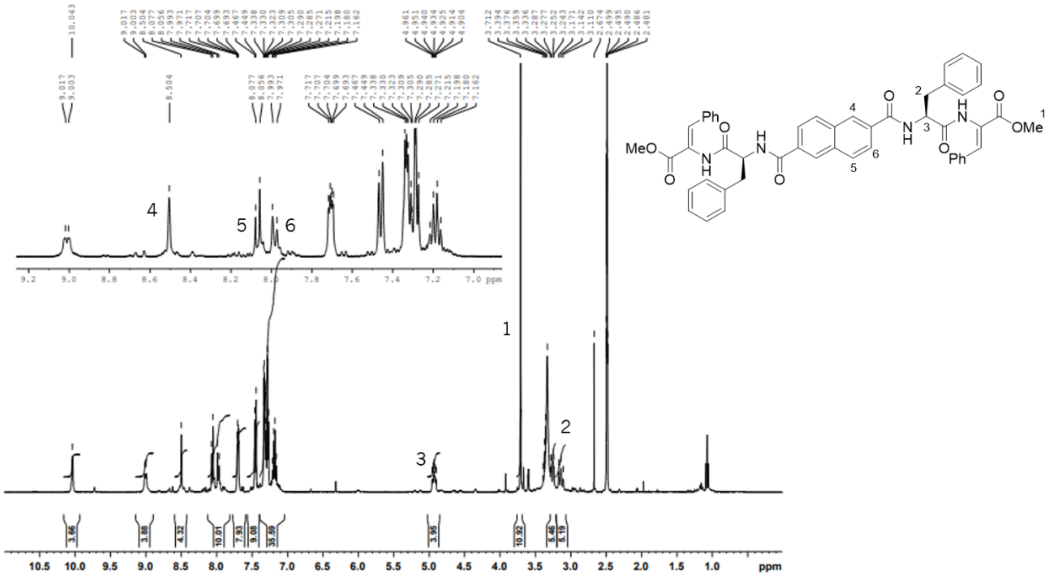

Figure 28: ^{1}H NMR spectrum of compound **20** in DMSO-d_6.

Figure 29 shows the ^{1}H NMR spectrum of compound **21** in DMSO-d_6. It is possible to observe two doublets at 8.00 ppm and 8.07 ppm and one singlet at 8.50 that correspond to the naphthalene protons, the two doublets at 6.68 ppm and 7.23 ppm were assigned to the aromatic protons of tyrosine.

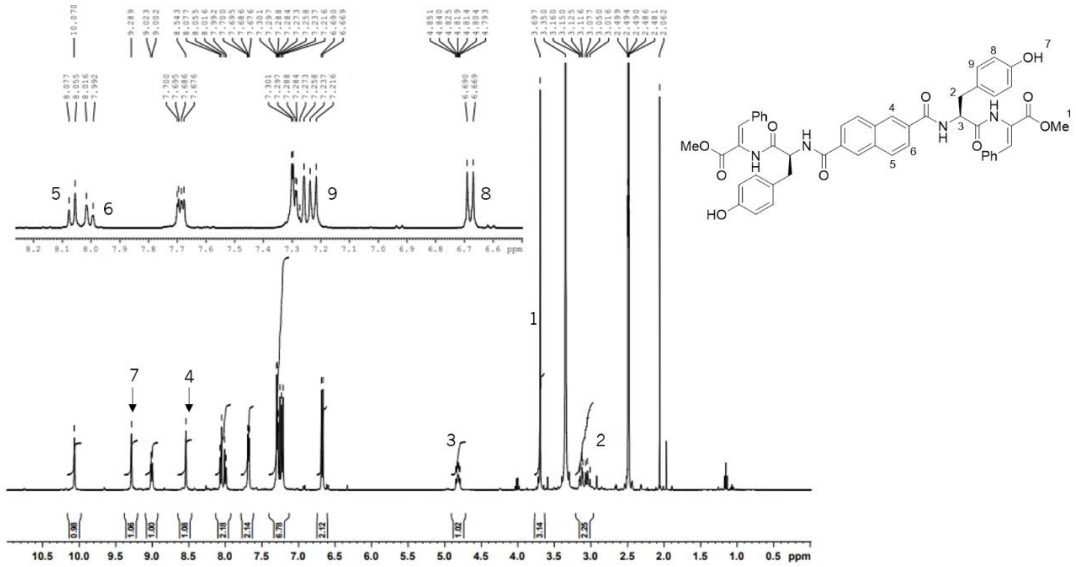

Figure 29: ^{1}H NMR spectrum of compound **21** in DMSO-d_6.

The final step in the synthesis of compounds **3** and **4** was the basic hydrolysis of the methyl esters using a solution of NaOH 1M in 1,4-dioxane. The ^{1}H NMR spectra of compound **3** and **4** in DMSO-d_6 (Figures 30 and 31) show broad singlets at 12.4 ppm and 12.3 ppm that correspond to the carboxylic acid proton (COO*H*).

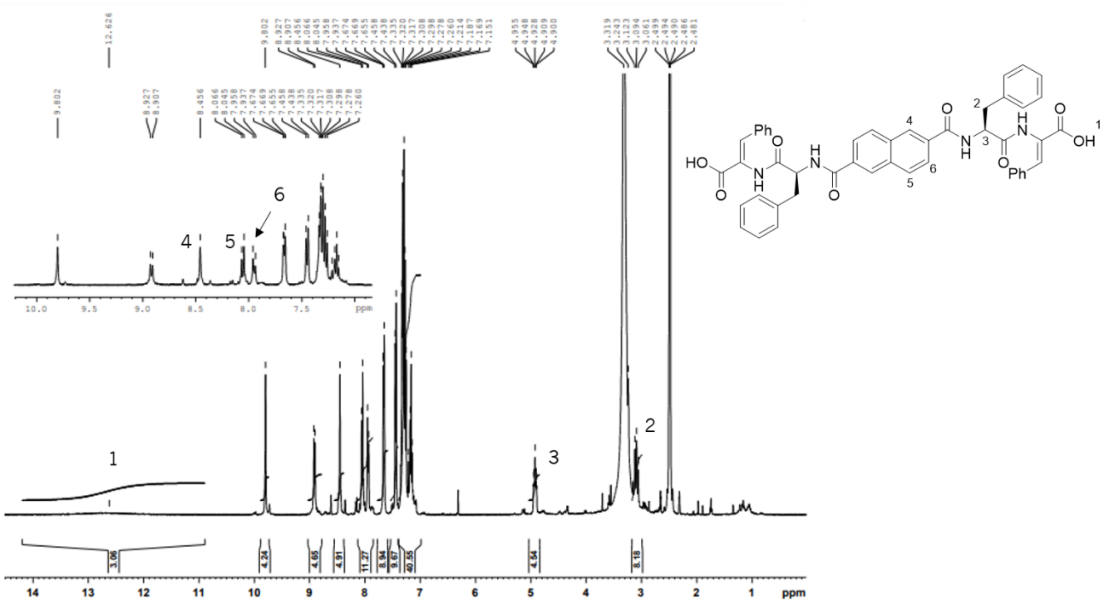

Figure 30: ^{1}H NMR spectrum of compound **3** in DMSO-d_6.

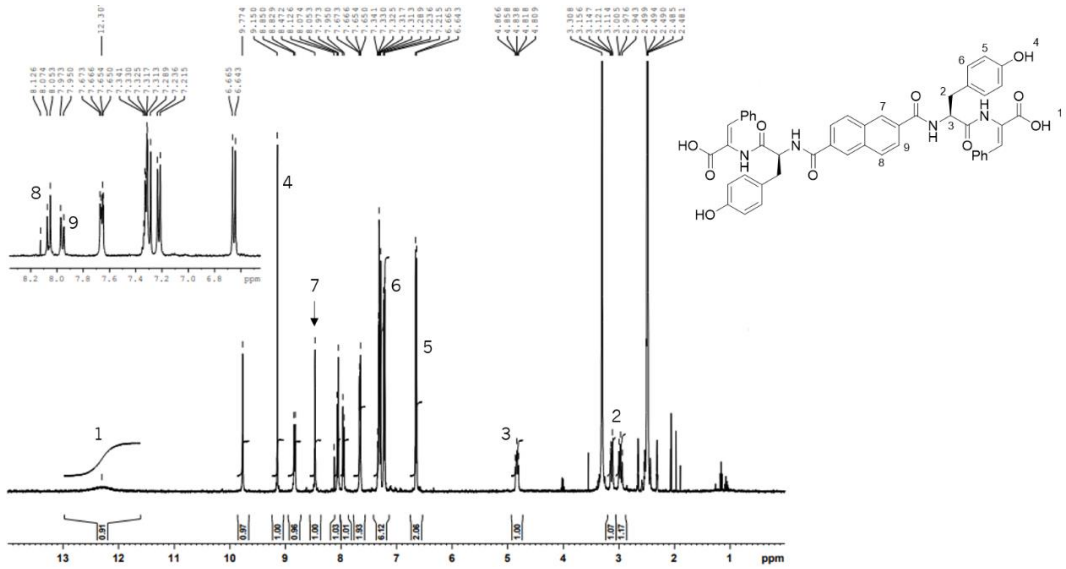

Figure 31: ^{1}H NMR spectrum of compound **4** in DMSO-d_6.

2.3 Preparation of hydrogels

The self-assembly and hydrogelation of small peptides relies on a fine balance between hydrophobicity and hydrophilicity. Dehydrodipeptides *N*-capped with aromatic groups give hydrogels using several types of triggers such as: pH, temperature or solvent exchange. [12]

Bola-dehydrodipeptides **1-4** showed limited solubility in buffer solutions in the physiological pH range (6.0-8.0). Nonetheless, these dimeric dehydropeptides could be dissolved in water upon pH adjustment to pH 10. Gel formation was triggered by a slow pH drop. The pH change was obtained by the aqueous hydrolysis of added D-glucono-δ-lactone (GdL) to D-gluconic acid. Generally, gelation using GdL is preferred over the addition of acids such as HCl, as D-gluconic acid formation is slower than diffusion leading to a more uniform change of pH. In these conditions, compounds **1-3** gave self-standing hydrogels (Figures 32 and 33). Bola-dehydrodipeptide **4** failed to give hydrogels using several gelification triggers such as pH, temperature and solvent exchange and concentrations between 0.3 wt% and 0.8 wt%. The critical gelation concentration (cgc) of compounds **1-3** was qualitatively assessed by varying the peptide concentrations and conducting a vial inversion test (Table 1).

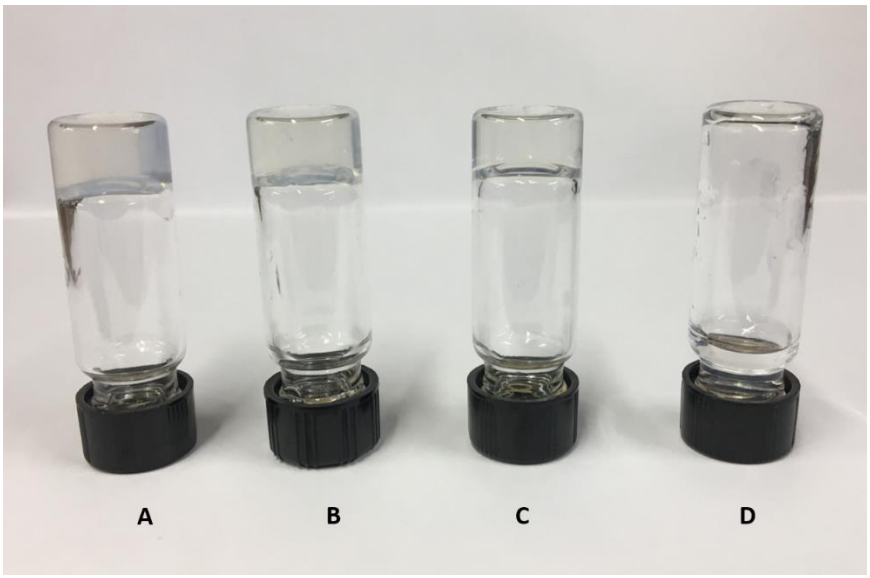

Figure 32: Optical images of hydrogelator **1** in concentrations ranging from 0.5 wt% (A) to 0.2 w% (D)

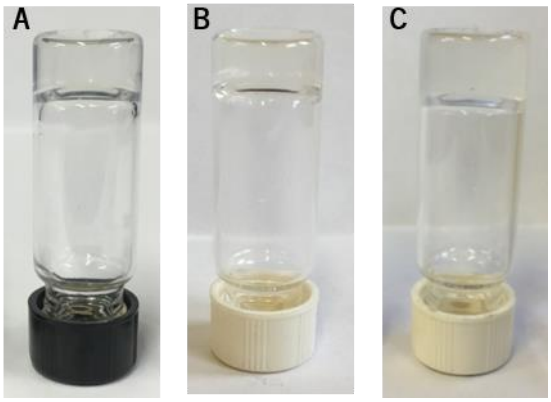

Figure 33: Optical images of hydrogels formed by hydrogelators **1** (A), **2** (B), **3** (C).

Table 1: Optimized conditions for gelation of peptide **1-4**.

Peptide	**Critical gelation concentration (cgc)**		**GDL Concentration (wt%)**	**pH**	**cLogP***
	wt%	mM			
1	0.3	4.0	0.4	5.10	5.53
2	0.4	5.1	0.4	4.15	4.57
3	0.3	3.7	0.4	5.30	6.69
4			No hydrogel		5.73

*cLogP value obtained from https//molinspiration.com

The cgcs of bolamphiphiles **1-3** are similar to those observed for the corresponding dehydrodipeptides *N*-capped with naproxen or with carboxybenzyl group although the triggers to induce gelation were in some cases different from that described for compounds **1-3**. (Figure 34). [25, 55, 56]

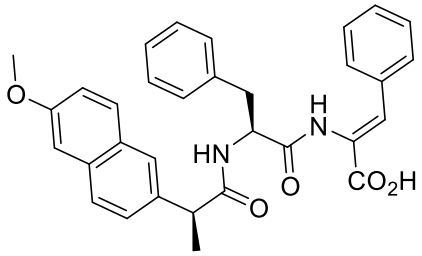

cgc 0.4 wt%, pH 8.0 [25]
cLogP 5.84

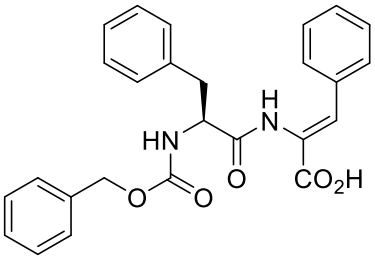

cgc 0.1 wt%, pH 7.3 [56]
cLogP 5.94

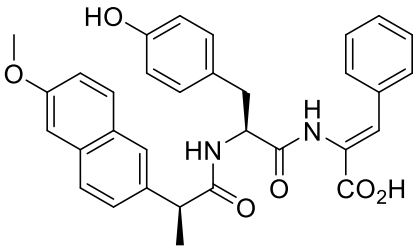

cgc 0.4 wt%, pH 6.0 [55]
cLogP 5.36

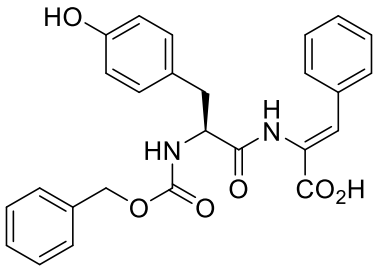

cgc 0.2 wt%, pH 6.0 [56]
cLogP 5.46

Figure 34: Critical gelation concentrations of phenylalanyldehydrophenylalanine and tyrosyldehydrophenylalanine *N*-capped with naproxen or with the carboxybenzyl group. [25, 55, 56]

A bolaamphphile based on the dipeptide phenylalanylphenylalanine and *bis*(10-carboxydecyle)disulphide (Figure 35) showed a considerably higher cgc (0.8 wt%) when compared with the cgcs of hydrogelators **1-3**. This could be due to the presence of an alkyl chain instead of an aromatic moiety linking the two dipeptides. The authors also found that by reducing the number of carbon atoms of the hydrophobic linker the bolamphiphile was unable to form hydrogels. The methodology used for obtaining the hydrogel from bola-phenylalanylphenylalanine was solvent exchange. [65]

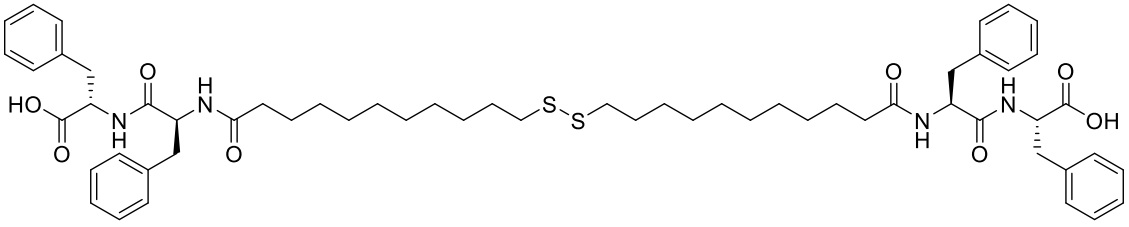

cgc 0.8 wt% (7.8 mM)
cLogP 8.14

Figure 35: Cgc of bola–phenylalanylphenylalanine. [65]

Although compounds **1-3** show low cgcs, the gelation pH values are more acidic than those reported for the *N*-protected dehydrodipeptides. [25, 55, 56] Dipeptides form gels when the carboxylic acid group is protonated and this happens bellow the pKa of the amino acid. It was found that the pKa of dipeptides contained within hierarchical structures are higher than those reported for the free dipeptide in solution. One explanation for this observation is that the acid group is incorporated into a highly hydrophobic environment. An alternative explanation consider that the higher pKa values are due to the stabilization of the carboxylic acid by a neighbouring molecule. In the case of bolaamphiphiles **1-3** the lower gelation pH may be due to the presence of two carboxylic acid functions one of which is not incorporated in a hydrophobic environment or it is not stabilized by neighbouring molecules.

According to Cameron *et al.* peptides should have an ideal hydrophobicity expressed in terms of LogP to be a hydrogelator. Peptides highly hydrophilic with LogP values below 2.8 or too hydrophobic with LogP values above 5.5 do not give stable hydrogels. The optimal LogP values for dipeptides to give hydrogels are between 3.4 and 5.5. [12, 27] The values of calculated cLogP for compounds **1-3** are between 4.6 and 6.7, only compound **2** have a calculated cLogP in the range reported as optimal for gelation. Moreover, the cLogP of the bola-FF described by Yan *et al.* is 8.14 which points to a compound too hydrophobic to give hydrogels (Figure 35). [63] It seems that for this type of compounds the observation relating dipeptide hydrogelation and LogP values cannot be applied.

2.4 STEM

The micro- and nanostructure of the supramolecular assemblies of compounds **1-4** was studied by scanning transmission electron microscopy (STEM). The STEM images show interlaced fibres that assemble into three-dimensional networks in hydrogels **1-3**. In general, the fibres appear to have several micrometres long and diameters between 15 and 50 nm (Figure 36).

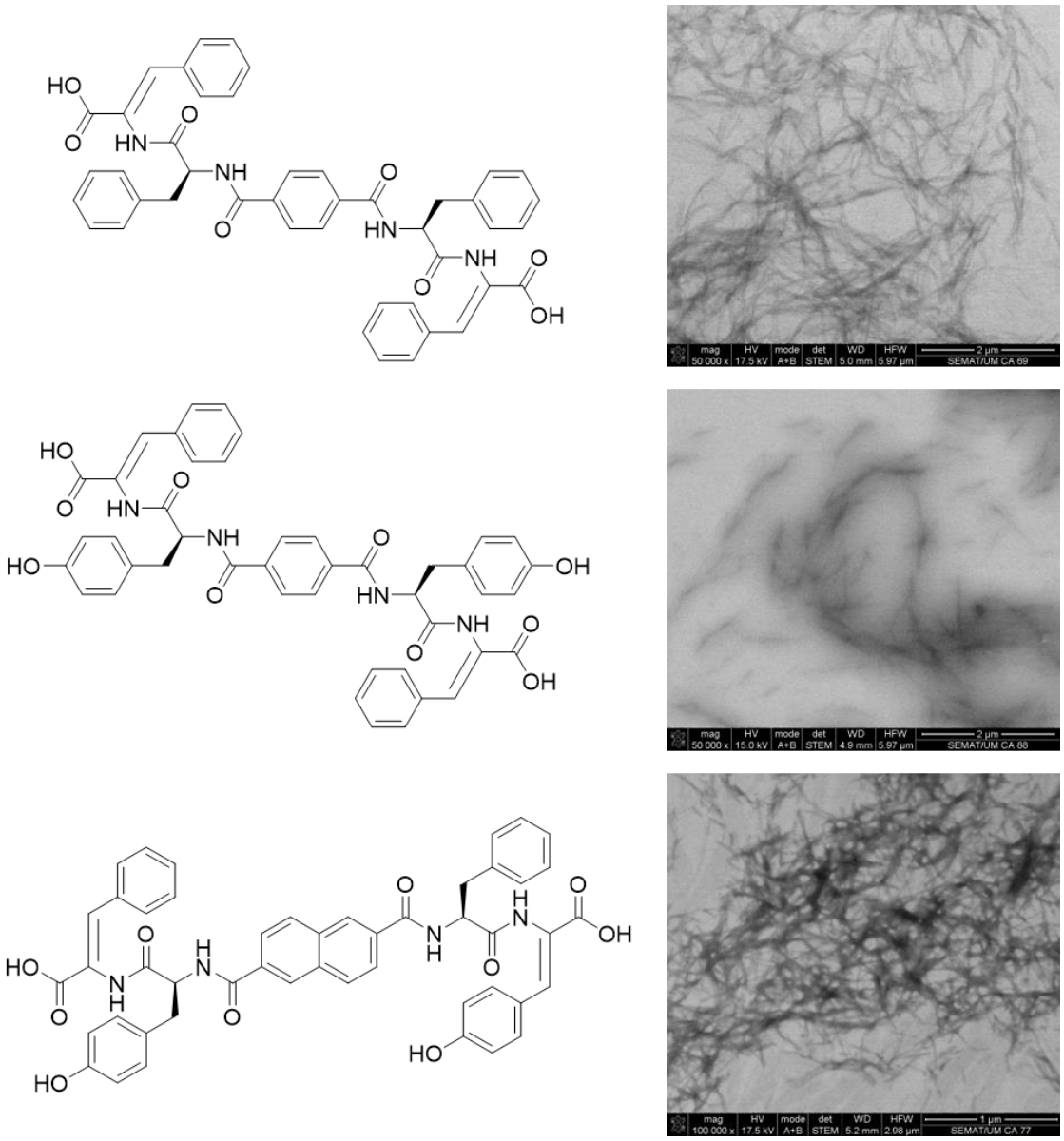

Figure 36: Scanning transmission electron microscopy (STEM) images of hydrogels **1-3** at 0.4 wt%.

The network of the hydrogel from compounds **1** and **3** with the phenylalanyldehydrophenylalanine moiety are similar. The fibers of hydrogel **2** with the tyrosine residue seem to be shorter and thicker than those observed for the other two hydrogels (Figure 36). This type of network was also observed for hydrogels of Phe-ΔPhe and Tyr-ΔPhe *N*-capped with the carboxybenzyl group (Figure 37). The average width reported for the fibres of these hydrogels was 26.1 nm however when comparing the length the dehydrodipeptides protected with Cbz have longer fibres. [56]

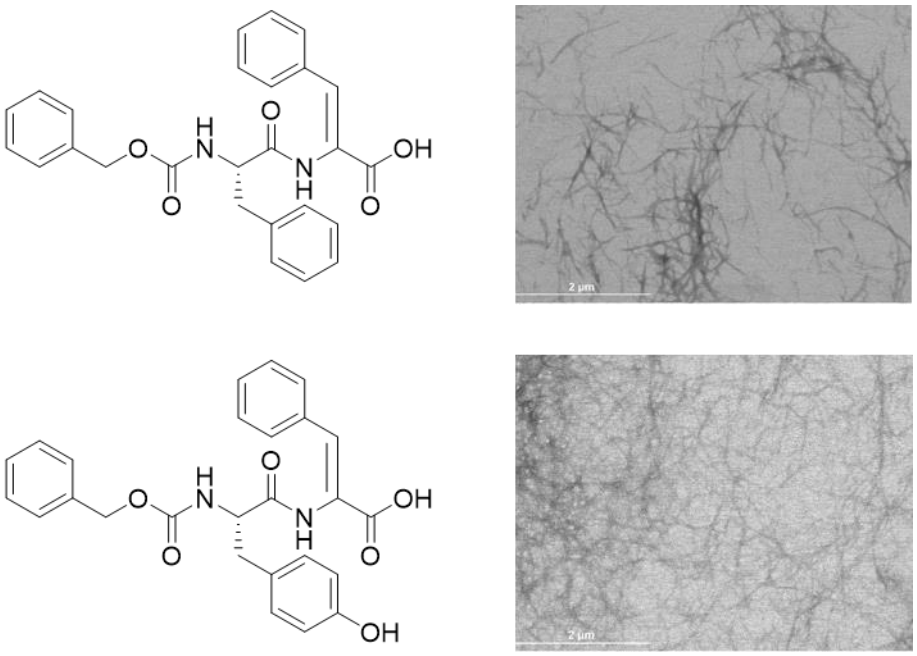

Figure 37: Scanning transmission electron microscopy (STEM) images of Cbz-Phe-ΔPhe-OH e Cbz-Tyr-ΔPhe-OH at 0.3 wt%. (adapted from 54) [56]

The STEM images of compound **4** that failed to give a hydrogel show that this compound self-assembles to form vesicles-like structures (Figure 38). This type of self-assemble might be the reason for compound **4** fail to give self-standing hydrogels.

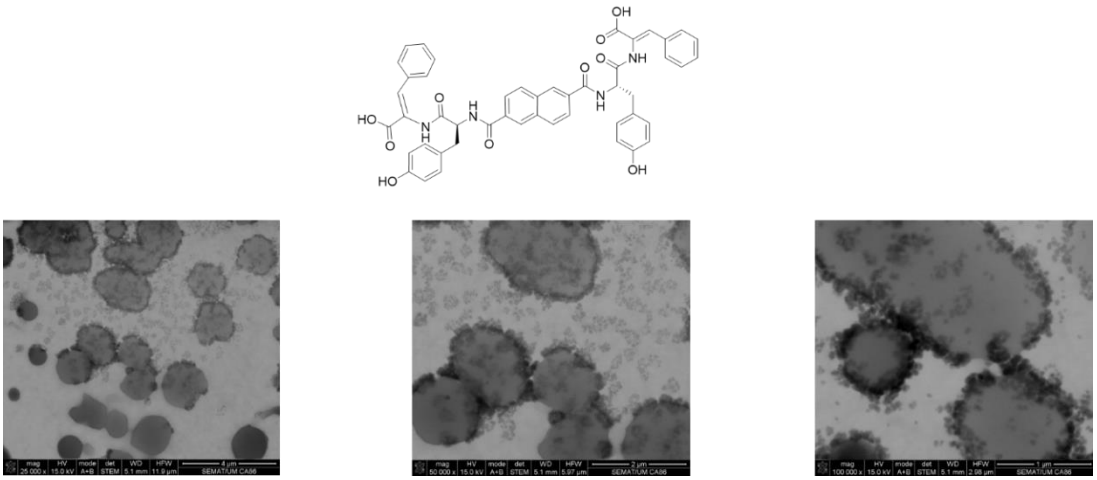

Figure 38: Scanning transmission electron microscopy (STEM) image of compound **4** at 0.4 wt%.

The tyrosyl bolaamphiphile reported by Lee *et al.* with an alkyl chain linking two tyrosine residues does not give hydrogels but SEM show that this compound aggregates to form spherical structures (Figure 39). [79] In this case the intermolecular interactions lead to the formation of interior-filled solid rigid spherical structures with different sizes. According to the authors the bulky, aromatic

side chain of tyrosine is supposed to be a potential factor in preventing a planar arrangement, resulting in rather spherical aggregates. The flexibility of the alkyl chain and the rigidity associated with the naphthyl moiety may explain the differences observed in the self-assembled structures of compound **4** and of the tyrosyl-bolaamphphile described by Lee *et al.*.

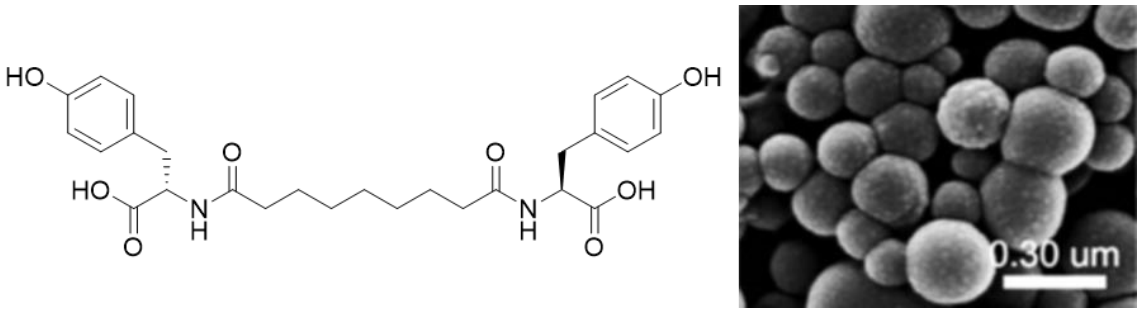

Figure 39: Structure and SEM images of a tyrosyl bolaamphiphile in water. (adapted from ref 79) [79]

Spherical aggregates were also observed as a result of the self-assembly of a bolaamphiphile having two L-DOPA residues linked by a central heptyl chain (Figure 40). [80] The molecules of this compound when dissolved in water, spontaneously self-assemble creating nanospheres with the DOPA catechol moiety exposed at the surface.

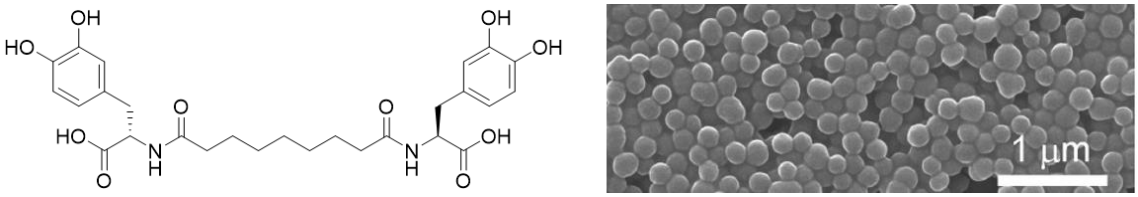

Figure 40: Structure and SEM images of a L-DOPA bolaamphiphile in water. (adapted from ref 80) [80]

The TEM image of the bola-phenylalanylphenylalanine hydrogel (Figure 41) revealed a network of cross-linked nanofibers similar but more compact than those observed for bola-dehydrodipeptides **1-3**.

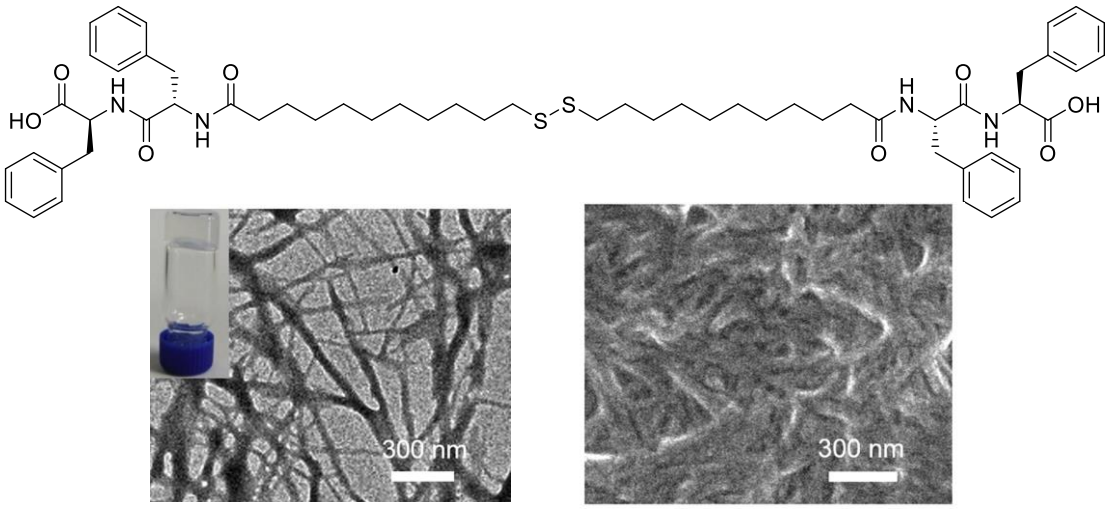

Figure 41: TEM and SEM images of bola-phenylalanylphenylalanine hydrogel (adapted from ref 65) [65]

A similar compound with a smaller alkane (2 carbon atoms) linking the phenylalanylphenylalanine dipeptides and the disulphide bond fail to give a hydrogel. The results suggest that the hydrophobic effect arising from the long alkane is crucial for the formation of the hydrogels, along with other noncovalent interactions. [65]

2.5 Circular Dichroism

Circular dichroism (CD) measures the difference in the absorption of left and right polarized light in optically active substances and constitutes a valuable tool for elucidation of the secondary structure of peptides and proteins. Peptides with a α-helix secondary structure give a CD spectrum with negative bands at 222 nm and 208 nm and a positive band at 193 nm. Peptides with an antiparallel β-sheet structure present in CD spectra negative bands at 218 nm and positive bands at 195 nm, while a random coil peptide show low ellipticity above 210 nm and negative bands near 195 nm. [45]

The CD spectrum of hydrogelators **1**, **2** and **3** are presented in Figure 42. The CD spectra were acquired with hydrogelator concentrations well-below the cgc owing to instrumental limitations. Therefore, the secondary structures determined by CD are only indicative, since less-ordered self-assembled fibrils are expected to exist in solution. However, it is expected that increasing the hydrogelator concentration is likely to result in progressive ordering of the secondary structure elements, already observed in solution.

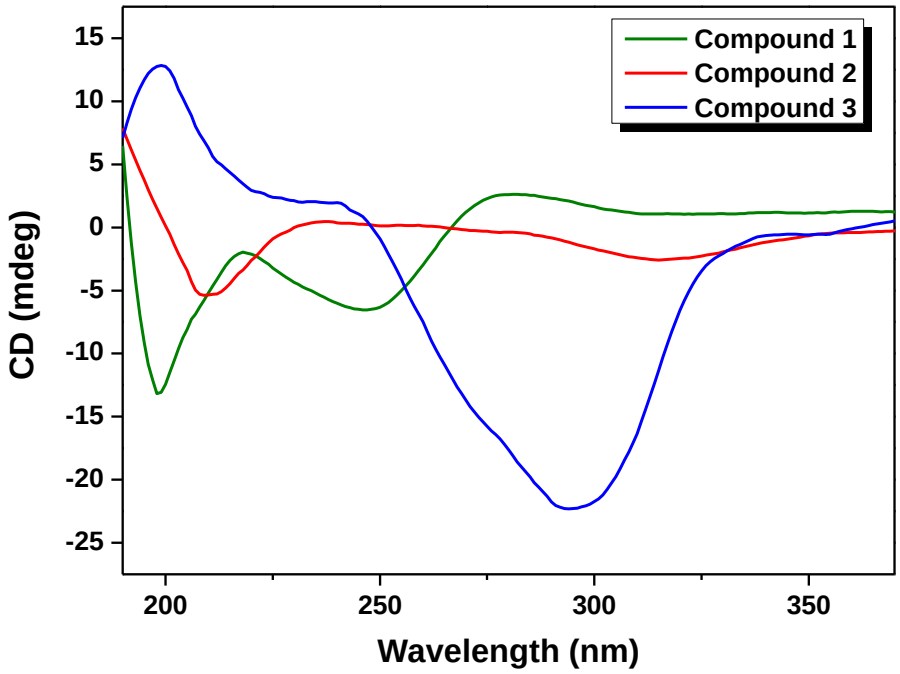

Figure 42: CD spectra of diluted aqueous solutions of compounds **1**, **2** and **3** (0.01 wt%).

The CD spectrum of compound **1** exhibits negative bands around 200 nm and 250 nm (Figure 42, green line) suggesting a contribution of a random coil structure. The CD spectrum of compound **2** shows a negative band at 220 nm and a negative broad peak around 320 nm (Figure 42, red line) This result points to a β-sheet aggregation pattern. Finally, the spectrum from compound **3** (Figure 42, blue line) show the importance that naphthalene interactions seem to have in self-assembly. The dehydrodipeptides phenylalanyldehydrophenylalanine and tyrosyldehydrophenylalanine *N*-protected with the carboxybenzyl group (Figure 43) gave CD spectra in dilute solution that suggest a predominance of random coil and a minor contribution of β-sheets. [56]

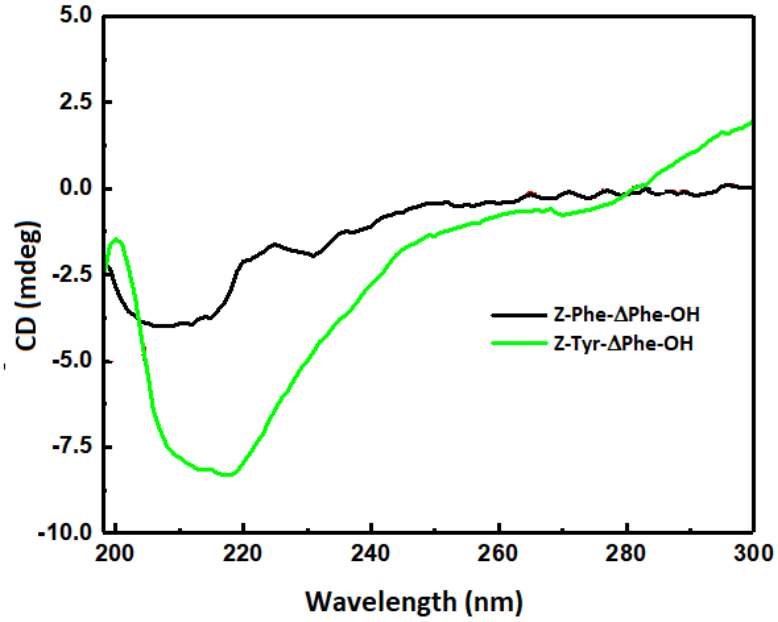

Figure 43: CD spectra of diluted aqueous solutions of Z-Phe-ΔPhe-OH e Z-Tyr-ΔPhe-OH (0.01 wt%). [56]

Unlike the CD spectra of compounds **1** and **3** the CD spectrum of bola-phenylalanylphenylalanine with a disulphide alkyl chain (Figure 44) indicate the presence of a β-sheet secondary structure. [65]

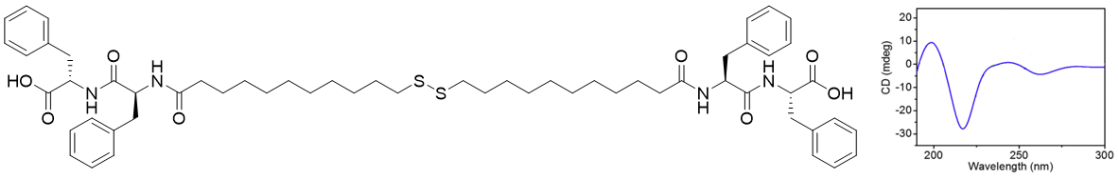

Figure 44: CD spectra of diluted aqueous solution of bola-phenylalanylphenylalanine (0.02 wt%). (adapted from ref 65) [65]

It seems like the substitution of a dehydrophenylalanine residue by its saturated counterpart and of an aromatic moiety by an alkyl chain have a significant effect on the self-assemble structure.

2.6 Rheology

Rheology provides structural information about the type, number and strength of the network responsible for hydrogelation. The gelation kinetics of compound **1**,**2** and **3** are presented in Figure 45. The scattering of data recorded with compound **3** does not allow a quantitative assessment of the gel kinetics. This is due to the rather small deformation used during this test to allow gel formation without disturbing the build-up of the network structure. In contrast to this, data for compounds **1** and **2** show that G' is significantly larger than G'' after 2 hours, which indicates that the hydrogels formed relatively

quickly, within the same time scale of gel formation for ultra-short carboxybenzyl-protected dehydropeptides [56] but faster than some Fmoc-dipeptides. [27] Bolaamphiphile **1** show an initial time lag of 2300 seconds before the significant rise in G' and the final slower equilibration step while for compound **2** this time is higher (4600s).

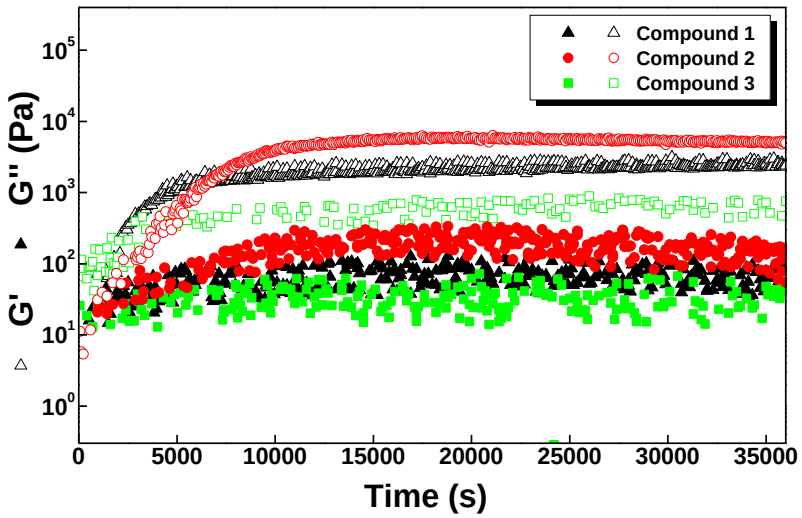

Figure 45: Elastic and viscous modulus during the kinetic process of gelation for compound **1**,**2** and **3**.

Several kinetics equations used in the literature were tested to quantify the gel kinetics reported in Figure 45. The first empirical model is a stretched exponential (KWW model) which has been reported to successfully describe the aggregation kinetics of various peptides. [81] A stretched exponential fit to the kinetics of compounds **1** and **2** is presented in Figures 46 and 47.

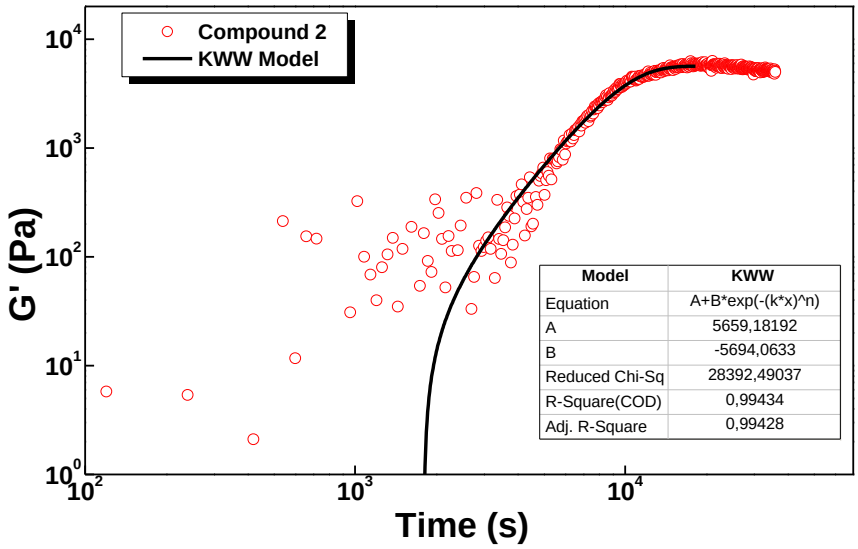

Figure 46: Time dependence of the storage modulus G' (symbols) of gelling compound **2** recorded at a frequency of 1 Hz and using a strain of 0.001%. The line is a fit of KWW model to the data.

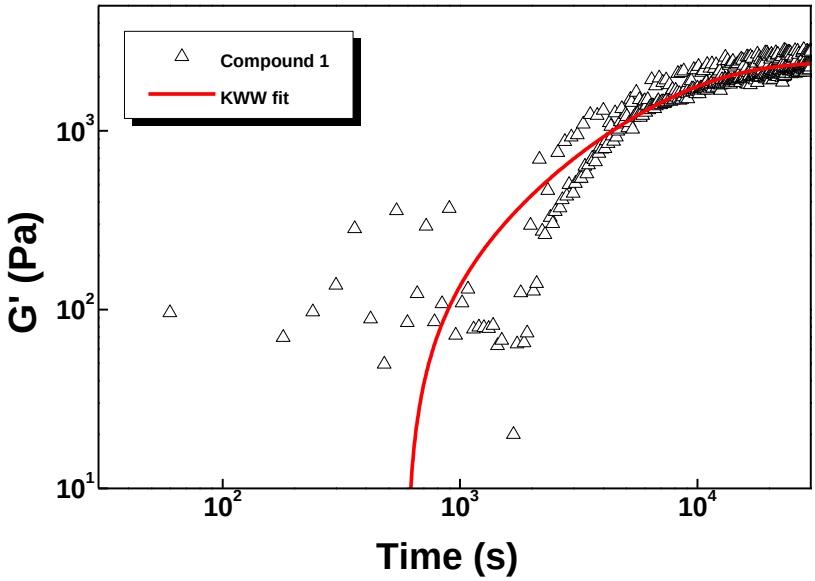

Figure 47: Time dependence of the storage modulus G' (symbols) of gelling compound **1** recorded at a frequency of 1 Hz and using a strain of 0.001%. The line is a fit of KWW model to the data.

Data in Figures 46 and 47 confirms that the stretched exponential cannot reproduce the time lag prior to the increase in the storage modulus G'. However, this model allows for a quantitative comparison between the kinetics of compound **1** and **2**, focusing on parameters *k* and *n* reported in Table 2.

Table 2: Characteristic time *k* and *n* of the stretched exponential model computed from the fits of this model to the kinetics of compound **1** and **2**. Parameters from the Saitô's equation computed from separate fits to the kinetics plotted in Figure 45 are also presented.

	Stretched exponential (KWW model)		**Saitô's model**			
Compound	***k* (10^{-4} s)**	***n***	***GO* (Pa)**	***dG* (Pa)**	k_n (h^{-1})	***k*** (h^{-1})
1	1.41 ± 0.05	1.00 ± 0.06	0 ± 57	2392 ± 66	0.40 ± 0.04	0.18 ± 0.10
2	1.03 ± 0.005	3.01 ± 0.05	0 ± 25	5722 ± 39	0.02 ± 0.001	1.84 ± 0.04

Essentially, the two compounds differ in the value of parameter *n*. In the original stretched exponential model used to describe distributions of relaxation phenomena in polymers [82], parameter *n* was bounded to $0 < n \leq 1$, as $n=1$ corresponds to a single relaxation process. Thus, the main information inferred from the KWW model is that the gel kinetics of compound **1** involves a single

process after the time lag, in contrast to the gel kinetics exhibited by compound **2**. However, the value of *n* for the latter does not bear any physical meaning.

A two steps model is often used to describe the nucleation (with rate constant k_n) and growth (with rate constant k) of aggregates of peptides [83]:

$$f(t) = G0 + dG\,\frac{\rho(e^{(1+\rho)kt}-1)}{1+\rho e^{(1+\rho)kt}}, \qquad (1)$$

where $\rho = \frac{k_n}{k}$, $G0$ is the initial storage modulus of the aggregate-free solution, and dG is the increment in the storage modulus during the kinetics.

A fit of equation (1) to the gel kinetics of compound **2** is presented in Figure 48, which shows that the model successfully reproduces the rheological data.

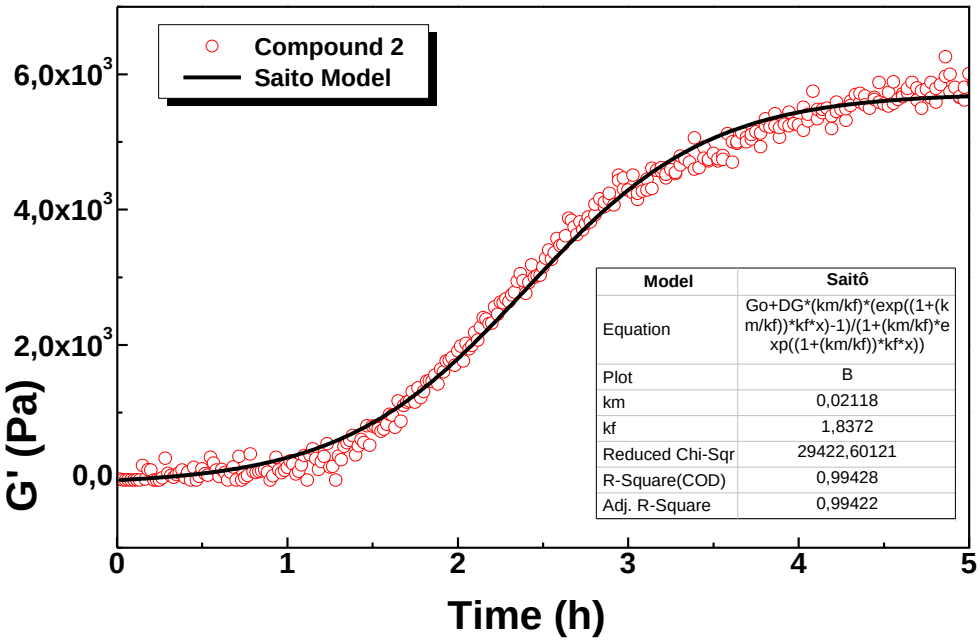

Figure 48: Same data as in Figure 45 but recast in hours and fitted with equation (1) – line.

A less successful fit was achieved for the kinetics for compound **1** (Figure 49). This is explained by the scatter in the data and by the fact that gelling is not fully completed after 10 hours. However, the errors in the values computed for the rate constants (Table 2) are small enough to offer a quantitative comparison between the gelling kinetics of the two compounds.

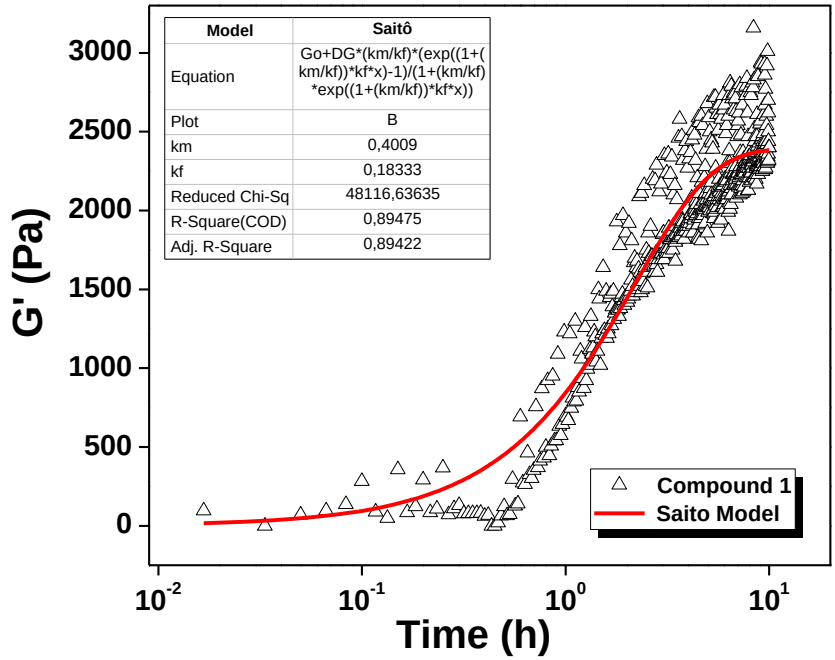

Figure 49: Time dependence of the storage modulus G' (symbols) recorded during the gelling of compound **1**.

A comparison of the parameters of equation (1) computed from fits to the rheological data of compounds **1** and **2** is shown in Table 2. The latter shows that nucleation and growth of peptide aggregates occurs on the same time scale for compound **1**, whereas nucleation is much slower for compound **2**. The values computed for the rate constants of compound **2** are consistent with the values reported recently from turbidity experiments of a hydrogel based on a dehydrodipeptide N-protected with a carboxybenzyl group. [56]

After reaching the structural equilibrium established by the reading of constant shear moduli G' and G'' with time (Figure 44), a frequency sweep from 100 Hz down to 0.1 Hz was performed with a strain of 0.01% to produce the mechanical spectra displayed in Figure 50.

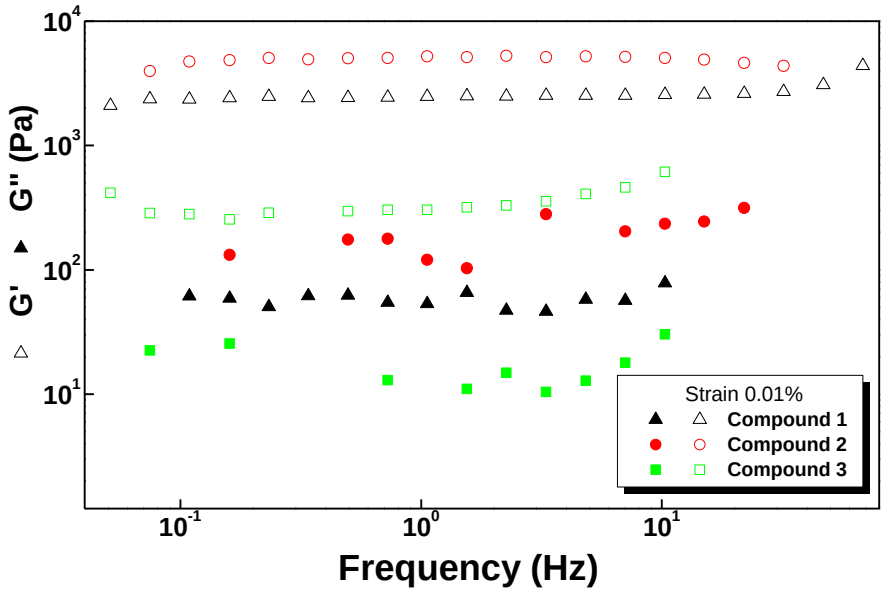

Figure 50: Frequency dependence of the shear elastic G' (empty symbols) and loss G'' (filled symbols) moduli for the compounds **1**,**2** and **3**.

Hydrogels from compounds **1**, **2** and **3**, G' is essentially constant over the frequency domain tested, whereas G'' presents a local minimum. Compound **3** show an increase of G' and G'' with the frequency at larger frequencies. However, this could be due to experimental issues (sample inertia) polluting the data in this frequency regime. Overall, all mechanical spectra are qualitatively similar, which suggests that the elastic network responsible for the gels mechanical response share structural similarities. As expected, the G' is higher than G'' for hydrogels of compounds **1**-**3** (Table 3).

Table 3: G' and G'' for hydrogel **1**, **2** and **3**.

Hydrogel	G' (Pa)	G'' (Pa)
1	2.5×10^3	6.5×10^1
2	4.5×10^3	1.4×10^2
3	3.7×10^2	$1,3 \times 10^1$

The thermal stability of gels formed by compounds **1**-**3** is depicted in Figure 51, which presents the shear moduli measured at a frequency of 1 Hz with a strain amplitude of 0.005%, during a heating and cooling cycle performed at a rate of 1 °C/min. Whereas the strain used with compound **3** is too small to detect any thermal variation in G', the data in Figure 51 show that the gel made with compound **1** is not thermally sensitive, whereas the gel made from compound **2** shows a thermal hysteresis. Overall, the results displayed in Figure 51 are the proof that these gels can sustain body

temperature with no significant structural changes.

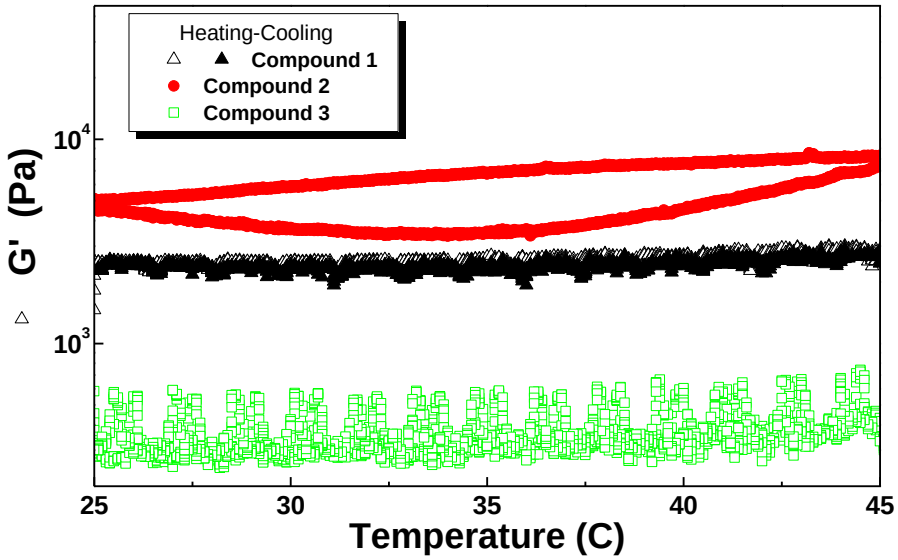

Figure 51: Thermal variation of the storage G' recorded during a heating and cooling cycle of gelled samples.

After the thermal cycle, gels were submitted to a strain sweep, whereas the frequency was maintained at 1 Hz. The hydrogel of compound **2** breaks up more easily than the other two hydrogels tested under applied strain (Figure 52). These results suggest that the thickness of the nanofibers does not have a direct correlation with the strength of the hydrogel. The hydrogel of compound **3** has thinner fibrils but shows an increase in G' before breaking (strain hardening) in contrast to the hydrogels from compounds **1** and **2** which show a continuous drop of G' before break. This suggests a different structure for hydrogel of bolaamphiphile **3**. Indeed, strain hardening is the hallmark of networks formed by condensed rod-like macromolecules [84], or by crosslinked biological filamentous networks [85], which combine a small elasticity with a significant strain stiffening originating from the enthalpic stretching of filaments having small bending elasticity [86]. The absence of strain hardening in gels of compounds **1** and **2** may have several structural reasons. First, the bending modulus of filaments might be much larger than their stretching modulus, thereby imparting an extended regime of linear viscoelasticity before the structural failure signalled by the crossover between G' and G'' moduli. Large bending modulus could be associated with the thicker filaments made of a larger number of bundled fibres. Alternatively, dual networks [87] or network with breakable links [88] might be called to explain the strain softening observed for hydrogels of compounds **1** and **2** shortly prior to break-up.

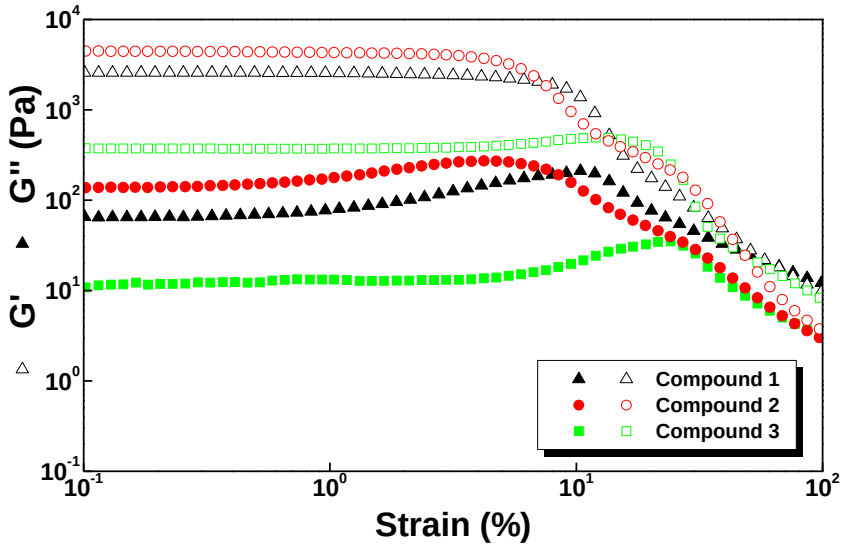

Figure 52: Strain dependence of the shear elastic G' (empty symbols) and loss G'' (filled symbols) moduli for compound **1**,**2** and **3**.

The mechanical spectra recorded 1 hour after the breakup of gels reported in Figure 52 indicate that they did not recover sufficient elasticity to be measured with a strain of 0.01%. This result is shown in Figure 53 where the low frequency regime does not indicate that G' is superior to G'' to define a solid-like behaviour. As such, there is no transient or breakable links in the present networks able to build a measurable elasticity within 1 hour. Additional studies at longer times and larger concentrations are needed to assess the possible healing properties of these hydrogels.

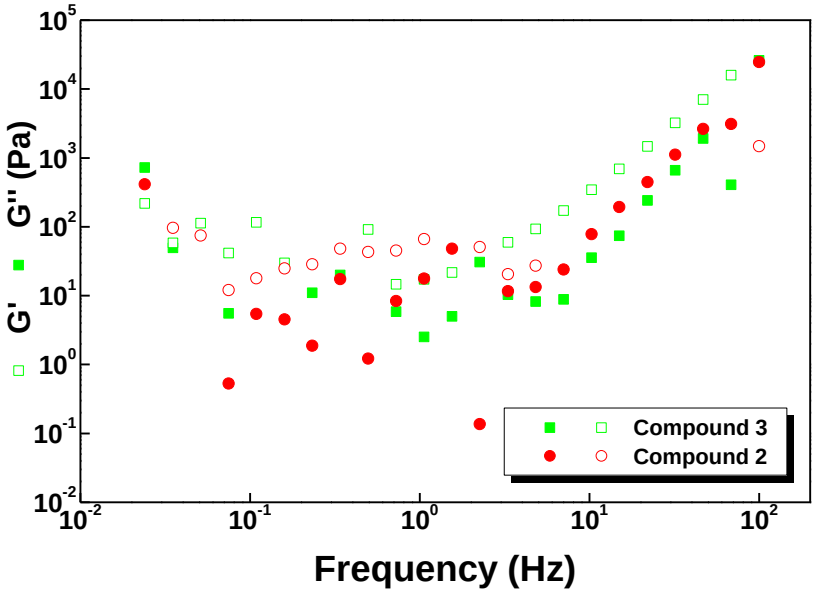

Figure 53: Strain dependence of the shear elastic G' (empty symbols) and loss G'' (filled symbols) for hydrogels of compounds **2** and **3** recorded 1 hour after the breakup of gels.

2.7 Biocompatibility and Cytotoxicity studies

The four compounds prepared were initially evaluated evaluated for their potential impact on the viability of human keratinocytes, namely the HaCaT cell line. The results show that compound **1**-**4** have small impact in cell viability (Figure 54). Interestingly compounds **1**, **3** and **4** exhibited a similar behaviour, with most concentrations tested eliciting a small apparent loss of cell viability of around 20%, which was independent of concentration. On the other hand, compound **2** was mostly devoid of any effect, with the exception of the two highest concentrations, which caused around 10% of viability loss.

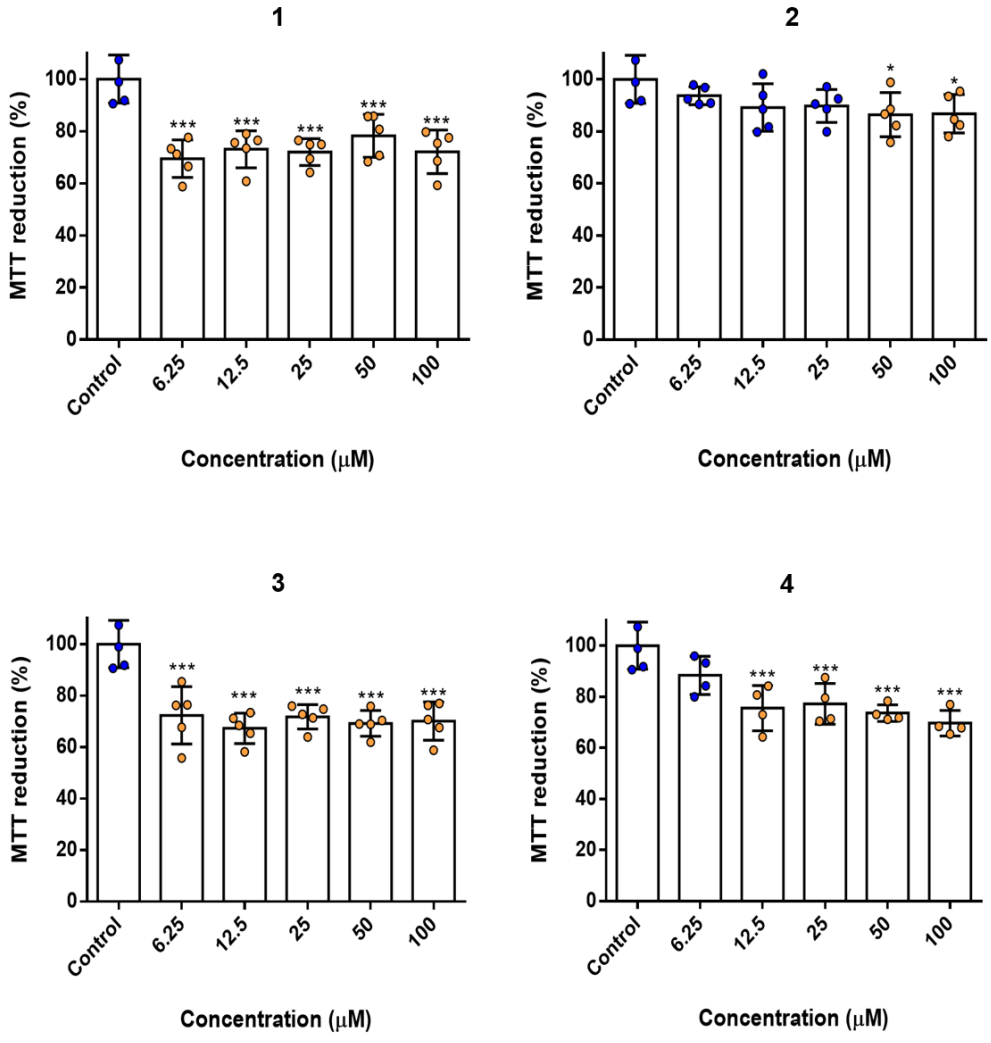

Figure 54: Viability of HaCaT cells treated with **1**/**2**/**3**/**4** for 24h, at the concentrations presented. *p<0.05, ***p<0.001.

In light of the results obtained for cell viability, it was decided to further characterize the effects caused by the molecules under study. One of the drawbacks of the MTT viability assay is that the absorbance values depend on the number of cells in each well. In order to clarify if the loss of viability identified could be related with fewer cells in hydrogelator-treated wells, the impact of the in cell DNA and protein content was evaluated, as a strategy to identify potential changes in cell proliferation and thus total number of cells. As shown in Figures 55 and 56, no statistically significant changes were found in any of the two parameters. These results show that the molecules under study have no identifiable impact in cell proliferation, despite having a small impact in cell viability.

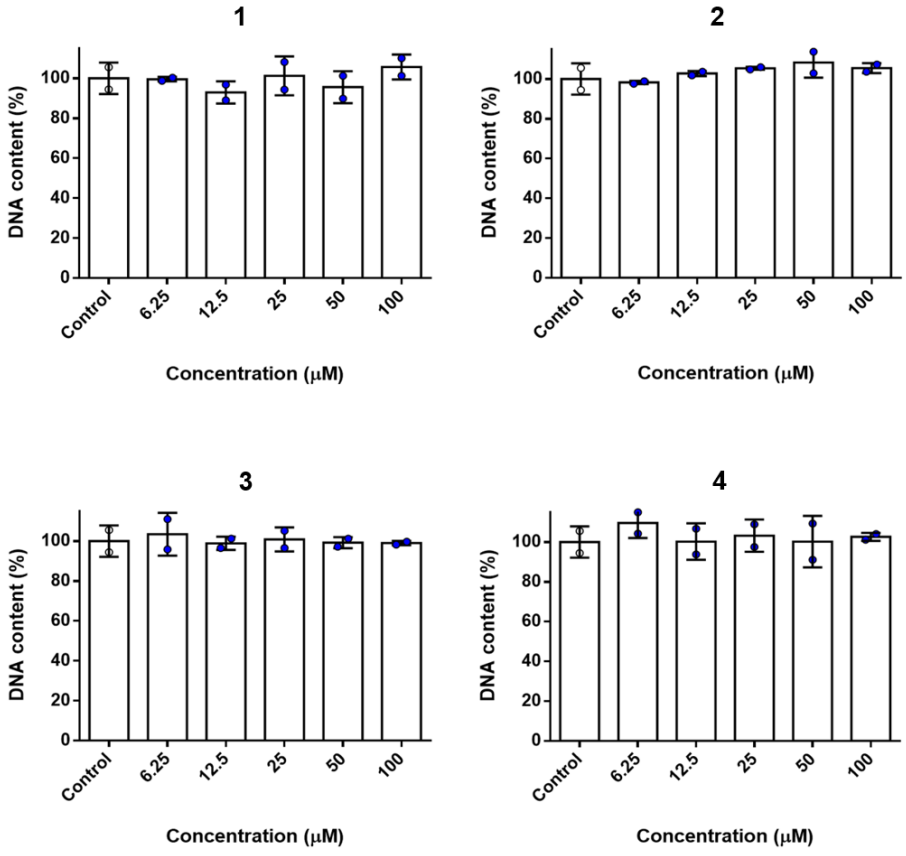

Figure 55: DNA content of HaCaT cells in the same conditions as Figure 54.

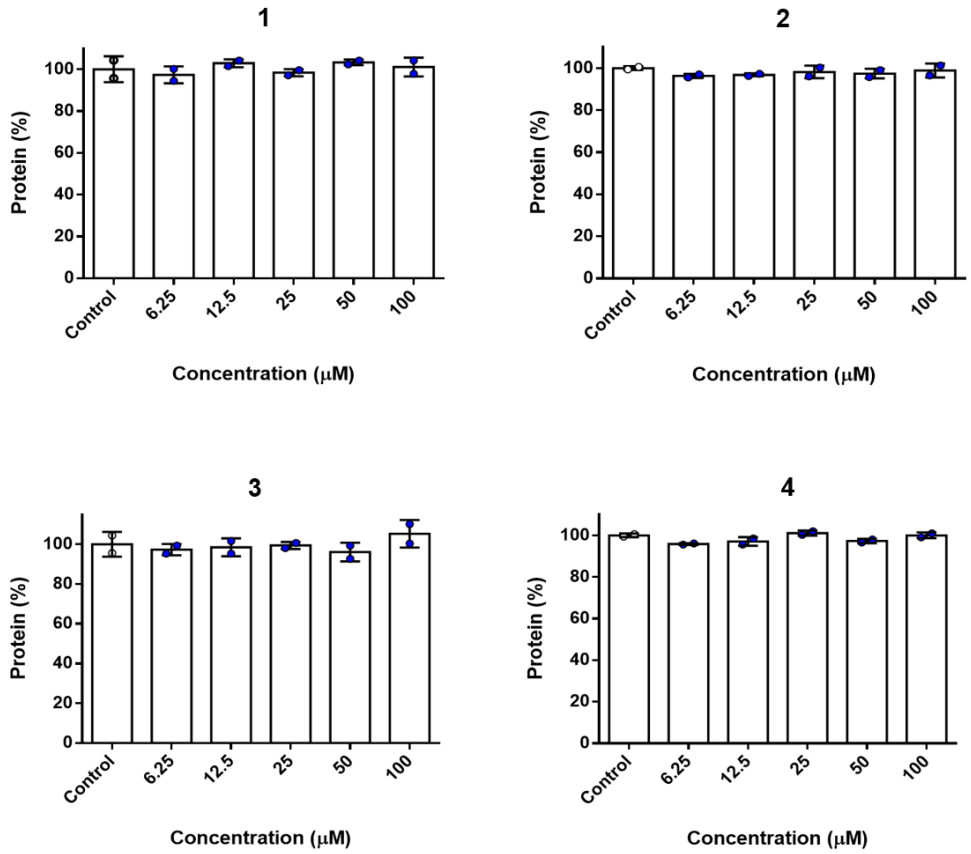

Figure 56: Protein content of HaCaT cells in the same conditions as Figure 54.

Given the marginal effect in cell viability, it was necessary to evaluate if the molecules could be eliciting necrosis in treated cells. To investigate this, the lactate dehydrogenase (LDH) release assay was carried out. Briefly, LDH is a cytosolic enzyme which presence in culture media is widely used as a suggestion that cells have lost membrane integrity, a hallmark of necrosis. As shown in Figure 57, none of the molecules elicited loss of membrane integrity in the concentrations tested.

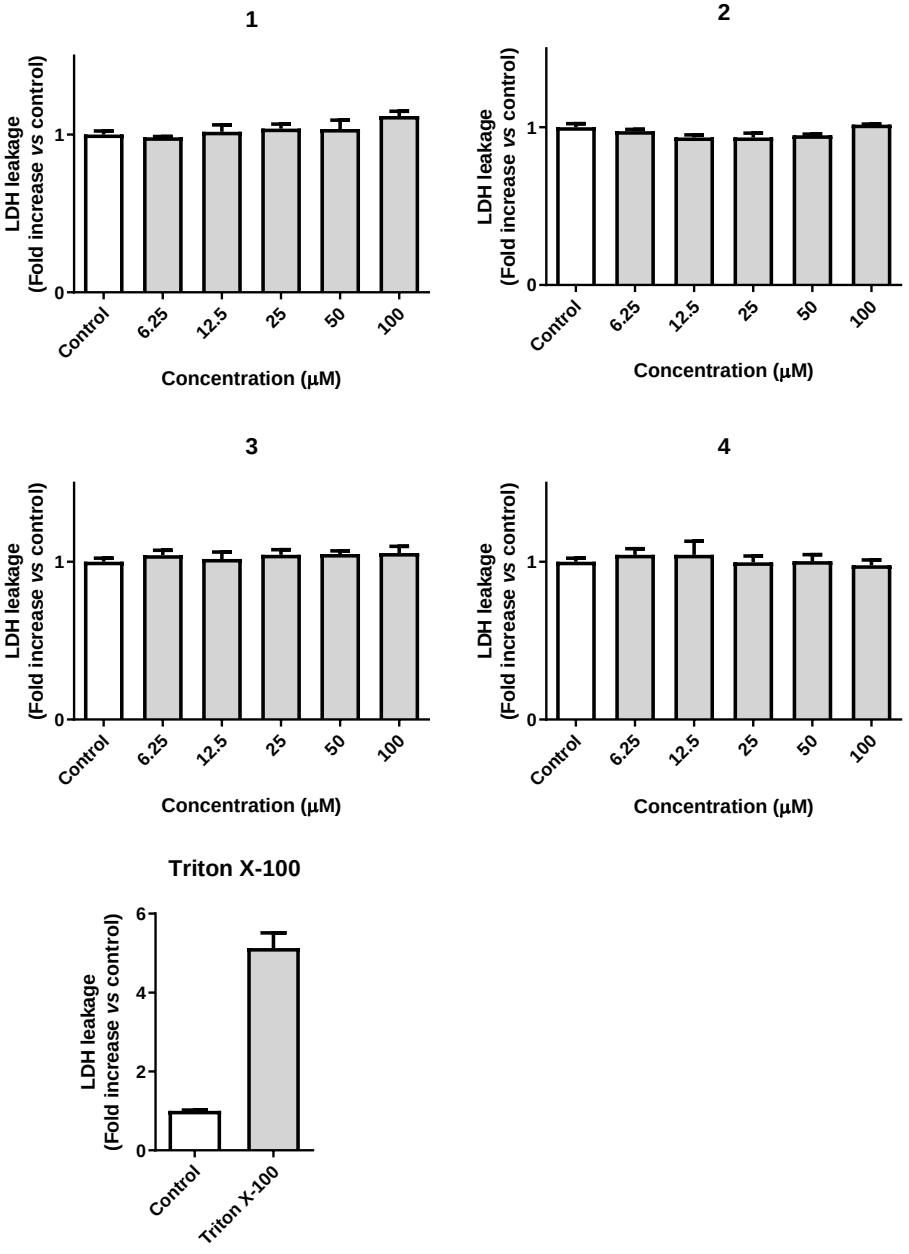

Figure 57: LDH activity found in the culture media of HaCaT cells treated with **1-4** for 24h, at the concentrations presented. Triton X-100 was used as positive control to lyse cells.

2.8 Drug Release studies

Supramolecular hydrogels have a great potential in the field of drug delivery and can often help to overcome pharmacological limitations of certain drugs, such as poor aqueous solubility or short half-lives *in vivo*. To study the ability of hydrogels **1-3** to entrap, and then release, model compounds, two dyes and an antibiotic were included in the hydrogel matrix. Thus, methylene blue (MB), ciprofloxacin and methyl orange (MO) were chosen as cationic, overall neutral and anionic cargo for modelling the drug release properties (Figure 58). The release of each cargo molecule from each hydrogel formed was studied.

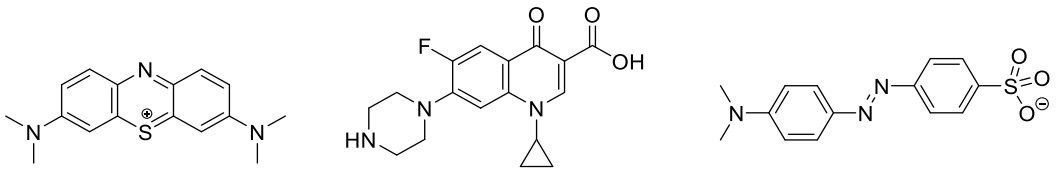

Figure 58: Small molecule cargo for release: methylene blue (MB), ciprofloxacin and methyl orange (MO).

Hydrogels containing the model compounds were prepared using the same conditions described previously, but with the water component (1mL) being replaced by a methylene blue solution (0.1 nM), a methyl orange solution (0.2 nM) or a ciprofloxacin (0.2 nM). In a modified version of the method described by Abraham *et al.* [89], water (1.5 mL) was carefully layered on top of hydrogel surface and then the percentage release of each model drug compound was recorded versus time.

The assays of hydrogels of compounds **1-3** with cationic MB, revealed that the top water layer remained almost colourless and transparent over several days, suggesting that very little MB was release from the hydrogel (Figure 59). The results obtained using UV-Vis spectroscopy showed that the cationic MB was retained by the hydrogels network. Similar studies were carried out with anionic MO. The results for the release of MO obtained by UV-vis spectroscopy showed that MO was released by the network of the hydrogels **1**,**2** and **3** (Figure 59). Hydrogelators **1** and **3**, which contain a phenylalanine residue, release nearly 60% of the anionic MO cargo (reaching a plateau after 3 days), whereas, hydrogel **2**, containing tyrosine residue, released more than 90% of MO. This might be due to the phenol group in the tyrosine side-chain which can be deprotonated, providing an additional repulsion of the anionic MO.

Ciprofloxacin was included as an overall neutral cargo (contains anionic and cationic groups), to provide a direct comparison between the cationic and anionic cargo. The amount of ciprofloxacin

present in the water layer was determined by HPLC. The results showed that the amount of ciprofloxacin released from hydrogels of compounds **1**,**2** and **3** was 32%, 58% and 20%, respectively and that a plateau was reached after 48 hours (Figure 59-61, Table 4). As observed for the anionic dye the hydrogel from bolaamphiphile **2** exhibit the greatest release capacity.

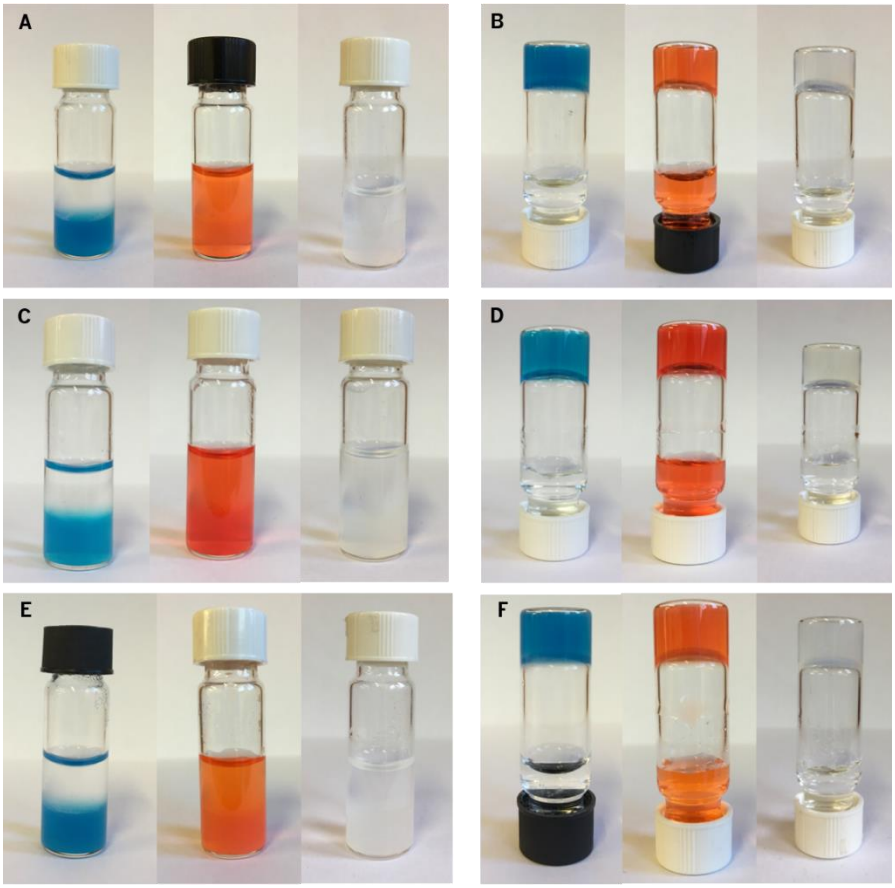

Figure 59: Representative images of hydrogels layered with water after a saturating release study (6 days). (A) Hydrogels of **1** loaded with MB (left), MO (centre) and ciprofloxacin (right), that were layered with 1.5 mL of H_2O. (B) Inverted vials from panel A. (C) Hydrogels of **2** loaded with MB (left), MO (centre) and ciprofloxacin (right), that were layered with 1.5 mL of H_2O (D) Inverted vials from panel D. (E) Hydrogels of **3** loaded with MB (left), MO (centre) and ciprofloxacin (right), that were layered with 1.5 mL of H_2O. (F) Inverted vials from panel E.

Table 4: Percentage release of cargo from hydrogels **1-3** after 6 days.

Hydrogelator	MB released (%)	MO released (%)	Ciprofloxacin released (%)
1	12.1	60.9	32.3
2	7.63	96.2	58.8
3	9.55	60.3	20.3

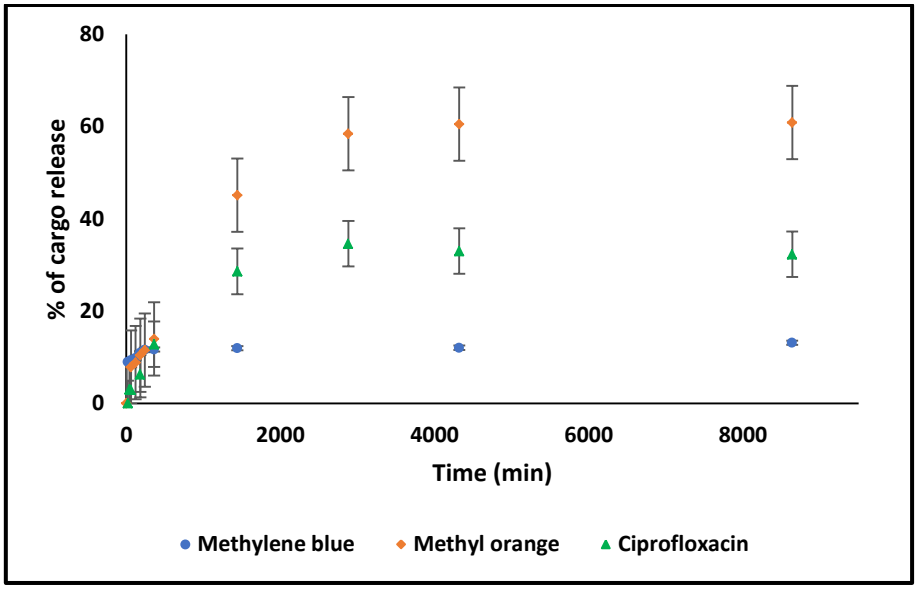

Figure 60: Percentage of cargo release vs time over 6 days. Release of methylene blue, methyl orange and ciprofloxacin from hydrogelator **1**.

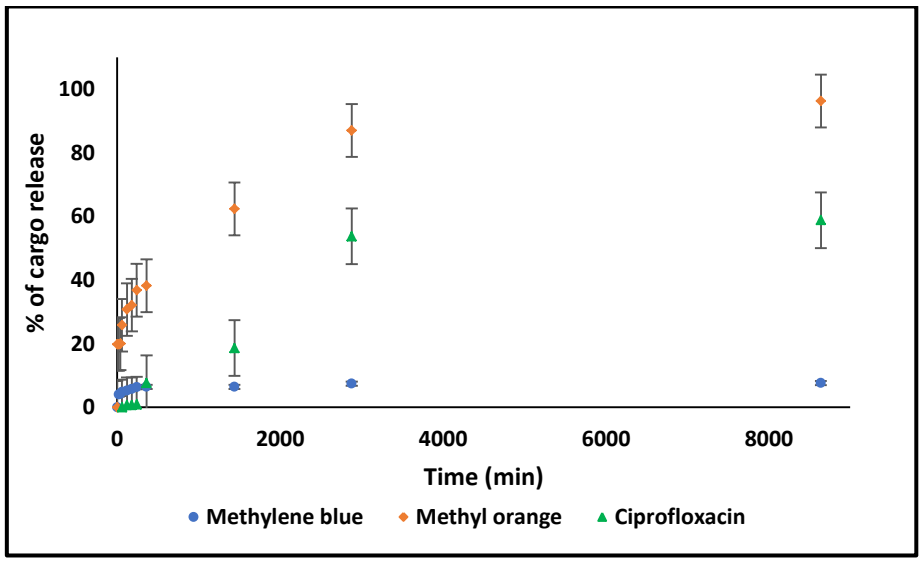

Figure 61: Percentage of cargo release vs time over 6 days. Release of methylene blue, methyl orange and ciprofloxacin from hydrogelator **2**.

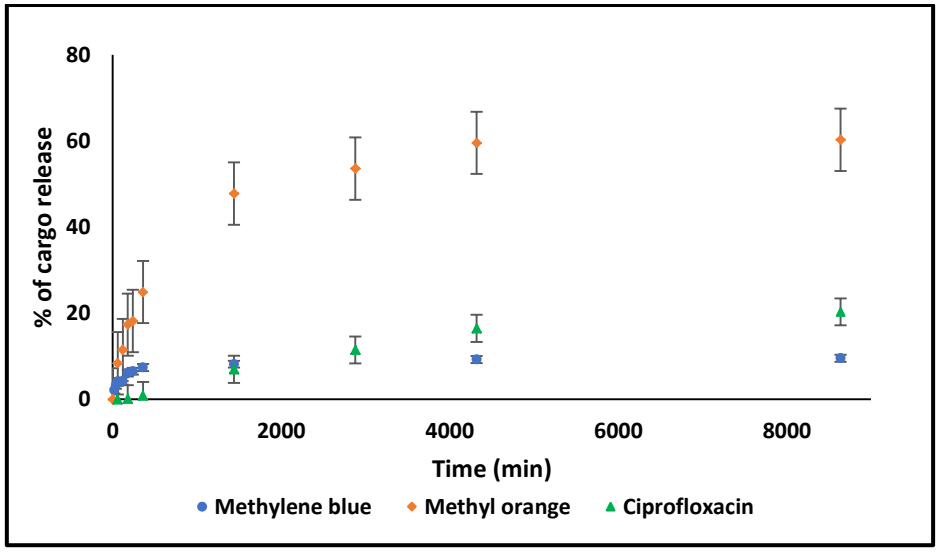

Figure 62: Percentage of cargo release vs time over 6 days. Release of methylene blue, methyl orange and ciprofloxacin from hydrogelator **3**.

Among the mathematical models used to describe the release of molecules from a gel network the Korsmeyer-Peppas model is the preferred model for polymeric systems. This model includes both diffusion and erosion of polymer (Figure 63 and 64). The following equation describes the Korsmeyer-Peppas model:

$$\frac{M_t}{M} = kt^n \qquad (2)$$

M_t: amount of cargo released at time t;

M: Total amount of cargo used for the release study;

k: release rate constant incorporating structural and geometric characteristics of drug dosage form;

n: release exponent.

In this model, the value n is associated with the diffusion mechanism of the drug as described in Table 5. [90, 91]

Table 5: Interpretation of diffusional release mechanisms.

Release exponent (n)	Drug transport mechanism
0.5	Fickian diffusion
$0.45 < n = 0.89$	Non – Fickian transport
0.89	Case II transport
Higher than 0.89	Super case II transport

The determined parameters of this model (k and n) and the value of R^2 are presented in Table 6 for hydrogels **1-3**. These results show that release of ciprofloxacin from hydrogel **1** is faster (higher k value) and is associated with a diffusion-controlled release mechanism (lower n value) when compared with hydrogels **2** and **3**. In the case of methyl orange, hydrogel **2** was the most effective hydrogel in releasing the anionic dye, as it presents the higher K and lower n.

Table 6: Release coefficients of the Korsmeyer-Peppas model obtained for methyl orange and ciprofloxacin release profiles in hydrogels **1**,**2** and **3**.

Cargo	Hydrogel	k	n	R^2
Methyl Orange	**1**	0.0200	0.4000	0.9509
	2	0.0900	0.2700	0.9785
	3	0.0400	0.3300	0.9497
Ciprofloxacin	**1**	0.0200	0.3300	0.8677
	2	0.0030	0.5800	0.8956
	3	0.0001	0.6300	0.9406

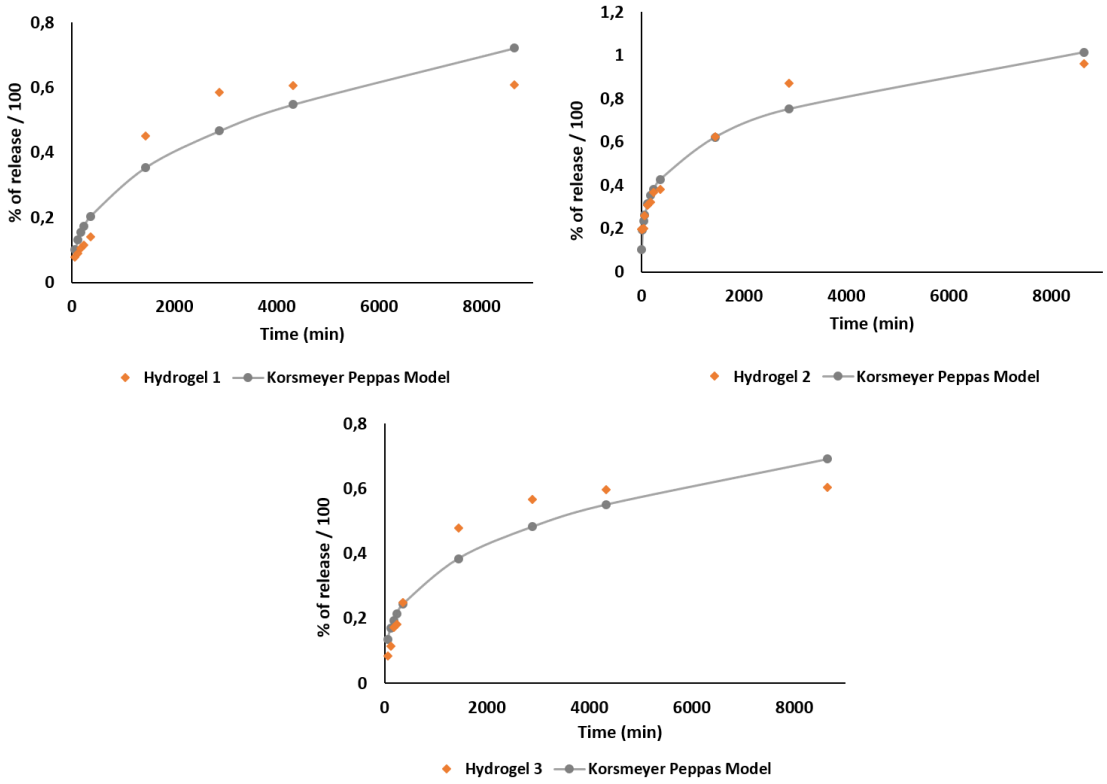

Figure 63: Data to Korsmeyer-Peppas Model to describe the release kinetics of methyl orange from hydrogels **1**, **2** and **3**.

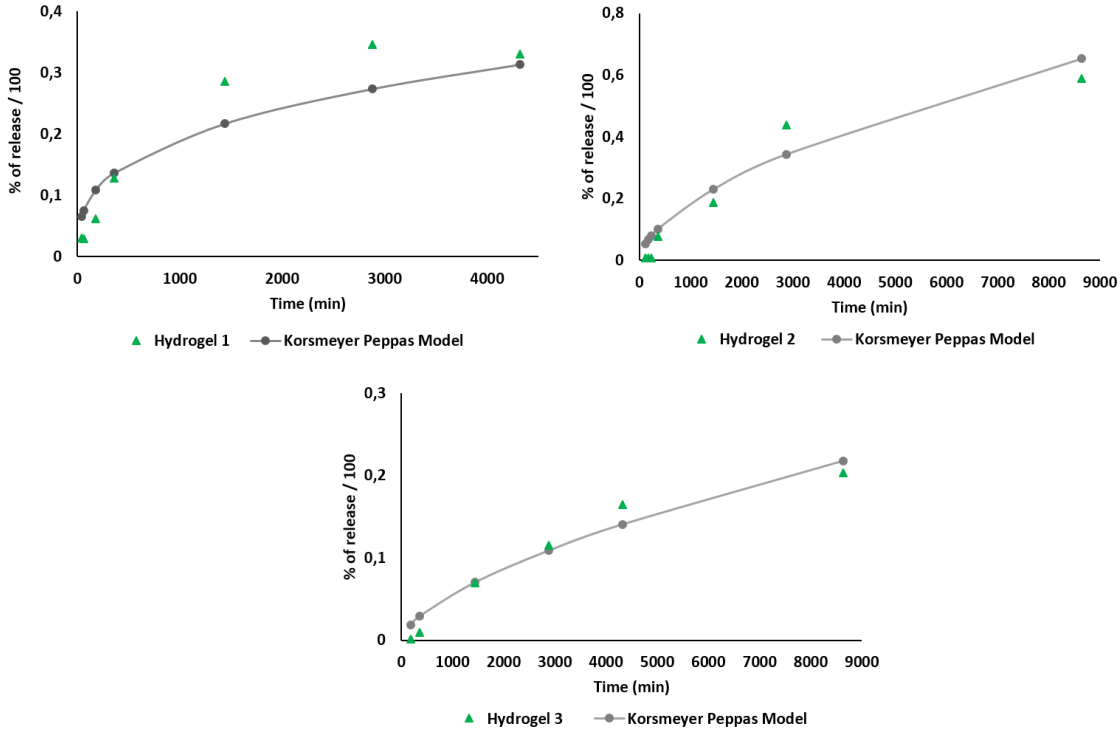

Figure 64: Data to Korsmeyer-Peppas Model to describe the release kinetics of ciprofloxacin from hydrogels **1**, **2** and **3**.

Chapter 3

Conclusions and Prospects

3 Conclusions and Prospects

In this work we describe the synthesis, characterisation and gelation properties of four new dehydrodipeptide symmetrical bolaamphiphiles, with a dehydrophenylalanine residue and a phenyl or naphthyl moiety linking the two hydrophilic heads. The saturated amino acids were phenylalanine or tyrosine. Three of the four compounds prepared behave as efficient hydrogelators, forming hydrogels with minimum gelation concentrations of 0.3-0.4 wt%. The rheologicaly properties of hydrogels prepared showed a storage modulus (G') significantly higher that their loss modulus (G'') which confirmed a viscoelastic behaviour characteristic of supramolecular hydrogels. STEM microscopy revealed that the hydrogels display fibrilar structures. The STEM images of the compound that failed to give hydrogels showed the self-assembly of the molecules into vesicle-like structures. Other authors reported for tyrosyl and L-DOPA bolaamphiphiles the self-assembly into spherical nanostructures. The phenolic side chain of tyrosine is supposed to be a potential factor in preventing a planar arrangement, resulting in rather spherical aggregates. The biocompatibility of these compounds was assessed by cytotoxicity assays. These compounds were initially evaluated for their potential impact on the viability of human keratinocytes (HaCaT cell line). The results show that the compounds synthetized have no identifiable impact on cell proliferation, despite having a small impact in cell viability.

Finally, in sustained release assays, the effects of the charge present on model drug compounds on the rate of release from the hydrogel networks was studied using cationic (methylene blue), anionic (methyl orange) and neutral cargo (ciprofloxacin). The hydrogels retain methylene blue inside the hydrogel network, and release methyl orange (60-90% release after 6 days) and ciprofloxacin (20-58% release after 6 days). In the experiments involving the methyl orange and ciprofloxacin, the hydrogel formed from compound **2**, containing tyrosine residues, released more (90% and 58%, respectively) model compounds than hydrogels **1** and **3**, which contain phenylalanine. This can be explained by the phenol group of tyrosine that increases the repulsive interactions between the model molecules and the hydrogel network.

Future work includes molecular dynamic simulations to try to explain the different self-assembly patterns observed for the bolaamphiphiles prepared in this work. Also, the small loss of cell viability observed for some of the compounds will be investigated together with drug release assays involving drug transport into small unilamellar vesicles (as biomembrane models). Also, other bolaamphiphiles will be prepared by changing the aromatic linking moieties by alkyl chains and the saturated amino acid by residues of aspartic acid or lysine. The objective of these studies is the development of new efficient drug delivery systems based on symmetrical bolaamphiphiles based on dehydrodipeptides.

Chapter 4

Experimental procedures

4 Experimental procedures

4.1 Reagents and instrumentation

Analytical grade reagents were purchased from Sigma-Aldrich and Acros and used without further purification. Analytical grade solvents were used and dried by the usual methods when required. The petroleum ether used refers to the fraction having a boiling point of 40-60°C. Distilled water was always used for the reactions when aqueous medium was needed. The reactions were monitored by thin layer chromatography (TLC) on Merck-Kieselgel plates 60 F254 and detection was made by examination under UV light (240 nm) or by adsorption of iodine vapour. The organic phases were dried using anhydrous magnesium sulphate (Riedel) and carbonate of anhydrous potassium (Merck). Chromatographic separations were performed on silica MN Kieselgel 60 M (230-400 mesh).

The ^{1}H and ^{13}C NMR spectra (assigned by DEPT, HSQC and HMBC techniques) were recorded on a Bruker Avance III 400 spectrometer, operating at 400.13 MHz and 100.62 MHz, for ^{1}H and ^{13}C NMR respectively. The NMR spectra were recorded at 25°C and in some cases at 75°C, using the residual solvent signals as reference. Deuterated dimethyl sulfoxide (DMSO-d_6) and deuterated chloroform ($CDCl_3$-d_1) were used as solvents. Chemical shifts are given in parts per million (ppm) and the coupling constants in Hertz (Hz). HRMS data were recorded by the mass spectrometry service of the University of Vigo, Spain. MS was recorded by a Thermo Finnigan LxQ (Linear Ion Trap) Mass Detector with Electro Spray Ionization (ESI).

For the formation of the hydrogel the compounds were weighted into a sample vial and water was added. While on stirring, NaOH (1M) was added till pH 10. The mixture was sonicated and then added GdL. The solutions were left standing overnight to form the hydrogel.

CD spectra were recorded under N_2 on a Jasco J815 CD spectrometer. The samples used were solutions from dilutions of the preparation of the hydrogels.

The viscoelastic characterization of hydrogels was performed with a stress-controlled rotational rheometer Anton Paar MCR300 (Anton Paar GmbH, Graz, Austria). Gel forming solutions were loaded in the shearing geometry (a Couette cell with 1 mL volume and 0.5 mm gap) at 25 °C. The liquid sample was pre-sheared at a shear rate of 5 s^{-1} during one minute to homogenise the sample in the shearing geometry. Then, the gelation kinetics was monitored during 10 hours by applying a small amplitude (0.001 %) oscillatory shear at 1 Hz and recording both storage (G') and loss (G'') moduli at each second.

STEM images were recorded using a NanoSEM – FEI Nova 200 (FEI Technologies, Inc., Hillsboro, Oregon, USA), operating at 15 kV, coupled to an Electron Dispersive Spectroscopic analyzer (EDS) and Electron Backscatter Diffraction EDAX – Pegasus X4M analyzer and detection system (EBSD) at SEMAT (Serviços de Caracterização de Materiais), Guimarães, Portugal.

The concentration of methylene blue or methyl orange in the experiments of sustained release assays was determined by measuring the absorbance at λ_{max} of the dye (666 nm for methylene blue and 465 nm for methyl orange) using a microplate reader (VARIAN, 50 MPR Microplate Reader) and then converting the value to percentage release (using a standard calibration curve). The concentration of ciprofloxacin was determined using analytical HPLC (Jasco, PU-980 Intelligent HPLC Pump; Jasco, UV-975, Intelligent UV/VIS Detector; Shimadzu, C-R6A, Chromatopac), where the integrated peak area was converted to a percentage release (using a standard calibration curve). The eluent used in the HPCL measures was a mixture of acetonitrile/water (50/50), filtering and degassing, with a flow of 1 mL/min. Each experiment was performed in triplicate, and the mean percentage cargo release was plotted against time.

4.2 Synthesis

4.2.1 Synthesis of Boc-L-Phe-D,L-Phe(β-OH)-OMe (13a)

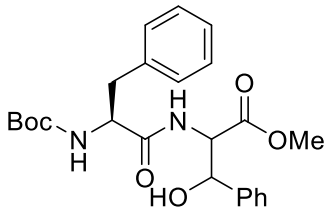

Boc-L-Phe-OH (1.0 equiv., 4.00 mmol, 1.10 g) was dissolved in MeCN (40 mL) and cooled to 0°C. H-D,L-Phe(β-OH)-OMe (1.0 equiv., 4.00 mmol, 0.93 g), Et_3N (3.0 equiv., 12.0 mmol, 1.67 mL) and HBTU (1.2 equiv., 4.80 mmol, 1.82 g) were added sequentially, with 2 min between each addition, and the mixture was stirred at rt overnight. The solvent was removed under reduced pressure to afford a residue that was partitioned between EtOAc (50 mL) and $KHSO_4$ (1M, 50 mL). After separation of the phases, the organic phase was thoroughly washed with $KHSO_4$ (1 M, 2 × 50 mL), $NaHCO_3$ (1 M, 3 × 50 mL), and brine (3 × 50 mL) and then dried with anhydrous $MgSO_4$. Filtration followed by removal of the sovent under reduced pressure afforded compound **13a** as a diasteroisomeric mixture with a 99% yield.

^{1}H NMR ($CDCl_3$, 400 MHz) δ): 1.39 (9H, s, $O_2C(CH_3)_3$), 2.79-2.94 (1H, m, β-CH_2 Phe), 2.95-3.06 (1H, m, β-CH_2 Phe), 3.87 and 3.71 (3H, s, OCH_3), 3.42 and 3.52 (1H, brs and d, J = 4.4, O*H*), 4.21-4.44 (1H, m, α-C*H* Phe), 4.72-4.78 (1H, m, α-C*H* Phe(β-O*H*), 4.91-5.04 (1H, m, N*H*), 5.18-5.29 (1H, m, β-C*H* Phe(β-O*H*), 6.80-6.89 (1H, m, N*H*), 7.18.7.35 (10H, m, Ph*H*) ppm.

4.2.2 Synthesis of Boc-L-Phe-*Z*-ΔPhe-OMe (12a)

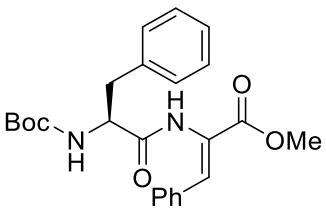

To a solution of compound **13a** (Boc-L-Phe-D,L-Phe(β-OH)-OMe) (1.0 equiv. 3.97 mmol, 1.75 g) in dry MeCN (20 mL), DMAP (0.12 equiv., 0.48 mmol, 0.06 g) and Boc_2O (1.2 equiv., 4.76 mmol, 1.04

g) were added under rapid stirring at rt. The mixture was monitored by ^{1}H-NMR and was stirred until all the starting material was consumed. *N,N,N',N'*- tetramethylguadinine (2% in volume, 0.4 mL) was added under continued stirring. The mixture was monitored by ^{1}H-NMR and stirred at rt until all the intermediate was consumed. Concentration under reduced pressure gave a residue that was partitioned between EtOAc (50 mL) and $KHSO_4$ (1M, 30 mL). After separation of the phases, the organic phase was washed with $KHSO_4$ (1 M, 2 × 30 mL), $NaHCO_3$ (1 M, 3 × 30 mL), and brine (3 × 30 mL) and then dried with anhydrous $MgSO_4$. Filtration followed by removal of the solvent under reduced pressure afforded compound **12a** as a yellow solid (1.16 g, 2.73 mmol, 69%).

^{1}H NMR ($CDCl_3$, 400 MHz, δ): 1.41 (9H, s, $O_2C(CH_3)_3$), 3.08 (1H, dd, J = 14.0 Hz, 7.2 Hz, β-CH_ACH_BPh Phe), 3.21 (1H, dd, J = 14.0 Hz, 6.4 Hz, β-CH_ACH_BPh Phe), 3.82 (3H, s, CO_2CH_3), 4.46-4.55 (1H, m, α-CH Phe), 4.97 (1H, br s, NH), 7.28-7.42 (11, m, PhH, α-CHPhe), 7.68 (1H, br s, NH) ppm.

^{13}C NMR ($CDCl_3$, 100.6 MHz, δ): 28.1 (3 x CH_3, $OC(CH_3)_3$), 37.5 (CH_2, β-CH_2 Phe), 52.5 (CH_3, CO_2CH_3), 80.3 (C, $OC(CH_3)_3$), 123.8 (C, α-C ΔPhe), 126.8 (CH, Ph), 128.49 (CH, Ph), 128.53 (CH, Ph), 129.3 (CH, Ph), 129.4 (CH, Ph), 129.7 (C, Ph), 132.7 (CH, β-CH ΔPhe), 133.3 (C, Ph), 136.4 (C, Ph), 165.3 (C, C=O ΔPhe), 170.3 (C, C=O Boc), 171.1 (C, C=O Phe) ppm.

4.2.3 Synthesis of H-L-Phe-*Z*-ΔPhe-OMe • TFA (11a)

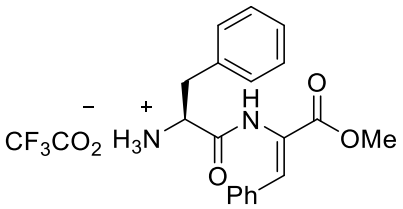

Boc-L-Phe-*Z*-ΔPhe-OMe, **12a**, (2.73 mmol, 2.16 g) was dissolved in TFA (5 mL) and the reaction mixture was stirred at rt for 20-30 minutes. The mixture was diluted with $CHCl_3$ (30 mL) and concentrated under reduced pressure. Additional $CHCl_3$ (2 × 30 mL) was added and then removed under reduced pressure (in order to completely remove the residual TFA), to afford compound **11a** as a white solid (1.19 g, 2.71 mmol, 99%). m.p. 87.0-88.0°C.

^{1}H-NMR (400 MHz, DMSO-d_6, δ): 2.94-3.00 (1H, dd, *J* = 8.8 and 14.0 Hz, β-CH_2 Phe), 3.24-3.29 (1H, dd, *J* = 4.8 and 14.0 Hz, β-CH_2 Phe), 3.73 (3H, s, OCH_3), 4.25 (1H, m, α-CH Phe), 7.30-7.41 (9H, m, Ar-H and β-CH ΔPhe), 7.58-7.60 (2H, dd, *J* = 2.0 and 4.0 Hz, Ar-H), 8.26 (3H, s br, NH_3^+), 10.37 (1H, s, NH ΔPhe) ppm.

^{13}C-NMR (100.6 MHz, DMSO-d_6, δ): 36.7 (CH_2, β-*C*H_2 Phe), 52.4 (CH_3, O*C*H_3), 53.6 (α-*C*H Phe), 125.0 (αC), 127.3 (CH), 128.6 (CH), 128.7 (CH), 129.6 (CH), 129.7 (CH), 130.0 (CH), 132.3 (CH, β-*C*H ΔPhe), 132.8 (C), 134.8 (C), 164.9 (C, *C*=O), 168.3 (C, *C*=O) ppm.

HRMS (micrOTOF): calcd. for $C_{19}H_{21}N_2O_3$ 325.15467; found 325.15545.

4.2.4 Synthesis of Boc-L-Tyr(*t*Bu)-D,L-Phe(β-OH)-OMe (13b)

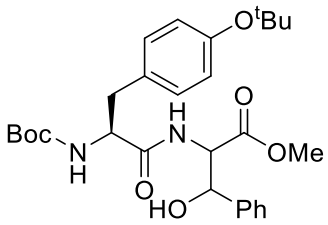

Boc-L-Tyr(*t*Bu)-OH (1.0 equiv., 6.47 mmol, 2.18 g) was dissolved in MeCN (60 mL) and cooled to 0°C. H-D,L-Phe(β-OH)-OMe (1.0 equiv., 6.47 mmol, 1.50 g), Et_3N (3.0 equiv., 19.4 mmol, 2.70 mL) and HBTU (1.2 equiv., 7.76 mmol, 2.71 g) were added sequentially, with 2 min between each addition, and the mixture was stirred at rt overnight. The solvent was removed under reduced pressure to afford a residue that was partitioned between ethyl acetate (50 mL) and $KHSO_4$ (50 mL, 1M). After separation of the phases, the organic phase was thoroughly washed with $KHSO_4$ (1 M, 2 × 50 mL), $NaHCO_3$ (1 M, 3 × 50 mL), and brine (3 × 50 mL) and then dried with anhydrous $MgSO_4$. Filtration followed by removal of the solvent under reduced pressure afforded compound **13b** as a diasteroisomeric mixture with a 94% yield.

^{1}H-NMR (400 MHz, DMSO-d_6, δ): 1.24 (9H, s, OC(C*H*$_3$)$_3$ Tyr), 1.26 and 1.28 (9H, s, O_2C(C*H*$_3$)$_3$ Boc), 2.30-2.37 (1H, m, β-C*H*$_2$ Phe), 2.63-2.74 (1H, m, β-C*H*$_2$ Phe), 3.61 and 3.66 (3H, s, OC*H*$_3$), 4.05-4.23 (1H, m, α-C*H* Phe(β-OH), 4.54-4.62 (1H, m, α-C*H* Phe), 5.12-5.17 (1H, m, β-C*H* Phe(β-O*H*), 5.94-5.98 (1H, m, *N*H), 6.71-7.42 (10H, m, Ar*H*), 8.00 and 8.20 (1H, m, N*H*) ppm

4.2.5 Synthesis of Boc-L-Tyr(*t*Bu)-*Z*-ΔPhe-OMe (12b)

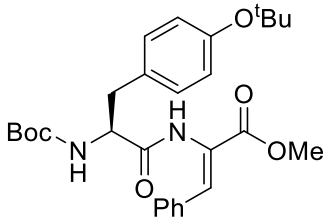

To a solution of compound **13b** (Boc-L-Tyr(*t*Bu)-D,L-Phe(β-OH)-OMe) (1.0 equiv. 6.07 mmol, 3.12 g) in dry MeCN (30 mL), DMAP (0.12 equiv., 0.728 mmol, 0.0890 g) and Boc_2O (1.2 equiv., 7.28 mmol, 1.59 g) were added under rapid stirring at rt. The mixture was monitored by ^{1}H-NMR and was stirred until all the starting material was consumed. *N,N,N',N'*- tetramethylguadinine (2% in volume, 0.6 mL) was added under continued stirring. The mixture was monitored by ^{1}H-NMR and stirred at rt until all the intermediate was consumed. Concentration under reduced pressure gave a residue that was partitioned between EtOAc (50 mL) and $KHSO_4$ (1M, 30 mL). After separation of the phases, the organic phase was washed with $KHSO_4$ (1 M, 2 × 30 mL), $NaHCO_3$ (1 M, 3 × 30 mL), and brine (3 × 30 mL) and then dried with anhydrous $MgSO_4$. Filtration followed by removal of the solvent under reduced pressure afforded compound **12b** (2.30 g, 4.64 mmol, 70%).

^{1}H-NMR (400 MHz, DMSO-d_6, δ): 1.26 (9H, s, OC(C*H*$_3$)$_3$ Tyr), 1.31 (9H,s O_2C(C*H*$_3$)$_3$ Boc), 2.70-2.77 (1H, app. t, β-C*H*$_2$ Phe), 2.98-3.02 (1H, dd, *J* = 3.6 and 13.6, β-C*H*$_2$ Phe), 3.70 (3H, s, OC*H*$_3$), 4.33 (1H, m, α-C*H* Phe), 6.87 (2H, d, *J* = 8.4 Hz, Ar*H* Tyr), 7.06 (1H, d, *J* = 8.4 Hz, N*H*), 7.26 (2H, d, *J* = 8.4 Hz, Ar*H* Try), 7.25 (1H, s, β-C*H* ΔPhe), 7.37-7.69 (5H, m, Ar*H* Phe), 9.77 (1H, s, α-N*H* ΔPhe) ppm.

^{13}C-NMR (100.6 MHz, DMSO-d_6 δ: 28.1 and 28.5 (C, O_2C(*C*H$_3$)$_3$ Try and Boc), 36.1 (CH$_2$, β-*C*H$_2$ Phe), 52.2 (CH$_3$, O*C*H$_3$), 56.0 (CH, α-C*H* Phe), 77.6 (C), 78.0 (C), 123.3 (CH, Ar*H* Try), 126.0 (C), 128.5 (CH), 129.4 (CH), 129.7 (CH, Ar*H* Try), 130.1 (CH), 131.9 (CH, α-*C*H ΔPhe), 132.8 (C), 133.3 (C),153.4 (C), 155.5 (C, *C*=O), 165.4 (C, *C*=O), 172.2 (C, *C*=O) ppm.

4.2.6 Synthesis of H-L-Tyr-*Z*-ΔPhe-OMe • TFA (11b)

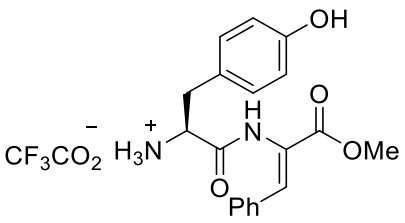

Boc-L-Tyr(*t*Bu)-*Z*-ΔPhe-OMe, **12b**, (2.30 g, 4.64 mmol) was dissolved in TFA (5 mL) and the reaction mixture was stirred at rt for 20-30 minutes. The mixture was diluted with $CHCl_3$ (20 mL) and concentrated under reduced pressure. Additional $CHCl_3$ (2 × 20 mL) was added and then removed under reduced pressure (in order to completely remove the residual TFA), to afford compound **11b** (2.03 g, 4.47 mmol, 97%) as a white solid.

^{1}H-NMR (400 MHz, DMSO-d_6, δ): 2.82-2.87 (1H, dd, *J* = 8.8 and 14 Hz, β-CH_AH$_B$ Tyr), 3.12-3.17 (1H, dd, *J* = 4.8 and 15.2 Hz, β-CH$_A$$H_B$ Tyr), 3.73 (3H, s, OCH_3), 4.12 (1H, m, α-C*H* Tyr), 6.73 (2H, d, *J* = 8.4 Hz, Ar*H* Tyr), 7.11 (2H, *J* = 8.4 Hz, Ar*H* Tyr), 7.30 (1H, s, β-C*H* ΔPhe), 7.40-7.42 (3H, m, Ar*H* Phe), 7.55-7.58 (2H, m, Ar*H* Phe), 8.17 (3H, s, NH_3^+), 9.38 (1H, s br, O*H* Tyr), 10.30 (1H, s, N*H* ΔPhe) ppm.

^{13}C-NMR (100.6 MHz, DMSO-d_6 δ: 36.0 (CH_2, β-*C*H$_2$ Phe), 52.3 (CH_3, O*C*H$_3$), 53.9 (CH, α-C*H* Phe), 115.5 (CH, Ar*H* Try), 124.7 (C), 125.1 (C), 128.7 (CH), 129.7 (CH), 130.0 (CH), 130.6 (CH, Ar*H* Try), 132.2 (CH, β-*C*H ΔPhe), 132.9 (C), 156.7 (C), 165.0 (C, *C*=O), 168.4 (C, *C*=O). ppm.

4.2.7 Synthesis of compound 17 [76]

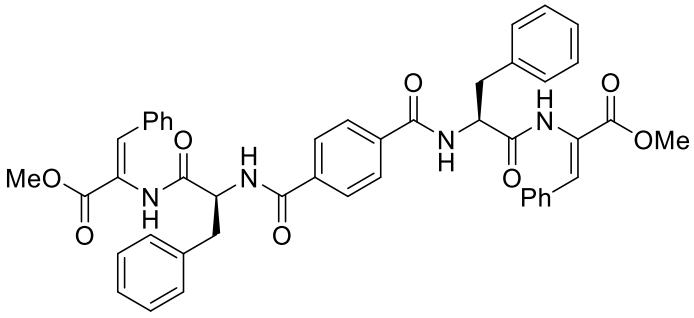

To a stirred suspension of terephthaloyl chloride (**16**) (1.0 equiv., 0.25 mmol, 0.05 g) in dry THF (5 mL), ET_3N (5.0 equiv., 1.25 mmol, 0.18 mL) and H-L-Phe-*Z*-ΔPhe-OMe • TFA, **11a**, (2.4 equiv.,

0.60 mmol, 0.26 g) were sequentially added under a nitrogen atmosphere. This mixture was stirred for 1 h at room temperature and then heated under reflux for 48 h at 80°C. The white precipitate was filtered and washed several times with cold water (25 mL) - (to remove the byproduct Et_3NHCl) and finally with diethyl ether (25 mL). This white solid was dried under vacuum, to provide compound **17** as a white solid (84 mg, 0.11 mmol, 44%).

^{1}H-NMR (400 MHz, DMSO-d_6, δ): 3.03-3.09 (2H, dd, *J* = 3.9 and 13.8 Hz, β-CH_AH_B); 3.21-3.24 (2H, dd, *J* = 10.8 and 12.8 Hz, β-CH_AH_B); 3.70 (6H, s, OCH_3); 4.83-4.89 (2H, m, α-C*H*); 7.16-7.35 (18H, m, Ar*H* and β-C*H* ΔPhe); 7.68 (4H, m, Ar*H*); 7.88 (4H, s, Ar*H* central ring); 8.84 (2H, d, *J* = 8.0 Hz, α-N*H* Phe); 9.96 (2H, s, α-N*H* ΔPhe) ppm.

^{13}C-NMR (100.6 MHz, DMSO-d^6, δ): 36.4 (CH_2, β-*C*H_2 Phe), 52.2 (CH_3, O*C*H_3), 55.2 (CH, α-*C*H Phe), 125.9 (C, α-*C* ΔPhe), 126.4 (CH), 127.4 (CH), 128.1 (CH), 128.6 (CH), 129.2 (CH), 129.5 (CH), 130.1 (CH), 132.0 (CH, β-C*H* ΔPhe), 133.3 (C), 136.3 (C), 138.3 (C), 165.4 (C, *C*=O), 165.9 (C, *C*=O), 171.5 (C, *C*=O) ppm.

HRMS (ESI): m/z: $[M+H]^+$ calcd. for $C_{46}H_{42}N_4O_8$ 779.30026; found 779.30759.

4.2.8 Synthesis of compound 1 [76]

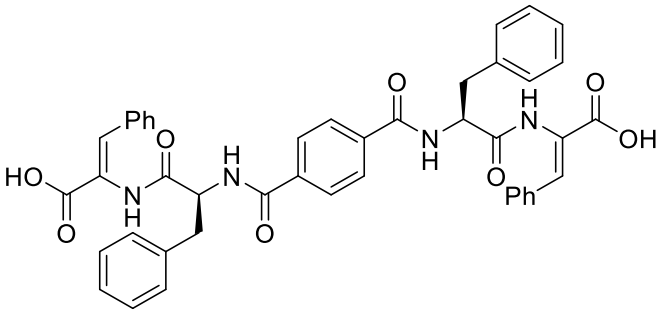

Compound **17** (0.11 mmol, 84.0 mg) was dissolved in 1,4-dioxane (3.21 mL) and NaOH (1M) (3.0 equiv., 0.32 mL). The reaction was monitored by TLC. When the starting material was consumed (typically 4 h), the organic solvent was removed under reduced pressure and the reaction mixture was acidified to pH 3 with $KHSO_4$ (1M). The solid precipitate was filtered, affording compound **1** (66.0 mg, 0.09 mmol, 82%), as a white solid, that decomposes at 218 °C.

^{1}H-NMR (400 MHz, DMSO-d_6, δ): 3.02-3.08 (2H, dd, *J* = 10.8 and 13.7 Hz, β-CH_AH_B); 3.21-3.24 (2H, dd, *J* = 3.6 and 13.7, β-CH_AH_B); 4.84-4.89 (2H, m, α-C*H*); 7.14-7.33 (14H, m, Ar*H* and β-

C*H* ΔPhe); 7.40-7.42 (4H, d, *J* = 7.2 Hz, Ar*H* Phe); 7.65-7.67 (4H, m, Ar*H* ΔPhe); 7.85-7.87 (4H, m, Ar*H* central ring); 8.79-8.81 (2H, d, *J* = 8.4 Hz; α-N*H* Phe); 9.79 (2H, s, α-N*H* ΔPhe), 12.7 (2H, s, CO_2H) ppm.

^{13}C-NMR (100.6 MHz, DMSO-d_6: δ): 36.5 (CH_2, β-*C*H_2 Phe), 55.2 (CH, α-*C*H Phe), 126.6 (C, α-*C* ΔPhe), 126.3 (CH), 127.3 (CH), 128.1 (CH), 128.5 (CH), 129.2 (CH), 129.2 (CH), 130.0 (CH), 131.9 (CH, β-*C*H ΔPhe), 133.6 (C), 136.3 (C), 138.4 (C), 165.8 (C, *C*=O), 166.2 (C, *C*=O), 171.1 (C, *C*=O) ppm.

HRMS (ESI): m/z: $[M+H]^+$ calcd. for $C_{44}H_{38}N_4O_8$ 751.26896; found 751.27670.

4.2.9 Synthesis of compound 18

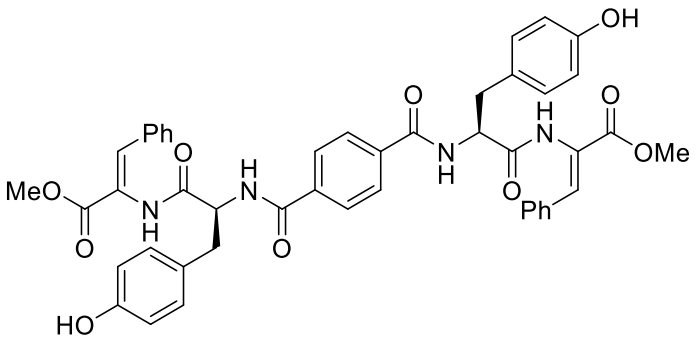

To a stirred suspension of terephthaloyl chloride (**16**) (1.0 equiv., 0.244 mmol, 0.050 g) in dry THF (5 mL), Et_3N (5.0 equiv., 1.22 mmol, 0.17 mL) and H-L-Tyr-*Z*-ΔPhe-OMe • TFA, **11b**, (2.4 equiv., 0.586 mmol, 0.266 g) were sequentially added under a nitrogen atmosphere. This mixture was stirred for 1h at room temperature and then heated under reflux for 48h at 80°C. The white precipitate was filtered and washed several times with cold water (25 mL) - (to remove the byproduct Et_3NHCl) and finally with diethyl ether (25 mL). This white solid was dried under vacuum, to provide compound **18** as a yellow solid (145 mg, 0.178 mmol, 73%).

^{1}H-NMR (400 MHz, DMSO-d_6, δ): 2.87-2.97 (2H, app.t, β-CH_AH$_B$ Tyr), 3.03-3.13 (2H, app.t, β-C$H_A$$H_B$ Try), 3.70 (6H, s, OCH_3), 4.75-4.80 (2H, m, α-C*H* Tyr), 6.65 (4H, d, *J* = 8.0 Hz, Ar*H* Tyr), 7.19 (4H, d, *J* = 8.0 Hz, Ar*H* Tyr), 7.26 (2H, s, β-C*H* ΔPhe), 7.34-7.35 (6H, m, Ar*H* ΔPhe), 7.66 (4H, s br., Ar*H* ΔPhe), 7.90 (4H, s, Ar*H* central ring), 8.77 (2H, d, *J* = 8 Hz, N*H* Tyr), 9.18 (2H, s, O*H*), 9.92 (2H, s, N*H* ΔPhe) ppm.

^{13}C-NMR (100.6 MHz, DMSO-d_6, δ): 35.7 (CH_2, β-*C*H_2 Tyr), 52.2 (CH_3, O*C*H_3), 55.6 (CH, α -*C*H Tyr), 115.0 (CH, Tyr), 126.0 (C), 127.4 (CH, central ring), 128.3 (C, *C*-Tyr), 128.5 (CH, *C*H ΔPhe),

129.5 (CH, *C*H ΔPhe), 130.1 (CH, *C*H ΔPhe), 130.1 (CH, *C*H Tyr), 132.0 (CH, β-*C*H ΔPhe), 133.3 (C, *C*-ΔPhe), 136.3 (C, central ring), 155.8 (C, Tyr *C*-OH), 165.4 (C, *C*=O), 165.8 (C, *C*=O), 171.6 (C, *C*=O) ppm.

HRMS (ESI): m/z: $[M+H]^+$ calcd. for $C_{46}H_{42}N_4O_{10}$ 811.2901; found 811.2956.

4.2.10 Synthesis of compound 2

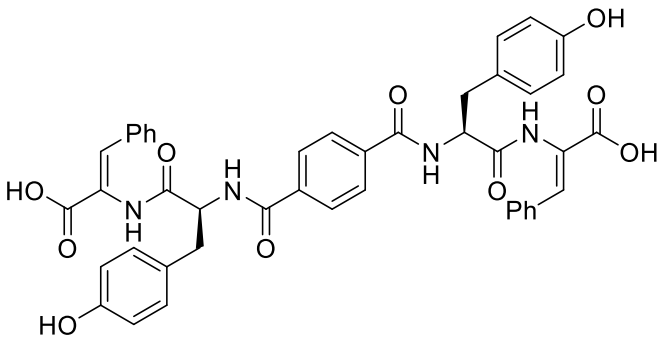

Compound **18** (0.178 mmol, 145 mg) was dissolved in 1,4-dioxane (3.60 mL) and NaOH (1M) (3.0 equiv., 0.40 mL). The reaction was monitored by TLC. When the starting material was consumed (typically 4 h), the organic solvent was removed under reduced pressure and the reaction mixture was acidified to pH 3 with $KHSO_4$ (1M). The solid precipitate was filtered, to afford compound **2** (75mg, 96 mmol, 81 %), as a white solid.

^{1}H-NMR (400 MHz, DMSO-d_6, δ): 2.90-2.96 (2H, app.t, β-CH_AH_B Tyr), 3.10-3.13 (2H, app.t, β-CH_AH_B Tyr), 4.75-4.81 (2H, m, α-C*H* Tyr), 6.64 (4H, d, *J* = 8 Hz, Ar*H* Tyr), 7.19 (4H, d, *J* = 8 Hz, Ar*H* Tyr), 7.29 (2H, s, β-C*H* ΔPhe), 7.32-7.33 (6H, m, Ar*H* ΔPhe), 7.63-7.66 (4H, m, Ar*H* ΔPhe), 7.88 (4H, d *J* = 4.0 Hz, Ar*H* central ring), 8.73 (2H, d, *J* = 8.0 Hz, N*H* Tyr), 9.17 (2H, s, O*H*), 9.74 (2H, s, N*H* ΔPhe), 12.5 (2H, s, CO_2H) ppm.

^{13}C-NMR (100.6 MHz, DMSO-d_6: δ): 35.8 (CH_2, β-*C*H_2 Tyr), 55.6 (CH, α-*C*H Tyr), 115.0 (CH, *C*H Tyr), 126.7 (C), 127.4 (CH, central ring), 128.4 (C, *C*-Tyr), 128.5 (CH, *C*H ΔPhe), 129.2 (CH, *C*H ΔPhe), 130.0 (CH, *C*H ΔPhe), 130.2 (CH, *C*H Tyr), 131.7 (CH, β-*C*H ΔPhe), 133.7 (C, *C*-ΔPhe), 136.4 (C, central ring), 155.8 (C, Tyr *C*-OH), 165.8 (C, *C*=O), 166.3 (C, *C*=O), 171.3 (C, *C*=O) ppm.

HRMS (ESI): m/z: $[M+H]^+$ calcd. for $C_{44}H_{38}N_4O_{10}$ 783.2588; found 783.2661.

4.2.11 Synthesis of compound 20

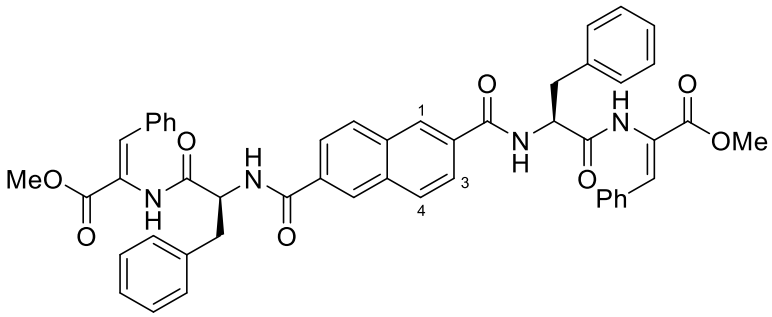

Naphthalene-2,6-dicarboxylic acid (**19**) (1.0 equiv., 0.53 mmol, 0.11 g) was dissolved in MeCN (6 mL) and cooled to 0°C. H-L-Phe-*Z*-ΔPhe-OMe • TFA (2.2 equiv., 1.16 mmol, 0.51 g), Et_3N (6.0 equiv., 3.17 mmol, 0.44 mL), and HBTU (2.4 equiv., 1.67 mmol, 0.48 g) were added sequentially, with 2 min between each addition, and the mixture was stirred at rt overnight. The solvent was removed under reduced pressure to afford a residue that was partitioned between EtOAc (50 mL) and $KHSO_4$ (1M, 50 mL). After separation of the phases, the organic phase was thoroughly washed with $KHSO_4$ (1 M, 3 × 50 mL), $NaHCO_3$ (1 M, 3 × 50 mL), and brine (3 × 50 mL) and then dried with anhydrous $MgSO_4$. Filtration followed by removal of the solvent under reduced pressure afforded compound **20** as a white solid (0.420 g, 0.510 mmol, 96 %)

^{1}H-NMR (400 MHz, DMSO-d_6, δ): 3.11-3.17 (2H, app. t, β-CH_AH$_B$ Phe), 3.24-3.29 (2H, dd, *J* = 3.6 and 14 Hz, β-CH$_A$$H_B$ Phe), 3.71 (6H, s, OCH_3), 4.90-4.96 (2H, m, α-C*H* Phe), 7.16-7.47 (18H, m, Ar*H* Phe), 7.69-7.72 (4H, m, Ar*H* ΔPhe), 7.97 (2H, d, *J* = 8.8 Hz, ArH_3 central ring), 8.10 (2H, d, *J* = 8.8 Hz, ArH_4 central ring), 8.50 (2H, s, ArH_1 central ring), 9.00 (2H, d, *J* = 6.8 Hz, α-N*H* Phe), 10.0 (2H, s, α-N*H* ΔPhe) ppm.

^{13}C-NMR (100.6 MHz, DMSO-d_6: δ): 36.5 (CH_2, β-*C*H$_2$ Phe), 52.2 (CH_3, O*C*H$_3$), 55.3 (CH, α-*C*H Phe), 125.1 (CH, C_3H central ring), 125.9 (C), 126.3 (CH), 127.6 (CH, C_1H central ring), 128.1 (CH), 128.5 (CH), 128.9 (CH, C_4H central ring), 129.2 (CH), 129.5 (CH), 130.1 (CH, *C*H ΔPhe), 132.1 (CH), 132.7 (C), 133.2 (C), 138.3 (C), 165.3 (C, *C*=O), 166.3 (C, *C*=O), 174.6 (C, *C*=O) ppm.

HRMS (ESI): m/z: $[M+H]^+$ calcd. for $C_{50}H_{44}N_4O_8$ 829.3159; found 829.3228.

4.2.12 Synthesis of compound 3

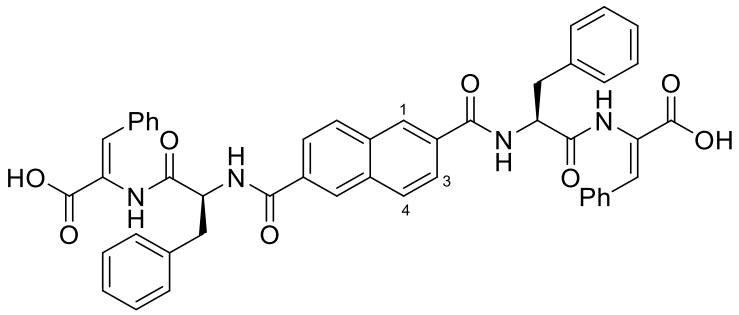

Compound **20** (0.51 mmol, 0.42 g) was dissolved in 1,4-dioxane (15 mL) and NaOH (1M) (3.00 equiv., 1.52 mL). The reaction was monitored by TLC. When the starting material was consumed (typically 4 h), the organic solvent was removed under reduced pressure and the reaction mixture was acidified to pH 3 with $KHSO_4$ (1M). The solid precipitate was filtered to afford compound **3** (0.400 g, 0.500 mmol, 98%), as a white solid.

^{1}H-NMR (400 MHz, DMSO-d_6, δ): 3.10-3.17 (2H, dd, *J* = 3.12 and 13.2 Hz, β-CH_AH$_B$ Phe), 3.26-3.29 (2H, app. t, β-CH$_A$$H_B$ Phe), 4.91-4.97 (2H, m, α-C*H* Phe), 7.14-7.45 (18H, m, Ar*H* Phe), 7.65-7.67 (4H, m, Ar*H* ΔPhe), 8.05 (2H, d, *J* = 8.4 Hz, ArH_3 central ring), 7.95 (2H, d, *J* = 8.4 Hz, ArH_4 central ring ,8.46 (2H, s, ArH_1 central ring), 8.89 (2H, d, *J* = 6.8 Hz, α-N*H* Phe), 9.76 (2H, s, α-N*H* ΔPhe), 12.6 (2H, s, CO_2H) ppm.

^{13}C-NMR (100.6 MHz, DMSO-d_6 δ): 36.6 (CH_2, β-*C*H$_2$ Phe), 55.4 (CH, α-*C*H Phe), 125.1 (CH, C_3H central ring), 125.9 (C), 126.3 (C), 126.9 (CH), 127.5 (CH, C_1H central ring), 128.1 (CH), 128.4 (CH), 128.9 (CH, C_4H central ring), 129.0 (CH), 129.1 (CH), 129.2 (CH), 130.0 (CH), 131.4 (CH), 132.8 (C), 133.2 (C), 133.8 (C), 138.4 (C), 166.3 (C, 2× *C*=O), 171.1 (*C*=O) ppm.

HRMS (ESI): m/z: $[M+H]^+$ calcd. for $C_{48}H_{44}N_4O_8$ 801.2846; found 801.2925.

4.2.13 Synthesis of compound 21

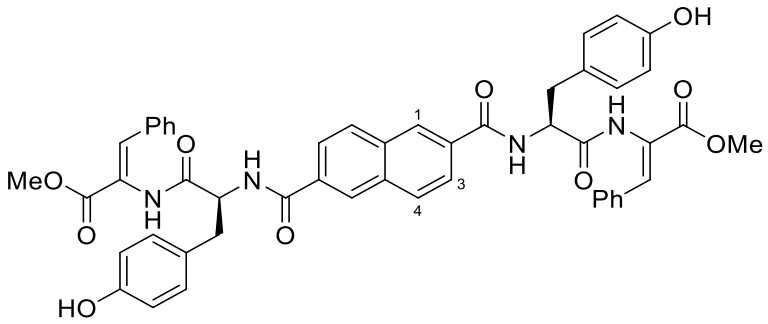

Naphthalene-2,6-dicarboxylic acid (**19**) (1.0 equiv., 0.23 mmol, 0.05 g) was dissolved in DMF (5 mL) and cooled to 0°C. NH_2-L-Tyr-*Z*-ΔPhe-OMe • TFA (2.4 equiv., 0.56 mmol, 0.25 g), Et_3N (6.0 equiv., 1.40 mmol, 0.10 mL), and HBTU (2.4 equiv., 0.56 mmol, 0.21 g) were added sequentially, with 2 min between each addition, and the mixture was stirred at rt for 2 days. The solvent was removed under reduced pressure to afford a residue that was partitioned between EtOAc (50 mL) and $KHSO_4$ (1M, 50 mL). After separation of the phases, the organic phase was thoroughly washed with $KHSO_4$ (1 M, 2 × 50 mL) and brine (3 × 50 mL) and then dried with anhydrous $MgSO_4$. Filtration followed by removal of the solvent under reduced pressure afforded compound **21** as a white solid (196 mg, 0.228 mmol, 98%).

^{1}H-NMR (400 MHz, DMSO-d_6, δ): 3.02-3.08 (2H, dd, *J* = 10.8 and 13.6 Hz, β-CH_AH_B Tyr), 3.12-3.16 (2H, dd, *J* = 4.0 and 14.0 Hz, β-CH_AH_B Tyr), 3.70 (6H, s, OCH_3), 4.79-4.85 (2H, m, α-C*H* Tyr), 6.68 (4H, d, *J* = 8.4 Hz, Ar*H* Tyr), 7.23 (4H, d, *J* = 8.4 Hz, Ar*H* Tyr), 7.26 (2H, s, β-C*H* ΔPhe), 7.27-7.30 (6H, m, Ar*H* ΔPhe), 7.68-7.70 (4H, m, Ar*H* ΔPhe), 8.00 (2H, d, *J* = 9.6 Hz, ArH_3 central ring), 8.07 (2H, d, *J* = 8.8 Hz, ArH_4 central ring), 8.54 (2H, s, ArH_1 central ring), 9.01 (2H, d, *J* = 8.4 Hz, N*H* Tyr), 9.29 (2H, s, O*H*), 10.1 (2H, s, N*H* ΔPhe) ppm.

^{13}C-NMR (100.6 MHz, DMSO-d_6 δ): 35.8 (CH_2, β-*C*H_2 Tyr), 52.2 (CH_3, O*C*H_3), 55.9 (CH, α-*C*H Tyr), 115.0 (CH, *C*H Tyr), 125.1 (CH, *C*$_3$H central ring), 126.0 (C), 127.6 (CH, *C*$_1$H central ring), 128.2 (C), 128.5 (CH, *C*H ΔPhe), 128.8 (CH, *C-4,* central ring), 129.4 (CH, *C*H ΔPhe), 130.1 (CH, *C*H ΔPhe), 130.2 (CH, *C*H Try), 132.1 (CH, β-*C*H ΔPhe), 132.7 (C), 133.2 (C), 133.3 (C), 155.9 (C), 165.4 (C, *C*=O), 166.2 (C, *C*=O), 171.8 (C, *C*=O) ppm.

HRMS (ESI): m/z: $[M+Na]^+$ calcd. for $C_{50}H_{44}N_4O_{10}$ 883.3057; found 883.2961.

4.2.14 Synthesis of compound 4

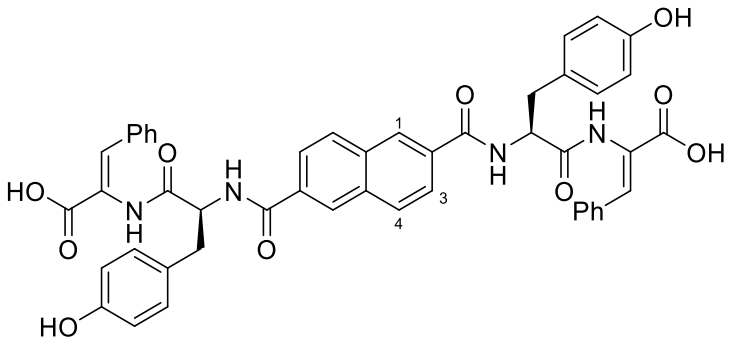

Compound **21** (0.228 mmol, 196 mg) was dissolved in 1,4-dioxane (7 mL) and NaOH (1M) (3.00 equiv., 0.7 mL). The reaction was monitored by TLC. When all the starting material was consumed (typically 4 h), the organic solvent was removed under reduced pressure and the reaction mixture was acidified to pH 3 with $KHSO_4$ (1 M). The solid precipitate was filtered to afford compound **4** (188 mg, 0.225 mmol, 98 %), as a white solid.

^{1}H-NMR (400 MHz, DMSO-d_6, δ): 3.10-3.17 (2H, app.t, β-CH_AH$_B$ Tyr), 3.26-3.29 (2H, dd, *J* = 3.6 and 14.0 Hz, β-CH$_A$$H_B$ Tyr), 4.81-4.87 (2H, m, α-C*H* Tyr), 6.66 (4H, d, *J* = 8.8 Hz, Ar*H* Tyr), 7.22 (4H, d, *J* = 8.4 Hz, Ar*H* Tyr), 7.29 (2H, s, β-C*H* ΔPhe), 7.31-7.34 (6H, m, Ar*H* ΔPhe), 7.66-7.67 (4H, m, Ar*H* ΔPhe), 7.96 (2H, d, *J* = 9.2 Hz, ArH_3 central ring), 8.06 (2H, d, *J* = 8.4 Hz, ArH_4 central ring), 8.47 (2H, s, ArH_1 central ring), 8.84 (2H, d, *J* = 10 Hz, N*H* Tyr), 9.15 (2H, s, O*H*), 9.77 (2H, s, N*H* ΔPhe), 12.3 (2H, s, CO_2H) ppm.

^{13}C-NMR (100.6 MHz, DMSO-d_6 δ): 35.8 (CH_2, β-*C*H$_2$ Phe), 55.8 (CH, α-*C*H Phe), 114.9 (CH, *C*H Tyr), 125.1 (CH, C_3H central ring), 126.7 (C), 127.6 (CH, C_1H central ring), 128.3 (CH), 128.4 (CH, CH ΔPhe), 128.8 (CH, C_4H central ring), 129.2 (CH, *C*H ΔPhe), 130.0 (CH, *C*H ΔPhe), 130.1 (CH, *C*H Try), 131.9 (CH, β-*C*H ΔPhe), 132.8 (C), 133.2 (C), 133.6 (C), 155.8 (C), 166.2 (C, 2× *C*=O), 171.4 (C, *C*=O) ppm.

HRMS (ESI): m/z: $[M+H]^+$ calcd. for $C_{48}H_{40}N_4O_{10}$ 833.2744; found 833.2819.

4.3 Sustained release assays

Hydrogels of **1**,**2** and **3** were prepared as described before to form 1 mL hydrogels containing the same concentration of the hydrogelators described above and the appropriate cargo – methylene blue (0.1 nM), methyl orange (0.2 nM) or ciprofloxacin (0.2 nM), in a slightly modified version of the procedure described by Abraham *et al.* [88] After allowing to stand overnight, 1.5 mL of water was carefully added to the surface of the hydrogels. Aliquots of the layered solution (100 μL) were removed at 1h, 2h, 3h, 4h, 6h, 24h, 72h and 6 days from the time the water was initially layered on top of the hydrogel. After removing each aliquot, the volume water was immediately replaced by and equal volume of water. The concentration of methylene blue or methyl orange in each aliquot was determined by measuring the absorbance at λ_{max} of the dye (666 nm for methylene blue and 465 nm for methyl orange) using a microplate reader and then converting the value to percentage release (using a standard calibration curve). The concentration of ciprofloxacin in each aliquot was determined using analytical HPLC, where the integrated peak area was converted to a percentage release (using a standard calibration curve). Each experiment was performed in triplicate, and the mean percentage cargo release was plotted against time.

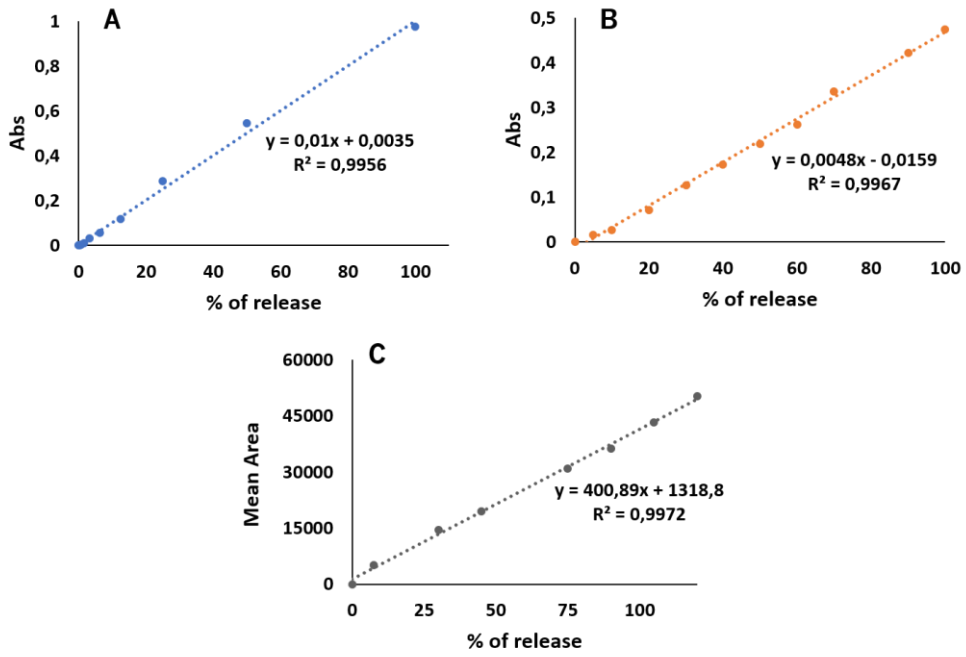

Figure 65: Calibration curve to determine the amount of cargo in present in the layered solution above the hydrogel. (A) Methylene blue was measured by UV-Vis spectroscopy by absorbance at 666 nm. Equation of linear correlation: y=0.01x + 0.0035. (B) Methyl orange was measured by UV-Vis spectroscopy by absorbance at 465 nm. Equation of linear correlation: y=0.0048x - 0.0159. (C) Ciprofloxacin was measured by HPLC by area under the curve of the ciprofloxacin peak. Equation of linear correlation: y=400.89x + 1318.8.

4.4 Cell Culture

Human keratinocytes cell line HaCaT was from ATCC. Cells were cultured in DMEM supplemented with 10% FBS and 1% penicillin/streptomycin and were incubated in an incubator at 37°C, in a humidified atmosphere of 5% CO_2.

4.5 MTT assay

Cells were seeded in 96-well plates (1.5×10^4 cells/well) and left to attach for 24h. After this period, cells were incubated with different concentrations of the molecules under study for another 24h. After this period, cell viability was evaluated based on the ability of metabolically active cells to convert MTT to formazan over the course of 2 hours. Absorbances were measured at 570 nm in a Multiskan GO plate reader (Thermo Fisher Scientific; Waltham, MA, USA) and results were expressed as percentage of the respective control and correspond to the mean ± standard error of the mean (SEM) of at least three independent experiments performed in triplicate.

4.6 DNA quantification

Cells were cultured at the same density described above for the MTT assay, in the presence of the molecules under study. After incubation, the culture medium was replaced by 50 µL of ultra-pure water, plates being incubated for 30 min at 37°C and immediately frozen at -80°C. DNA quantification was performed in a triplicate pool using a Qubit™ dsDNA HS Assay Kit according to manufacturer's instructions. Results are expressed as percentage of the respective control and correspond to the mean ± SEM of three independent experiments performed in triplicate.

Chapter 5

References

5 References

[1] G. Fichman, E. Gazit, "Self-assembly of short peptides to form hydrogels: Design of building blocks, physical properties and technological applications", *Acta Biomaterialia*, **2014**, vol. 10, pp. 1671-1682, DOI: https://doi.org/10.1016/j.actbio.2013.08.013

[2] M.C.I.M. Amin, N. Ahmad, M. Pandey, M.M. Abeer, N. Mohamad, "Recent advances in the role of supramolecular hydrogels in drug delivery", *Expert Opinion on Drug Delivery*, **2015**, vol.12, pp. 1149-1161, DOI: 10.1517/17425247.2015.997707

[3] N.N. Ferreira, L.M.B. Ferreira, V.M.O. Cardoso, F.I. Boni, A.L.R. Souza, M.P.D. Gremião, "Recent advances in smart hydrogels for biomedical applications: From self-assembly to functional approaches", *European Polymer Journal*, **2018**, vol. 99, pp. 117-133, DOI: https://doi.org/10.1016/j.eurpolymj.2017.12.004

[4] S.M. Bindu, V. Ashok, C. Arkendu, "As A Review on Hydrogels as Drug Delivery in the Pharmaceutical Field", *International Journal of Pharmaceutical and Chemical Sciences*, **2012**, vol. 1, pp.642-661

[5] T.R. Hoare, D.S. Kohane, "Hydrogels in drug delivery: Progress and Challenges", *Polymer*, **2008**, vol. 49, pp. 1993-2007, DOI: https://doi.org/10.1016/j.polymer.2008.01.027

[6] M. Hamidi, A. Azadi, P. Rafiei, "Hydrogel nanoparticles in drug delivery", *Advanced Drug Delivery Reviews*, **2008**, vol. 60, pp. 1638-1649, DOI: https://doi.org/10.1016/j.addr.2008.08.002

[7] N.A. Peppas, P. Bures, W. Leobandung, H. Ichikawa, "Hydrogels in pharmaceutical formulations", *European Journal of Pharmaceutics and Biopharmaceutics*, **2000**, vol. 50, pp. 27-46, DOI: https://doi.org/10.1016/S0939-6411(00)00090-4

[8] S.K.H. Gulrez, S-Al-Assaf, G.O. Phillips, "Hydrogels: Methods of Preparation, Characterisation and Applications", *Progress in Molecular and Environmental Bioengineering - Analysis and Modeling to Technology Applications*, **2011**, vol. 5, pp. 117-150, DOI: 10.5772/24553

[9] N. Chirani, L. Yahia, L. Gritsch, F.L. Motta, S. Chirani, S. Faré, "History and Applications of Hydrogels", *Journal of Biomedical Sciences*, vol. 4, pp. 2-13, **2015**, DOI: 10.4172/2254-609x.100013

[10] X. Du, J. Zhou, B. Xu, "Supramolecular Hydrogels Made of Basic Biological Building Blocks", *Chemistry an Asian Journall*, **2014**, vol. 6, pp. 1446-1472, DOI: 10.1002/asia.201301693

[11] P.R.A. Chivers, D.K. Smith, "Shaping and structuring supramolecular gels", *Nature Reviews Materials*, **2019**, vol. 4, pp. 463-478, DOI: https://doi.org/10.1038/s41578-019-0111-6

[12] E.K. Johnson, D.J. Adams, P.J. Cameron, "Peptide based low molecular weight gelators",

Journal of Materials Chemistry, **2011**, vol. 21, pp. 2024-2027, DOI: https://doi.org/10.1039/C0JM03099F

[13] K. Tao, A. Levin, L. Alder-Abramovich, E. Gazit, "Fmoc-modified amino acids and short peptides: simples bio-inspired building blocks for the fabrication of functional materials", *Chem. Soc. Rev.*, **2016**, vol. 45, pp. 3935-3953, DOI: https://doi.org/10.1039/C5CS00889A

[14] E.R. Draper, D.J. Adams, "Low-Molecular-Weight Gels: The State of the Art", *Chem*, **2017**, vol. 3, pp. 391-410, DOI: https://doi.org/10.1016/j.chempr.2017.07.012

[15] M. Reches, E. Gazit, "Self-Assembly of Peptide Nanotubes and Amyloid-like Structures by Charged-Termini-Capped Diphenylalanine Peptide Analogues", *Israel Journal of Chemistry*, **2005**, vol. 45, pp. 363-371, DOI: https://doi.org/10.1560/5MC0-V3DX-KE0B-YF3

[16] C. Tang, A.M. Smith, R.F. Collins, R.V. Ulijn, A. Saiani, "Fmoc-Diphenylalanine Self-Assembly Mechanism Induces Apparent pKa Shifts", *Langmuir*, **2009**, vol. 25, pp. 9447–9453, DOI: https://doi.org/10.1021/la900653q

[17] J. Raeburn, G. Pont, L. Chen, Y. Cesbron, R. Levyc, D.J. Adams, "Fmoc-diphenylalanine hydrogels: understanding the variability in reported mechanical properties", *Soft Matter*, **2012**, vol. 8, pp. 1168-1174, DOI: https://doi.org/10.1039/C1SM06929B

[18] A.D. Martin, P. Thordarson, "Beyond Fmoc: a review of aromatic peptide capping groups", *J. Mat. Chem. B*, **2020**, vol. 8, pp. 863-877, DOI: https://doi.org/10.1039/c99tb02539a

[19] Z. Yang, G. Liang, M. Ma, Y. Gao, B. Xu, "Conjugates of naphthalene and dipeptides produce molecular hydrogelators with high efficiency of hydrogelation and superhelical nanofibers", *Journal of Materials Chemistry*, **2007**, vol. 17, pp. 850-854, DOI: https://doi.org/10.1039/B611255B

[20] C.J. Bowerman, W. Liyanage, A.J. Federation, B.L. Nilsson, "Tuning β-Sheet Peptide Self-Assembly and Hydrogelation Behavior by Modification of Sequence Hydrophobicity and Aromaticity", *Biomacromolecules*, **2011**, vol. 12, pp. 2735-2745, https://doi.org/10.1021/bm200510k

[21] D.M. Murali, G. Shanmugam, "The aromaticity of the phenyl ring imparts thermal stability to a supramolecular hydrogel obtained from low molecular mass compound", *New J. Chem.*, **2019**, vol. 43, pp. 12396-12409, DOI: 10.1039/C9NJ01781J

[22] H. Vilaça, A.C.L. Hortelão, E.M.S. Castanheira, M.J.R.P. Queiroz, L. Hulliou, I.W. Hamley, J.A. Martins, P.M.T. Ferreira, "Dehydrodipeptide Hydrogelators Containing Naproxen *N*-Capped Tryptophan: Self-Assembly, Hydrogels Characterization, and Evaluation as Potencial Drug Nanocarriers", *Biomacromolecules*, **2015**, vol. 16, pp. 3562-3573, DOI: 10.1021/acs.biomac.5b01006

[23] N.M. Sangeetha, U. Maitra, "Supramolecular gels: Functions and uses", *Chemical Society*

Reviews, **2005**, vol. 34, pp. 821-836, DOI: https://doi.org/10.1039/B417081B

[24] D.J. Adams, "Dipeptide and Tripeptide Conjugates as Low-Molecular-Weight Hydrogelators", *Macromolecular Bioscience*, **2011**, vol. 11, pp. 160-173, DOI: 10.1002/mabi.201000316

[25] H. Vilaça, G. Pereira, T.G. Castro, B.F. Hermenegildo, J. Shi, T.Q. Faria, N. Michêlo, R.M.M. Brito, B.Xu, E.M.S. Castanheira, J.A. Martins, P.M.T. Ferreira, "New self-assembled supramolecular hydrogels based on dehydropeptides", *Journal of Materials Chemistry B*, **2015**, vol. 3, pp. 6355-6367, DOI: https://doi.org/10.1039/C5TB00501A

[26] D.J. Adams, M.F. Butler, W.J. Frith, M. Kirkland, L. Mullen, P. Sanderson, "A new method for maintaining homogeneity during liquid-hydrogel transitions using low molecular weight hydrogelators", *Soft Matter*, **2009**, vol. 5, pp. 1856-1862, DOI: https://doi.org/10.1039/B901556F

[27] D.J. Adams, L.M. Mullen, M. Berta, L. Chen, W.J. Frith, "Relationship between molecular structure, gelation behaviour and gel properties of Fmoc-dipeptides", *Soft Matter*, **2010**, vol. 6, pp. 1971-1980, DOI: https://doi.org/10.1039/B921863G

[28] L. Chen, K. Morris, A. Laybourn, D. Elias, M.R. Hicks, A. Rodger, L. Serpell, D.J. Adams, "Self-Assembly Mechanism for a Naphthalene-Dipeptide Leading to Hydrogelation", *Langmuir*, **2010**, vol. 26, pp. 5232-5242, DOI: https://doi.org/10.1021/la903694a

[29] L. Chen, S. Revel, K. Morris, L.C. Serpell, D.J. Adams, "Effect of Molecular Structure on the Properties of Naphthalene-Dipeptide Hydrogelators", *Langmiur*, **2010**, vol. 26, pp. 13466-13471, DOI: https://doi.org/10.1021/la102059x

[30] R. Vegners, I. Shestakova, I. Kalvinish, R.M. Ezzell, P.A. Janmey, "Use of a Gel-forming Dipeptide Derivative as a Carrier for Antigen Presentation", *Journal of Peptide Science*, **1995**, vol. 1, pp. 371-278, DOI: https://doi.org/10.1002/psc.310010604

[31] S. Debnath, A. Shome, D. Das, P.K. Das, "Hydrogelation Through Self-Assembly of Fmoc-Peptide Functionalized Cationic Amphiphiles: Potent Antibacterial Agent", *The Journal of Physical Chemistry B*, **2010**, vol. 114, pp. 4407-4415, DOI: https://doi.org/10.1021/jp909520w

[32] Z. Yang, G. Liang, B. Xu, "Enzymatic Hydrogelation of Small Molecules", *Accounts of Chemical Research*, **2008**, vol. 41, pp. 315-326, DOI: 10.1021/ar7001914

[33] S. Toledano, R.J. Williams, V. Jayawarna, R.V. Ulijn, "Enzyme-Triggered Self-Assembly of Peptide Hydrogels via Reversed Hydrolysis", *Journal of the American Chemical Society*, **2006**, vol. 128, pp. 1070-1071, DOI: https://doi.org/10.1021/ja056549l

[34] Z. Yang, G. Liang, M. Ma, Y. Gao, B. Xu, "In Vitro and In Vivo Enzymatic Formation of Supramolecular Hydrogels Based on Self-Assembled Nanofibers of a β-Amino Acid Derivative", *Nano*

Micro Small, **2007**, vol. 3, pp. 558-562, DOI: https://doi.org/10.1002/smll.200700015

[35] Q. Wang, Z. Yang, Y. Gao, W. Ge, L. Wang, B. Xu, "Enzymatic hydrogelation to immobilize an enzyme for high activity and stability", *Soft Matter*, **2008**, vol. 4, pp. 550-553, DOI: https://doi.org/10.1039/B715439A

[36] J. Shi, Y. Gao, Y. Zhang, Y. Pan, B. Xu, "Calcium Ions to Cross-Link Supramolecular Nanofibers to Tune the Elasticity of Hydrogels over Orders of Magnitude", *Langmuir*, **2011**, vol. 27, pp. 14425-14431, DOI: 10.1021/la2033862

[37] L. Chen, G. Pont, K. Morris, G. Lotze, A. Squires, L.C. Serpell, D.J. Adams, "Salt-induced hydrogelation of functionalised-dipeptides at high pH", *Chemical Communications*, **2011**, vol. 47, pp. 12071-12073, DOI: https://doi.org/10.1039/C1CC15474E

[38] M.M. Piepenbrock, G.O. Lloyd, N. Clarke, J.W. Steed, "Metal- and Anion-Binding Supramolecular Gels", *Chemical Reviews*, **2010**, vol. 110, pp. 1960-2004, DOI: https://doi.org/10.1021/cr9003067

[39] G. Yu, X. Yan, C. Han, F.Huang, "Characterization of supramolecular gels", *Chemical Society Reviews*, **2013**, vol.42, pp. 6697-6622, DOI: https://doi.org/10.1039/C3CS60080G

[40] A.H. Karoyo, L.D. Wilson, "Physicochemical properties and the gelation process of supramolecular hydrogels: a review", *Gels*, **2017**, vol. 1, pp. 1-18, DOI: https://doi.org/10.3390/gels3010001

[41] X.Li, K.Yi, J.Shi, Y.Gao, H.Lin, B.Xu, "Multifunctional. Biocompatible Supramolecular Hydrogelators Consist Only of Nucleobase, Amino Acid, and Glycoside", *Journal of the American Chemical Society*, **2011**, vol. 43, pp. 17513-17518, DOI: https://doi.org/10.1021/ja208456k

[42] L. Whitmore, B.A. Wallace, "Protein Secondary Structure Analyses from Circular Dichroism Spectroscopy: Methods and References Databases", *Biopolymers*, **2007**, vol. 89, pp. 392-400, DOI: https://doi.org/10.1002/bip.20853

[43] S.M. Kelly, T.J. Jess, N.C. Price, "How to study proteins by circular dichroism", *Biochimica et Biophysica Acta (BBA) – Proteins and Proteomics*, **2005**, vol. 1751, pp. 119-139, DOI: https://doi.org/10.1016/j.bbapap.2005.06.005

[44] NJ. Greenfield, "Using circular dichroism collected as a function of temperature to determine the thermodynamics of protein unfolding and binding interactions", *Nature Protocols*, **2006**, vol.1, pp. 2527-2535, DOI: 10.1038/nprot.2006.204

[45] N. J. Greenfield, "Using circular dichroism spectra to estimate protein secondary structure," *Nature Protocols*, **2007**, vol. 1, no. 6, pp. 2876–2890, DOI: 10.1038/nprot.2006.202

[46] C. D. Ramos CHI, "The use of circular dichroism spectroscopy to study protein folding, form and function", *African Journal Biochemistry Research*, **2009**, vol. 3, pp. 164–173

[47] S.J. Pennycook, M.F. Chisholm, A.R. Lupini, M. Varela, A.Y. Borisevich, M.P. Oxley, W.D. Luo, K.V. Benthem, S.H. Oh, D.L. Sales, S.I. Molina, J. Garcia-Barriocanal, C. Leon, J. Santamaría, S.N. Rashkeev, S.T. Pantelides, "Aberration-corrected scanning transmission electron microscopy: from atomic imaging and analysis to solving energy problems", *Philosophical Transactions of the Royal Society A*, **2009**, vol. 367, pp. 3709-3733, DOI: https://doi.org/10.1098/rsta.2009.0112

[48] J. Nanda, A. Banerjee, "β-Amino acid containing proteolytically stable dipeptide based hydrogels: encapsulation and sustained release of some important biomolecules at physiological pH and temperature", *Soft Matter*, **2012**, vol. 12, pp. 3380-3386, DOI: https://doi.org/10.1039/C2SM07168A

[49] S. Shankar, J.U. Rahim, R. Rai, "Self-Assembly in Peptides Containing β- and γ-amino Acids", *Current Protein & Peptide Science*, **2020**, vol. 21, pp. 584-597, DOI: 10.2174/1389203721666200127112244

[50] J. Li, Y. Kuang, Y. Gao, X. Du, J. Shi, B. Xu, "D-Amino Acids Boost the Selectivity and Confer Supramolecular Hydrogels of a Non-steroidal Anti-inflammatory Drug (NSAID)", *Journal of the American Chemical Society*, **2013**, vol. 2, pp. 545-545, DOI: 10.1021/ja310019x

[51] C.A. Miller, J.A.H. Ortiz, N.L. Abbott, S.H. Gellman, J.J. Pablo, "Dipole-induced self-assembly of helical β-peptide", *J. Chem. Phys.*, **2008**, vol. 129, pp. 015102, DOI: 10.1063/1.2928700

[52] C.K. Thota, N. Yadav, V.S. Chauhan, "A novel highly stable and injectable hydrogel based on a conformationally restricted ultrashort peptide", *Scientific Reports*, **2016**, vol.6, DOI: 10.1038/srep31167

[53] H. Vilaça, T. Castro, F.M.G. Costa, M. Melle-Franco, L. Hilliou, I.W. Hamley, E.M.S. Castanheira, J.A. Martins, P.M.T. Ferreira, "Self-assembly RGD dehydropeptide hydrogels for drug delivery applications", *Journal Materials Chemistry B*, **2017**, vol. 5, pp. 8607-8617, DOI: https://doi.org/10.1039/C7TB01883E

[54] S.R.S. Veloso, C.A.B. Magalhães, A.R.O. Rodrigues, H. Vilaça, M.J.R.P. Queiroz, J.A. Martins, P.J.G. Coutinho, P.M.T. Ferreira, E.M.S. Castanheira, "Novel dehydropeptide-based magnetogels containing manganese ferrite nanoparticles as antitumor drug nanocarriers", *Physical Chemistry Chemical Physics*, **2019**, vol. 21, pp. 10377-10390, DOI: https://doi.org/10.1039/C9CP00352E

[55] A. Carvalho, J. Gallo, D.M. Pereira, P. Valentão, P.B. Andrade, L. Hilliou, P.M.T. Ferreira, M. Bañobre-López, J.A. Martins, "Magnetic Dehydrodipeptide-Based Self-Assembled Hydrogels for

Theragnostic Applications", *Nanomaterials*, **2019**, vol. 9, pp. 541-557, DOI: 10.3390/nano9040541

[56] S.R.S. Veloso, P.J. Jervis, J.F.G. Silva, L. Hilliou, C. Moura, D.M. Pereira, P.J.G. Coutinho, J.A. Martins, E.M.S. Castanheira, P.M.T. Ferreira, "Supramolecular ultra-short carboxybenzyl-protected dehydropeptide-based hydrogels for drug delivery", *Materials Science and Engineering: C*. **2011**, vol. 122, pp. 111869, DOI: https://doi.org/10.1016/j.msec.2021.111869

[57] N. Naruje, H. Bai, K. Su, "Bolaamphiphilic molecules: Assembly and applications", *Progress in Polymer Science*, **2013**, vol. 38, pp. 302-343, DOI: https://doi.org/10.1016/j.progpolymsci.2012.09.003

[58] J.R. Hughes, A.S. Miller, C.E. Wallace, G.N. Vemuri, P.M. Lovine, "Biomedically Relevant Applications of Bolaamphiphiles and Bolaamphiphile-Containing Materials", *Medicinal and Pharmaceutical Chemistry*, **2021**, vol. 8, DOI: https://doi.org/10.3389/fchem.2020.604151

[59] F. Qiu, Y. Chen, C. Tang, Q. Zhou, C. Wang, Y.K. Shi, X. Zhao, "De Novo Design of a Bolaamphiphilic Peptide with only natural amino acids", *Macromolecular Bioscience*, **2008**, vol. 8, pp. 1053-1059, DOI: https://doi.org/10.1002/mabi.200800180

[60] M. Fariya, M. Jain, V. Dhawan, S. Shah, M.S. Nagarsenker, "Bolaamphiphiles: a pharmaceutical review", *Adv Pharm Bull.*, **2014**, vol. 4, pp. 483-491, DOI: 10.5681/apb.2014.072

[61] P. Dhasaiyan, B.L.V. Prasad, "Self-Assembly of Bolaamphiphilic Molecules", *The Chemical Record*, **2016**, vol. 17, pp. 597-640, DOI: https://doi.org/10.1002/tcr.201600085

[62] L.A. Estroff, A.D. Hamilton, "Water Gelation by Small Organic Molecules", *Chemical Reviews*, **2004**, vol. 104, pp. 1201-1217, DOI: https://doi.org/10.1021/cr0302049

[63] X. Dou, P. Li, D. Zhang, C.L. Feng, "C_2-symmetric benzene-based hydrogels with unique layered structures for controllable organic dye adsorption", *Soft Matter*, **2012**, vol. 8, pp. 3231-3238, DOI: 10.1039/c2sm06927j

[64] A.K. Das, I. Maity, H.S. Parmar, T.O. McDonald, M. Konda, "Lipase-Catalyzed Dissipative Self-Assembly of a Thixotropic Peptide Bolaamphiphile Hydrogel for Human Umbilical Cord Stem-Cell Proliferation", *Biomacromolecules*, **2015**, vol. 16, pp. 1157-1168, DOI: https://doi.org/10.1021/bm501835v

[65] Q. Zou, R. Chang, R. Xing, C. Yuan, X, Yan, "Injectable self-assembled bola-dipeptide hydrogels for sustained photodynamic prodrug delivery and enhanced tumor therapy", *Journal of Controlled Release*, **2020**, vol. 319, pp. 344-351, DOI: https://doi.org/10.1016/j.jconrel.2020.01.002

[66] C. Liu, Q. Zhang, S. Zhu, H. Liu, J. Chen, "Preparation and applications of peptide-based injectable hydrogels", *RSC Advances,* **2019**, vol. 9, pp. 28299-28311, DOI:

https://doi.org/10.1039/C9RA05934B

[67] M.J. Sis, M.J. Webber, "Drug Delivery with Designed Peptide Assemblies", *Trends in Pharmacological Sciences*, **2019**, vol. 40, pp. 747-762, DOI: https://doi.org/10.1016/j.tips.2019.08.003

[68] Y. Ben-Nun, G. Fichman, L. Alder-Abramovich, B. Turk, E. Gazit, G. Blum, "Cathepsin nanofiber substrates as potential agents for targeted drug delivery", *Journal of Controlled Release*, **2017**, vol. 257, pp. 60-67, DOI: https://doi.org/10.1016/j.jconrel.2016.11.028

[69] P. Zhang, A.G. Cheetham, Y. Lin, H. Cui, "Self-assembled tat nanofibers as effective drug carrier and transporter", *ACS Nano*, **2013**, vol. 7, pp. 5965-5977, DOI: https://doi.org/10.1021/nn401667z

[70] N.Yadav, M.K. Chauhan, V.S. Chauhan, "Short to ultrashort peptide-based hydrogels as a platform for biomedical applications", *Biomaterials Science*, **2020**, vol.8, pp.84-100, DOI: https://doi.org/10.1039/C9BM01304K

[71] A. Dasgupta, J.H. Mondal, D. Das, "Peptide hydrogels", *RSC Advances*, **2013**, vol. 3, pp. 9117-9149, DOI: https://doi.org/10.1039/C3RA40234G

[72] Z. Yang, K. Xu, L. Wang, H. Gu, H. Wei, M. Zhang, B.Xu, "Self-assembly of small molecules affords multifunctional supramolecular hydrogels for topically treating simulated uranium wounds", *Chemical Communicationd*, **2005**, vol. 35, pp. 4414-4416, DOI: 10.1039/b507314f

[73] J. Li, Y. Kuang, J. Shi, Y. Gao, J. Shou, B. Xu, "The conjugation of nonsteroidal anti-inflammatory drugs (NSAID) to small peptides for generating multifunctional supramolecular nanofibers/hydrogels", *Beilstein Journal of Organic Chemistry*, **2013**, vol.9, pp. 908-917, DOI: 10.3762/bjoc.9.104

[74] R. Moreira, P.J. Jervis, A. Carvalho, P.M.T. Ferreira, J.A. Martins, P. Valentão, P.B. Andrade, D.M. Pereira, "Biological Evaluation of Naproxen–Dehydrodipeptide Conjugates with Self-Hydrogelation Capacity as Dual LOX/COX Inhibitors", *Pharmaceutics*, **2020**, vol. 2, DOI: 10.3390/pharmaceutics12020122

[75] C. Bonauer, T. Walenzyk, B. Konig, "α,β-Dedydroamino acids", *Synthesis*, **2006**, vol. 1, pp. 1-20, DOI: 10.1055/s-2005-921759

[76] Juliana Justino de Andrade, "Self-Assembled noncovalent hydrogels based on dedydropeptides", **2012**, University of Minho

[77] P.M.T. Ferreira, L.S. Monteiro, G. Pereira, L. Ribeiro, J. Sacramento, L. Silva, "Reactivity of Dehydroamino Acids and Dehydrodipeptides Towards *N*-Bromosuccinimide: Synthesis of β-Bromo- and

β,β-Dibromodehydroamino Acid Derivatives and of Substituted 4-Imidazolidinones", *Eur. J. Org. Chem.,* **2007**, vol. 2007, pp. 5934-5949, DOI: https://doi.org/10.1002/ejoc.200700669

[78] E. Valeur, M. Bradley, "Amide bond formation: beyond the myth of coupling reagents", *Chem. Soc. Rev.*, **2009**, vol. 38, pp. 606-631, DOI: https://doi.org/10.1039/B701677H

[79] J. Kwak, S.S. Nam, J. Cho, E. Sim, S. Lee, "Interior-filled self-assemblies of tyrosyl bolaamphiphiles regulated by hydrogen bonds", *Phys. Chem. Chem. Phys.*, **2017**, vol. 19, pp. 10274-10281, DOI: https://doi.org/10.1039/C6CP08863E

[80] C. Lee, S. Lee, "Mussel-inspired bolaamphiphile sticky self-assemblies for the preparation of magnetic nanoparticles", *Colloids and Surface B: Biointerfaces*, **2015**, vol. 127, pp. 89-95, DOI: https://doi.org/10.1016/j.colsurfb.2014.11.024

[81] S.S.S. Wang, Y.T. Chen, P.H. Chen, K.N. Liu, "A kinetic study on the aggregation behavior of β-amyloid peptides in different initial solvent environments", *Biochemical Engineering Journal*, **2006**, vol. 29, pp. 129-138, DOI: https://doi.org/10.1016/j.bej.2005.02.037

[82] G. Williams, D.C. Watts, "Non-symmetrical dielectric relaxation behaviour arising from a simple empirical decay function", *Trans. Faraday Soc.*, **1970**, vol. 66, pp. 80-85, DOI: 10.1039/TF9706600080

[83] M. Kamihira, A. Naito, S. Tuzi, A.Y. Nosaka, H. Saito, "Conformational transitions and fibrillation mechanism of human calcitonin as studied by high-resolution solid-state ^{13}C NMR", **2000**, vol. 9, pp. 864-877, DOI: https://doi.org/10.1110/ps.9.5.867

[84] M. Doi, N.Y. Kuzuu, "Nonlinear elasticity of rodlike macromolecules in condensed state", *Polymer Physics*, **1980**, vol. 18, pp. 409-419, DOI: https://doi.org/10.1002/pol.1980.180180301

[85] M.L. Gardel, J.H. Shin, F.C. MacKintosh, L. Mahadevan, P. Matsudaira, D.A. Weitz, "Elastic behavior of cross-linked and bundled actin networks", *Science*, **2004**, vol. 304, pp. 1301-1305, DOI: 10.1126/science.1095087

[86] R.H. Pritchard, Y.Y.S. Huang, E.M. Terentjev, "Mechanics of biological networks: from the cell cytoskeleton to connective tissue", *Soft Matter*, **2014**, vol. 10, pp. 1864-1884, DOI: 10.1039/C3SM52769G

[87] H. Yang, S. Ghiassinejad, E.V. Ruymbeke, C.A. Fustion, "Tunable Interpenetrating Polymer Network Hydrogels Based on Dynamic Covalent Bonds and Metal-Ligand Bonds", *Macromolecules*, **2020**, vol. 53, pp. 6956-6967, DOI: https://doi.org/10.1021/acs.macromol.0c00494

[88] F. Meng, E.M. Terentjev, "Theory of Semiflexible Filaments and Networks", *Polymers*, **2017**, vol. 9, pp. 52-80, DOI: https://doi.org/10.3390/polym9020052

[89] B.L. Abraham, E.S. Toriki, N.D.J. Tucker, B.L. Nilsson, “Electrostatic interactions regulate the release of small molecules from supramolecular hydrogels”, *Journal of Materials Chemistry B*, **2020**, vol. 8, pp. 6366-6377, DOI: 10.1039/d0tb01157f

[90] S. Dash, P.N. Murthy, L. Nath, P. Chowdhury, “Kinetic modelling on drug release from controlled drug delivery systems”, *Acta Poloniae Pharmaceutica*, **2010**, vol. 67, pp. 217-223

[91] S. Kini, D. Bahadur, D. Panda, “Mechanism of Anti-Cancer Activity of Benomyl Loaded Nanoparticles in Multidrug Resistant Cancer Cells”, *Journal of Biomedical Nanotechnology*, **2014**, vol. 10, pp. 1-13, DOI: 10.1166/jbn.2014.1998